## Title

Activation of Hydrogen Peroxide by Iron-Containing Minerals and Catalysts in Circumneutral pH Solutions: Implications for ex situ and in situ Treatment of Contaminated Water and Soil



## Author

Pham, Anh

## Publication Date

2012

Peer reviewed|Thesis/dissertation

# Activation of Hydrogen Peroxide by Iron-Containing Minerals and Catalysts in Circumneutral pH Solutions: Implications for *ex situ* and *in situ* Treatment of Contaminated Water and Soil

by

Anh Le Tuan Pham

A dissertation submitted in partial satisfaction of the

requirements for the degree of

Doctor of Philosophy

in

Engineering – Civil and Environmental Engineering

in the

Graduate Division

of the

University of California, Berkeley

Committee in charge:

Professor David L. Sedlak, Co-Chair

Professor Fiona M. Doyle, Co-Chair

Professor James R. Hunt

Professor Ronald Gronsky

Fall 2012

# Activation of Hydrogen Peroxide by Iron-Containing Minerals and Catalysts in Circumneutral pH Solutions: Implications for *ex situ* and *in situ* Treatment of Contaminated Water and Soil



By Anh Le Tuan Pham

Abstract

Activation of Hydrogen Peroxide by Iron-Containing Minerals and Catalysts in Circumneutral pH Solutions: Implications for *ex situ* and *in situ* Treatment of Contaminated Water and Soil

by

Anh Le Tuan Pham

Doctor of Philosophy in Civil and Environmental Engineering

University of California, Berkeley

Professor David Sedlak, Co-Chair
Professor Fiona Doyle, Co-Chair

The decomposition of hydrogen peroxide ($H_2O_2$) on iron minerals can generate hydroxyl radical ($^{\bullet}OH$), a strong oxidant capable of transforming a wide range of contaminants. This reaction is critical to *ex situ* advanced oxidation processes employed in waste treatment systems, as well as *in situ* chemical oxidation processes used for soil and groundwater remediation. Unfortunately, the process in the *ex situ* treatment systems is relatively inefficient at circumneutral pH values. In this research, the development of iron-containing catalysts with improved efficiency was investigated. In addition, little is known about the factors that control the performance of *in situ* treatment systems. Another aim of this dissertation was to elucidate those factors to provide a basis for improving the efficiency of the remediation method.

Two types of silica- and alumina-containing iron (hydr)oxide catalysts were synthesized by sol-gel processing techniques (Chapter 2). Relative to iron oxides, such as hematite and goethite, these catalysts were 10 to 80 times more effective in catalyzing the production of $^{\bullet}OH$ from $H_2O_2$ under circumneutral conditions. The higher efficiency makes these catalysts promising candidates for *ex situ* advanced oxidation processes. Moreover, because alumina and silica alter the reactivity of the iron oxides with $H_2O_2$, understanding the activity of iron associated with natural aluminosilicates and silica-containing minerals in the subsurface is crucial to explaining the variability of $^{\bullet}OH$ production observed in *in situ* treatment systems.

In addition to the sol-gel technique used in Chapter 2, silica-containing iron (hydr)oxide catalysts were synthesized by immobilizing iron oxide onto mesoporous silica supports, such as SBA-15 (Chapter 5). The iron-containing SBA-15 was 10 times more effective than iron oxides in catalyzing the production of $^{\bullet}OH$ from $H_2O_2$. Moreover, this catalyst could be employed for selective oxidation of small organic contaminants based on size exclusion. However, a major drawback of the mesoporous silica-based catalysts is their instability under circumneutral conditions (Chapter 6). The dissolution of mesoporous silica materials raises questions about their use for water treatment, because silica dissolution might compromise the behavior of the material.

To gain insight into factors that control $H_2O_2$ persistence and $^{\bullet}OH$ yield in *in situ* processes, the decomposition of $H_2O_2$ and transformation of contaminants were investigated in the presence of iron-containing minerals and aquifer materials (Chapter 3). Consistent with the observation described in Chapter 2, iron-containing aluminosilicates were more effective than iron oxides in converting $H_2O_2$ into $^{\bullet}OH$. In both iron-containing mineral and aquifer material systems, the yield of $^{\bullet}OH$ was inversely correlated with the rate of $H_2O_2$ decomposition. In the aquifer material systems, the yield also inversely correlated with the Mn content, consistent with the fact that the decomposition of $H_2O_2$ on manganese oxides does not produce $^{\bullet}OH$. The inverse correlation between Mn content and $H_2O_2$ loss rate and $^{\bullet}OH$ yield suggests that the amount of Mn in aquifer materials could serve as a proxy for predicting $H_2O_2$ decomposition rates and contaminant oxidation efficiency.

In addition to the surface and structure properties of iron solids, the presence of solutes, such as dissolved silica, also affected the decomposition of $H_2O_2$ (Chapter 4). The adsorption of dissolved silica onto mineral surfaces altered the catalytic sites, thereby decreasing the reactivity of iron- and manganese-containing minerals with $H_2O_2$. Therefore, the presence of dissolved $SiO_2$ could lead to greater persistence of $H_2O_2$ in groundwater, which should be considered in the design of *in situ* $H_2O_2$-based treatment systems. In addition to *in situ* treatment, dissolved silica also can affect the reactivity of iron-containing catalysts used in *ex situ* processes. Therefore, its presence in contaminated industrial wastewater should be considered when *ex situ* treatment systems are designed.

*This dissertation is dedicated to my Mother, who always encourages me to become a scientist.*

# Table of Contents

# Acknowledgments

First and foremost, I would like to express my utmost gratitude to my supervisors, David Sedlak and Fiona Doyle, for all the help, advice and supports they provided me. Working with David and Fiona was altogether challenging and fun. Their abilities to balance between guidance and instruction, demands and expectations, critiques and encouragements have emboldened me to find my own scholarly path. The freedom and flexibility, together with the guidance they provided me help stimulate my passion to research and my desire to become an academic. I am particularly thankful to David for instilling in me the love of environmental chemistry, and Fiona for showing me the wonder of the world of materials science. Outside research, I also have learned from them about the importance of collegiality, intellectual exchange and scholarly commitment. Above all, I am in debt to David and Fiona for sharing with me their life experience, and for their unbounded supports through the entire process.

I am grateful to Changha Lee, who was a former postdoctoral research of the Sedlak Lab, and who is my mentor and close friend. His help during my first days in the laboratory was the cornerstone to my overall wonderful experience in the graduate school. I really appreciate the support that Changha has provided me, and look forward to a lifetime friendship and collegiality with him.

I would like to thank James Hunt and Ronald Gronsky for reviewing my dissertation and for serving on my Qualifying Exam committee. Their insightful comments and suggestions are greatly appreciated. I would also like to thank Thomas Devine for serving on my Qualifying Exam committee, and Garrison Sposito and Kara Nelson for serving on my Preliminary Exam committee.

I have the fortune to interact with all of the current and former members of the Sedlak Lab, including Changha Lee, Patrick Ulrich, Christy Keenan Remucal, Erika Houtz, Scott Mansell, Eva Agus, Justin Jasper, Amanda Ackerman, Ekrem Karpuzcu, Janel Grebel, Haizhou Liu, Joonseon Jeong, Jorge Loyo-Rosales, Urs Jans, and Antoine Ghauch. Their supports and friendship have made my time in the lab altogether fun. Other members of O'Brien Hall, including Ariel Grostern, Paul Koster van Groos, Mi Tra Nguyen, Xinwei Mao, Weiqin Zhuang and Shan Yi, have also made O'Brien Hall a fun and friendly place to work.

I am grateful to my friends around Bay Area, including Khuyen and Trung, anh Dinh, the family of anh Tuan and chi Giang, and the family of Phuong and Xo. They welcomed me when I first came to Bay Area, and their love and friendship through years make Bay Area my true home. Though they all will be missed a lot, I am sure that our paths will cross again. I am looking forward to meeting them in the future.

My late grandfather, Ong Ngoai, has been my true role model. I still remember inspiring conversations I had with him about philosophy, physics, and education. His life and work ethics,

and love of science have encouraged me and other family members to pursue career in science and education, and to be good members of society.

I am in debt to my parents for their boundless love, and for encouraging me to follow their footstep and become a chemist. Their vision, advice and supports help navigate me to the right path, and to find a career that I love. I am also grateful to my brother, Nhim, for being a great friend, and for taking care of my parents while I am away.

The completion of this dissertation would not have been possible without the support of my wife, Trang. Though being busy with her own Ph.D. research at Duke University, she has been patiently listening to me talking about environmental science and water treatment, the stuffs that have no relation to her own work. She has provided me with critiques and suggestions, and has helped me edit many of my manuscripts, job applications, and this dissertation. Above all, I am in debt to her unconditional love and support. I know that it has been very difficult to be apart, and I am grateful to her for staying strong through all those years. I am looking forward to sharing with her our journey ahead.

# Chapter 1. Introduction

## 1.1 Motivation

Redox-active metals and ultraviolet light can convert hydrogen peroxide ($H_2O_2$) into hydroxyl radical ($^{\bullet}OH$), a powerful oxidant capable of oxidizing many organic compounds in water (*e.g.*, benzene, phenol, trichloroethylene, polycyclic aromatic hydrocarbons) [1-3]. The conversion of $H_2O_2$ into $^{\bullet}OH$ (*i.e.*, the activation of $H_2O_2$) has been widely exploited in advanced oxidation processes (AOPs) for water treatment. However, UV light is expensive and the application of dissolved iron requires acidification and produces a large amount of precipitate waste. Therefore, the development of alternative approaches of converting $H_2O_2$ into $^{\bullet}OH$ is important to reducing water treatment costs and improving water quality.

Recently, iron-containing minerals, including iron oxides, iron-containing clays and sands have been demonstrated to catalyze the conversion of $H_2O_2$ into $^{\bullet}OH$ [4-6]. Several researchers have proposed their use in both *ex situ* and *in situ* water treatment technologies. Iron-containing minerals are attractive for *ex situ* treatment because they are inexpensive, readily available, and have the potential to activate $H_2O_2$ under a wide range of conditions [3, 7]. The ability of iron-containing clays and sands in the subsurface to activate $H_2O_2$ serves as the basis for *in situ* chemical oxidation, a practice in which $H_2O_2$ is injected into the subsurface to remediate contaminated groundwater and soils. This $H_2O_2$-based *in situ* remediation technology is potentially a better choice than the traditional energy-intensive, ineffective pump-and-treat remediation technologies [8, 9]. Despite these advantages, the employment of iron-containing solids in water treatment systems is often limited by the extremely low $^{\bullet}OH$ yield, because under environmentally relevant pH conditions (*i.e.*, circumneutral pH values ranging from 6 to 9), most $H_2O_2$ is decomposed into $O_2$ and $H_2O$ without producing $^{\bullet}OH$ [7, 9, 10]. Therefore, the development of approaches for improving $^{\bullet}OH$ production is critical to making the use of $H_2O_2$-based oxidation technologies more cost-effective.

The incorporation of silica and alumina into the structure of iron-containing solids increases the rate at which $H_2O_2$ is converted into $^{\bullet}OH$ under *acidic* conditions [11-14]. Therefore, synthetic silica- and alumina-containing iron catalysts have the potential to be more effective than pure iron oxides in activating $H_2O_2$. To date, however, the synthesis of such catalysts has occurred mainly through a process of trial-and-error because the exact mechanism through which silica and alumina affect the reactivity of iron is not well understood. Increased knowledge on the role of alumina and silica on $H_2O_2$ activation is needed to develop more efficient catalysts for *ex situ* treatment. In addition, the effect of silica and alumina on iron-catalyzed $H_2O_2$ activation at *circumneutral* pH also needs to be investigated. As silica and alumina are common components of natural soils and sediments, and circumneutral pH is typical of groundwater, this understanding may also provide a basis for understanding and optimizing *in situ* treatment systems.

In addition to being controlled by the surface and structure properties of iron solids, the decomposition of $H_2O_2$ is also affected by the presence of solutes that change the surface reactivity by interacting with iron (*e.g.*, phosphate, bicarbonate, and dissolved silica). While phosphate and bicarbonate are known to decrease the reactivity of many iron minerals with $H_2O_2$ [6, 15, 16], the effect of dissolved silica on iron reactivity with $H_2O_2$ has not been explored.

Dissolved silica, omnipresent in the environment due to dissolution of silica-containing minerals, is known to alter iron reactivity in many natural and engineered processes [17-19]. In this dissertation, it is hypothesized that dissolved silica also alters the reactivity of iron-containing solids with $H_2O_2$. An understanding of the role of dissolved silica on the activation of $H_2O_2$ is important for predicting and optimizing the performance of *ex situ* and *in situ* treatment systems.

## 1.2 Use of hydrogen peroxide for *ex situ* water treatment

Hydrogen peroxide ($H_2O_2$) is used in advanced oxidation processes (AOPs) to oxidize organic contaminants and pathogens in wastewater and drinking water. Although $H_2O_2$ does not react directly with organic molecules at appreciable rates, it can be converted into hydroxyl radical ($^{\bullet}OH$) by UV light (reaction 1.1) [2]:

$$H_2O_2 + \text{UV light} \rightarrow 2\ {}^{\bullet}OH \qquad (1.1)$$

The $^{\bullet}OH$ produced in reaction 1.1 reacts with most organic compounds at near diffusion-controlled rates [20]. Many of the products of these reactions are more susceptible to microbial oxidation than the parent compounds.

Under the conditions used in advanced oxidation processes, the activation of $H_2O_2$ by UV light is a relatively inefficient way of generating $^{\bullet}OH$, because UV lamps are expensive and consume a considerable amount of energy. In addition, the efficiency of the process decreases in waters with high concentrations of suspended solids and organic compounds, because these components compete with $H_2O_2$ for absorption of UV light. Therefore, UV/$H_2O_2$-based AOPs have mainly been employed to treat dilute hazardous wastes and drinking water [2].

Hydrogen peroxide can also be converted into $^{\bullet}OH$ by dissolved iron. The mixture of Fe(II) and $H_2O_2$, also known as Fenton's reagent [21], can generate $^{\bullet}OH$ via the following reaction [22]:

$$Fe^{2+} + H_2O_2 \rightarrow Fe^{3+} + {}^{\bullet}OH + OH^- \qquad (1.2)$$

In the presence of excess $H_2O_2$, the $Fe^{3+}$ produced in reaction 1.2 can be reduced by $H_2O_2$ to regenerate $Fe^{2+}$:

$$Fe^{3+} + H_2O_2 \rightarrow Fe^{2+} + HO_2^{\bullet} + OH^- \qquad (1.3)$$

Therefore, the $H_2O_2$ activation can be initiated by either dissolved iron(II) or iron(III) ions, and the cycling between $Fe^{2+}$ and $Fe^{3+}$ will continuously catalyze the conversion of $H_2O_2$ into $^{\bullet}OH$.

The use of Fenton's reagent as an AOP offers several advantages over UV/$H_2O_2$. First, the production of $^{\bullet}OH$ by the Fenton reaction does not require additional energy input and

expensive UV lamps [7]. In addition, high concentrations of suspended solids and dissolved organic carbon does not cause a deleterious effect on the rate of $^{\bullet}OH$ productions. As a result, Fenton's reagent is attractive for treating water that contains relatively high concentrations of organic compounds, such as wastewater from dye and pulp bleaching processes, landfill leachates, agricultural and food processing wastes, and other industrial wastewaters [7]. However, the major drawback of the Fenton reaction is that it is most effective under acidic conditions [23]. Therefore, wastewater effluents have to be acidified prior to the treatment and neutralized prior to discharge [7]. Furthermore, due to the low solubility of Fe(III) species produced in reaction 1.2, the Fenton reaction often generates large amounts of iron precipitates that requires disposal. The need to remove iron-containing solid wastes and complicated pH adjustment steps not only increases the treatment cost but also prevents the application of this method for *in situ* treatment of groundwater and soil, where pH adjustment can be impractical or destructive.

Although initially considered as wastes in Fenton reaction, it was later observed that iron precipitates could also activate $H_2O_2$ into $^{\bullet}OH$ [6, 24]. As a result, the reaction between iron-containing solids and $H_2O_2$, also known as the heterogeneous Fenton reaction, has been proposed as an alternative for the Fenton reaction [4, 5]. The advantage of this approach is that the iron-containing solids can be separated and reused. Furthermore, iron-containing solids could be used over a wider pH range [4, 24]. Numerous studies over the past two decades, however, have indicated that the $H_2O_2$ activation by iron minerals (*e.g.*, ferrihydrite, goethite, iron-containing minerals and clays) is relatively slow and inefficient, especially under circumneutral pH solutions [6, 25-29]. Although a consensus explanation does not exist, the low efficiency has been attributed to the scavenging of $^{\bullet}OH$ by iron oxides [6]. An alternative explanation for the low efficiency of $H_2O_2$ conversion into $^{\bullet}OH$ involves a series of competing reactions in which $H_2O_2$ is converted into $H_2O$ and $O_2$ on the surface without $^{\bullet}OH$ production (these non-radical reactions are represented collectively by reaction 1.4) [30, 31]. Irrespective of the explanation, the absence of iron-containing catalysts that can effectively convert $H_2O_2$ into $^{\bullet}OH$ at circumneutral pH currently limits the use of heterogeneous Fenton process in water treatment.

$$2\ H_2O_2 \rightarrow 2\ H_2O + O_2 \qquad (1.4)$$

## 1.3 Use of hydrogen peroxide for *in situ* treatment of groundwater and soil

*In situ* remediation technologies for the cleanup of contaminated groundwater and soils became popular in the late 1980s [8]. These technologies involve the injection of chemicals into the subsurface to stimulate the growth of microorganisms (*i.e.*, *in situ* bioremediation) or to initiate chemical reactions (*i.e.*, *in situ* chemical remediation) that can lead to the transformation of toxic contaminants. Compared with the pump-and-treat treatment methods (*i.e.*, *ex situ* remediation), *in situ* remediation is usually less expensive, faster and more effective [8].

Hydrogen peroxide was first employed in *in situ* bioremediation as an oxygen ($O_2$) source for subsurface aerobic microorganisms [32-34]. In this practice, dilute $H_2O_2$ solutions are injected into groundwater or added to soils. Upon contacting metal oxides (*e.g.*, iron and manganese oxides) and enzymes (*e.g.*, catalase), $H_2O_2$ is converted into $H_2O$ and $O_2$, thereby supplying $O_2$ to areas where the biological degradation of contaminants is limited by the availability of $O_2$ [35]. The injection of $H_2O_2$, together with nutrients, accelerates the biological transformation of many hydrocarbons and petroleum products, such as benzene, toluene, ethyl benzene, xylene, and polychlorinated phenols [36].

In the early 1990s, several researchers demonstrated that the addition of $H_2O_2$ to soils and sediments also could initiate the transformation of contaminants via abiotic pathways. For example, Ravikuma and Gurol reported the transformation of pentachlorophenol and trichloroethylene in sterilized sand upon the addition of $H_2O_2$ [4]. Miller and Valentine also observed the transformation of quinoline and phenol during the decomposition of $H_2O_2$ in the presence of sand [5, 37]. The transformation of organic compounds was attributable to the conversion of $H_2O_2$ into $^{\bullet}OH$, because the organic compounds did not react directly with $H_2O_2$ and the transformation reactions were inhibited by the presence of high concentration of an $^{\bullet}OH$ scavenger (*i.e.*, tert-butanol) [37].

Since these first observations of abiotic contaminant transformation, the use of $H_2O_2$ has evolved from being an $O_2$ source for *in situ* bioremediation into a reagent for *in situ* chemical oxidation (ISCO). A recent survey indicated that $H_2O_2$ and potassium permanganate ($KMnO_4$) are the most frequently used oxidants in ISCO remediation [38]. The popularity of $H_2O_2$ appears to be related to several factors. First, $^{\bullet}OH$ is a powerful oxidant that provides a means of oxidizing contaminants that cannot be transformed readily by microorganisms or weaker oxidants (*e.g.*, $KMnO_4$) [10]. Second, compared with other oxidants used in ISCO technologies (*i.e.*, permanganate, ozone and persulfate), $H_2O_2$ is relatively inexpensive, easy to transport and introduce into the subsurface, and the byproducts of its decomposition, namely $O_2$ and $H_2O$, are benign [9]. Third, the conversion of $H_2O_2$ into $^{\bullet}OH$ is relatively fast, allowing the remediation of contaminated soil and groundwater by $H_2O_2$-based *in situ* chemical oxidation to be completed in days to months [9].

Despite the advantages mentioned above, $H_2O_2$-based ISCO is not an ideal solution for remediating contaminated groundwater and soils. In fact, studies conducted at contaminated sites where $H_2O_2$-based ISCO has been applied indicate that contaminants' removal was sometimes not achieved [39, 40]. This failure might, at least partially, be due to the rapid $H_2O_2$ decomposition [37, 41, 42]. Rapid $H_2O_2$ decomposition upon injection is often problematic because $H_2O_2$ may be consumed before it reaches contaminated areas. In addition, since $H_2O_2$ decomposition is an exothermic reaction, the oxygen evolution and temperature increase that occur when $H_2O_2$ reacts with surfaces can cause problems, such as melting of plastic pipelines, stripping of volatile organic compounds, and reduction of aquifer permeability (due to the formation of oxygen bubbles) [9, 10, 39, 40]. Although various remedies have been proposed to slow the rate of $H_2O_2$ decomposition (*e.g.*, by addition of an $H_2O_2$ stabilizer such as phosphate, phytate, and citrate [16, 42]), these approaches are either expensive or could create other problems (*e.g.*, phosphate could stimulate bacterial growth in the subsurface).

The extremely low yield of $^{\bullet}OH$ during the decomposition of $H_2O_2$ in the subsurface is another major drawback of $H_2O_2$-based ISCO. For example, Miller and Valentine reported that the loss of 24 mM of $H_2O_2$ on an aquifer materials resulted in the transformation of only 0.02 mM of quinoline [5]. This result indicates that over 99% of the added $H_2O_2$ underwent reactions that did not transform quinoline. As a result, a large excess of $H_2O_2$ would be needed in ISCO remediation. The authors postulated that the low $H_2O_2$ utilization efficiency was due to the consumption of $^{\bullet}OH$ by surface scavengers rather than by quinoline. However, it is also possible that most of the $H_2O_2$ was decomposed via pathways that did not produce $^{\bullet}OH$ (*i.e.*, reaction 1.4) [30, 31]. In addition, the low $^{\bullet}OH$ yield also may have been associated with aquifer materials containing high concentration of manganese oxides, because manganese oxides are known to rapidly decompose $H_2O_2$ without producing $^{\bullet}OH$ [35, 43, 44].

In spite of these limitations, $H_2O_2$ is still being used widely in ISCO. Therefore, a better understanding of factors controlling $H_2O_2$ decomposition and $^{\bullet}OH$ production would be critical for the optimization of current $H_2O_2$-based ISCO systems and for the design of novel systems.

## 1.4 Activation of hydrogen peroxide by iron-containing solids

As mentioned above, the ability of iron-containing solids to convert $H_2O_2$ into $^{\bullet}OH$ has important implications for *ex situ* and *in situ* treatment of contaminated waters and soils. Therefore, understanding of the fundamental mechanism of $H_2O_2$ decomposition and $^{\bullet}OH$ generation in this process may lead to the development of better catalysts for AOPs and optimization of $H_2O_2$-based ISCO systems.

### 1.4.1 Decomposition of hydrogen peroxide in the presence of iron oxides

Most mechanistic insights into the decomposition of $H_2O_2$ on iron-containing surfaces have been obtained by studying pure iron(III) oxide/$H_2O_2$ systems. Under acidic conditions, the decomposition of $H_2O_2$ in these systems appears to be catalyzed by both iron on the surface and dissolved iron, with the latter resulting from the dissolution of iron oxides [30, 45]. At circumneutral pH values, the contribution of dissolved iron to $H_2O_2$ decomposition is expected to be negligible because Fe(III) is sparingly soluble [46]. Therefore, the decomposition of $H_2O_2$ under circumneutral pH conditions is likely a surface-catalyzed process.

The process through which $H_2O_2$ is decomposed on the surface of iron oxides appears to be catalyzed by the redox cycling between surface iron(II) and iron(III) (*i.e.*, ≡Fe(II) and ≡Fe(III), reaction 1.5 and 1.6) via the reactions that are analogous to those in the homogeneous Fenton system (*i.e.*, reaction 1.2 and 1.3) [24, 30, 31]:

$$\equiv Fe(III) + H_2O_2 \rightarrow \equiv Fe(II) + HO_2^{\bullet} + H^+ \quad (1.5)$$

$$\equiv Fe(II) + H_2O_2 \rightarrow \equiv Fe(III) + {}^{\bullet}OH + OH^- \quad (1.6)$$

Some investigators have postulated that, as in the homogeneous Fenton system, reaction (1.5) actually consists of a series of reactions, beginning with the formation of a complex between the surface and $H_2O_2$ [24, 47]:

$$\equiv Fe(III) + H_2O_2 \Leftrightarrow \equiv Fe(III)(H_2O_2)_{(s)} \quad (1.7)$$

$$\equiv Fe(III)(H_2O_2)_{(s)} \rightarrow \equiv Fe(II)(HO_2^{\bullet})_{(s)} + H^+ \quad (1.8)$$

$$\equiv Fe(II)(HO_2^{\bullet})_{(s)} \rightarrow \equiv Fe(II) + HO_2^{\bullet} \quad (1.9)$$

Therefore, the decomposition of $H_2O_2$ in this system is also controlled by the affinity of $H_2O_2$ for iron oxide surfaces, the availability of surface sites for $H_2O_2$ adsorption, and the rate at which ≡Fe(III) is reduced.

Regarding the rate of $H_2O_2$ decomposition, in the heterogeneous Fenton system the reduction of ≡Fe(III) to ≡Fe(II) (reaction 1.5 or reactions 1.7 – 1.9) is considered as the rate-limiting step in the heterogeneous Fenton system because the rate of $H_2O_2$ loss exhibited a first order dependence on both the surface of iron(III) oxides and $H_2O_2$ under a wide range of pH and $H_2O_2$ concentration [24]:

$$\frac{d[H_2O_2]}{dt} = - k \times [\text{surface of iron(III) oxide}] \times [H_2O_2] \quad (1.10)$$

In the above expression, the value of k depends on experimental conditions and the properties of the iron oxide. For example, Chou and Huang [48] observed that the rate of $H_2O_2$ decomposition in the presence of lepidocrocite (*i.e.*, γ-FeOOH) increased as the pH increased from 2.8 to 7.5. This observation was attributed to the change in iron surface speciation with varying pH (reaction 1.11 and 1.12), which alters the binding strength with $H_2O_2$.

$$\equiv Fe(III)OH_2^+ \Leftrightarrow \equiv Fe(III)OH + H^+ \qquad pK_{a1,\ lepidocrocite} = 5.3\ [48] \quad (1.11)$$

$$\equiv Fe(III)OH \Leftrightarrow \equiv Fe(III)O^- + H^+ \qquad pK_{a2,\ lepidocrocite} = 8.8\ [48] \quad (1.12)$$

Another important factor is the crystallinity of the iron oxides. Valentine and Wang [6] measured the rate of $H_2O_2$ decomposition catalyzed by a poorly crystalline (*i.e.*, ferrihydrite), a semi-crystalline, and a crystalline (*i.e.*, goethite) iron oxide at pH 7.7. The comparison of the surface-area-normalized $k_{obs}$ values showed that ferrihydrite was approximately 2 times more reactive than goethite. Huang *et al*. [26] reported that in a pH 6 – 8 solution, hematite, a material that is more crystalline than goethite and ferrihydrite, was less reactive with $H_2O_2$ than the other two oxides. Contrary to the observations of Valentine and Wang [6] and Huang *et al.* [26], Hermanek *et al.* [49] reported that among iron oxide nanoparticles, amorphous nanoparticles were significantly less reactive than crystalline nanoparticles. The authors postulated that in addition to surface area and crystallinity, particle shape could also play a role in the decomposition of $H_2O_2$.

Inorganic and organic solutes also could affect the rate of $H_2O_2$ decomposition. For example, the presence of phosphate and bicarbonate decreases the rate of $H_2O_2$ decomposition [6, 15]. Organic ligands capable of forming complex with the surface (*e.g.*, oxalate or natural organic matter) also slow the rate of $H_2O_2$ decomposition [6, 42]. This inhibitory effect of certain solutes can be explained by their adsorption onto iron surfaces, which blocks surface reactive sites. For this reason, several researchers have proposed the use of phosphate, citrate, malonate and phytate as a $H_2O_2$ stabilizing agent to enhance the persistence of $H_2O_2$ in *in situ* treatment systems [16, 42].

### 1.4.2 The oxidation of organic contaminants in the iron oxide/hydrogen peroxide systems

The decomposition of $H_2O_2$ on iron oxides generates $^{\bullet}OH$ (reaction 1.6) and $O_2$ (reaction 1.4). While $O_2$ does not oxidize contaminants at appreciable rates, $^{\bullet}OH$ is an extremely reactive species capable of oxidizing a wide range of organic contaminants and reduced inorganic species (*e.g.*, $AsO_3^{3-}$) at near diffusion-controlled rates [20]. The utility of the iron oxide/$H_2O_2$ systems for contaminant oxidation could be evaluated by stoichiometric efficiency ($E = \frac{\Delta[contaminant]}{\Delta[H_2O_2]}$), which is defined as the amount of contaminant transformed per mole of $H_2O_2$ decomposed. The stoichiometric efficiency depends on both $^{\bullet}OH$ yield and the proportion of $^{\bullet}OH$ reacting with the contaminant versus with other solutes (*i.e.*, $^{\bullet}OH$ scavengers).

The yield of $^{\bullet}OH$ in the heterogeneous Fenton systems is affected by several other reactions in addition to the initiation reactions (*i.e.*, reactions 1.5 and 1.6). Specifically, these reactions are those producing reactive oxygen species that can in turn propagate the redox cycling of iron species [24, 30, 50]:

$$HO_2^{\bullet} \Leftrightarrow O_2^{\bullet-} + H^+ \qquad (pK_a = 4.8) \tag{1.13}$$

$$^{\bullet}OH + H_2O_2 \rightarrow O_2^{\bullet-} (HO_2^{\bullet}) + (H^+) + H_2O \tag{1.14}$$

$$\equiv Fe(III) + O_2^{\bullet-}(HO_2^{\bullet}) \rightarrow \equiv Fe(II) + O_2 + (H^+) \tag{1.15}$$

$$\equiv Fe(II) + O_2^{\bullet-}(HO_2^{\bullet}) \rightarrow \equiv Fe(III) + O_2^{2-} (HO_2^-) \tag{1.16}$$

$$\equiv Fe(II) + {}^{\bullet}OH \rightarrow \equiv Fe(III) + OH^- \tag{1.17}$$

Among these reactions, reactions 1.16 and 1.17 are usually unimportant, because oxidation of ≡Fe(II) by $H_2O_2$ (*i.e.*, reaction 1.6) is faster at high concentration of $H_2O_2$ [24].

If reaction 1.14 contributes significantly to the production of $HO_2^{\bullet}$ in the heterogeneous Fenton system, the decomposition of $H_2O_2$ will proceed via a chain reaction formed by reaction 1.6, 1.14 and 1.15 (scheme 1) [30]. When this chain reaction is sufficiently long, the yield of $^{\bullet}OH$ (η) will approach 0.5 [30]. In contrast, when reaction 1.14 is unimportant, the decomposition of $H_2O_2$ will proceed via a non-chain pathway (scheme 2), and η would be 0.67 [51].

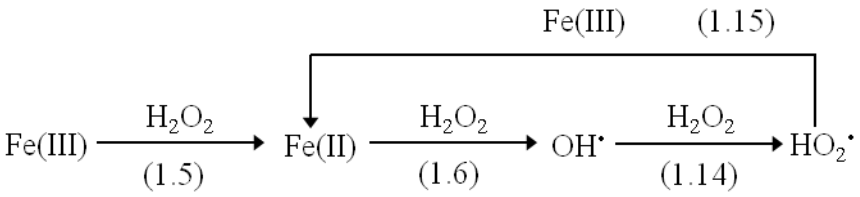


Scheme 1. Decomposition of $H_2O_2$ via the chain process initiated by reaction 1.5.

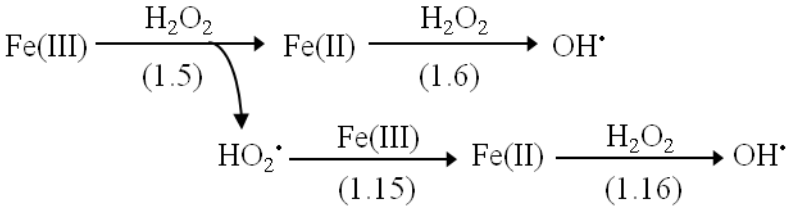


Scheme 2. Decomposition of $H_2O_2$ via the non-chain process.

The decomposition of $H_2O_2$ in the homogeneous Fenton system proceeds mainly via the chain reaction (Scheme 1) [47, 50]. In contrast, there is plenty of evidence showing that $H_2O_2$ decomposition in the iron oxide systems proceeds mainly via the non-chain reaction (Scheme 2). For example, Lin and Gurol successfully described the rate of $H_2O_2$ loss in the presence of goethite without including reaction 1.14 in their kinetics model [24]. Kwan and Voelker reported that the presence of an $^{\bullet}OH$ scavenger did not change the rate of $H_2O_2$ loss catalyzed by ferrihydrite to an appreciable extent [30]. These observations suggest that reaction 1.14 was unimportant and, therefore, the process was not controlled by the chain process. However, it is unclear if the chain process is also unimportant in systems that are catalyzed by other iron minerals and catalysts. Regardless which mechanism dominates, the yield of $^{\bullet}OH$ in the heterogeneous Fenton system is expected to be between 0.5 and 0.67.

The $^{\bullet}OH$ produced in the heterogeneous Fenton system reacts quickly with not only contaminants, but also with $H_2O_2$ (reaction 1.14), and other competing solutes, such as natural organic matter, bicarbonate, and chloride. Therefore, the fraction of $^{\bullet}OH$ available for contaminant oxidations depends on the concentration of these solutes, as well as the rate at which they react with $^{\bullet}OH$. (Some important $^{\bullet}OH$ sinks, their reaction rate constants with $^{\bullet}OH$ (k), and their typical concentration in contaminated groundwater are presented in Table 1-1). The fraction of $^{\bullet}OH$ that reacts with the contaminant can be calculated as follow:

$$F = \frac{the\ amount\ of\ OH^{\bullet}\ reacted\ with\ the\ contaminant}{total\ amount\ of\ OH^{\bullet}\ reacted\ with\ all\ solutes} = \frac{k_{cont}[contaminant]}{k_{cont}[contaminant] + k_{H_2O_2}[H_2O_2] + k_{HCO_3^-}[HCO_3^-] + \dots}$$

If the presence of the contaminant and other $^{\bullet}OH$ scavengers have a minimal impact on the yield of $^{\bullet}OH$ (*i.e.*, η), the stoichiometric efficiency E can be estimated by multiplying η by F:

$$E = \frac{\Delta[contaminant]}{\Delta[H_2O_2]} \times 100\% = \frac{k_{cont}[contaminant]}{k_{cont}[contaminant] + k_{H_2O_2}[H_2O_2] + k_{HCO_3^-}[HCO_3^-] + \ldots} \times \eta \times 100\% \quad (1.18)$$

Under conditions typically employed in studying of iron oxide/$H_2O_2$ systems (*i.e.*, ca. 100 mM of $H_2O_2$ and 0.1 to 1 mM of organic contaminant and negligible amount of other $^{\bullet}OH$ scavengers), the major $^{\bullet}OH$ sinks are $H_2O_2$ and the organic contaminant. Therefore, equation (1.18) can be simplified to:

$$E = \frac{k_{cont}[contaminant]}{k_{cont}[contaminant] + k_{H_2O_2}[H_2O_2]} \times \eta \times 100\% \quad (1.19)$$

Despite the large number of previous studies on iron oxide/$H_2O_2$ systems, few attempts have been made to measure E (Table 1-2). These studies provide two important insights. First, as with the rate of $H_2O_2$ decomposition, the stoichiometric efficiency depends on the crystallinity of iron oxide [6, 26]. For example, despite being less reactive with $H_2O_2$ than semi-crystalline iron oxide and ferrihydrite, goethite was the most effective catalyst for quinoline oxidation (*i.e.*, it exhibits the highest stoichiometric efficiency) [6]. Second, the measured stoichiometric efficiency is always much lower than the theoretical maximum (see footnote of Table 1-2). At circumneutral pH, E ranged from 0.001 to 1%, which is 1 to 4 orders of magnitude lower than the value calculated using equation 1.19 (footnote of Table 1-2). The stoichiometric efficiency appeared to be higher under acidic conditions but was still much lower than the maximum value.

Several explanations for the low stoichiometric efficiency in iron oxide/$H_2O_2$ systems have been proposed. Miller and Valentine postulated that most $^{\bullet}OH$ was scavenged by the surface of iron oxide (*i.e.*, reaction 1.17) because the stoichiometric efficiency in their study decreased at higher iron oxide concentrations [5]. However, a significant amount of ≡Fe(II) would have to be present on the surface before reaction 1.18 could outcompete other ≡Fe(II) sinks, such as the oxidation of ≡Fe(II) by $H_2O_2$ (reaction 1.6). Lin and Gurol suggested that most $^{\bullet}OH$ would only react with solutes on or near the surface because it is too reactive to diffuse into the solution, implying that the stoichiometric efficiency would be lower for contaminants with low surface affinity (*e.g.*, contaminants that are repulsed by the surface due to electrostatic interactions) [24]. However, this explanation is inconsistent with the low stoichiometric efficiency in systems with uncharged compounds that are not repelled by surfaces, such as quinoline and chlorophenol.

**Table 1-1.** Important hydroxyl radical sinks, their typical concentration in wastewater and groundwater, and their reaction rate constants with the hydroxyl radical.

| Solute | Typical concentration | Reaction with $^{\bullet}OH$ | Rate constant |
|---|---|---|---|
| Organic contaminants | $10^{-6} – 10^{-3}$ M | React with $^{\bullet}OH$ via 3 mechanisms: hydroxyl addition, hydrogen abstraction, and electron abstraction. | $k = 10^{9} – 10^{10}$ $M^{-1}s^{-1}$ [20] |
| $H_2O_2$ | $10^{-3} – 10^{0}$ M | $^{\bullet}OH + H_2O_2 \rightarrow O_2^{\bullet-} + H^{+} + H_2O$ | $k = 3.3 \times 10^{7}$ $M^{-1}s^{-1}$ [52] |
| $HCO_3^{-}$ | $10^{-3} – 10^{-2}$ M | $^{\bullet}OH + HCO_3^{-} \rightarrow OH^{-} + HCO_3^{\bullet}$ | $k = 8.5 \times 10^{6}$ $M^{-1}s^{-1}$ [20] |
| $Cl^{-}$ | $10^{-5} – 10^{-3}$ M | $^{\bullet}OH + Cl^{-} \Leftrightarrow ClOH^{\bullet-}$ | $k_{forward} = 4.3 \times 10^{9}$ $M^{-1}s^{-1}$ [20]<br>$k_{reverse} = 6.1 \times 10^{9}$ $M^{-1}s^{-1}$ [53] |
| Natural organic matter | 0.1 – 10 mg/L | reacts with $^{\bullet}OH$ via mechanisms similar to those of organic contaminants | $k = 2.5 \times 10^{4}$ $(mgC/L)^{-1}s^{-1}$ [54] |

**Table 1-2.** Experimental conditions and reported stoichiometric efficiency in the iron oxide/$H_2O_2$ systems.

| Solid type and organic compound | Experimental conditions | Stoichiometric efficiency [a] | Reference |
|---|---|---|---|
| Ferrihydrite, semi-crystalline iron oxide, goethite<br><br>Quinoline | pH = 7<br>[quinoline] = 10 mg/L<br>[oxide] = 0.5 – 12.5 g/L<br>[$H_2O_2$] = 500 mg/L | $E_{maximum}$ = 0.18% | Valentine and Wang [6] |
| Ferrihydrite, goethite, hematite<br><br>2-chlorophenol | pH = 4.36 – 8.45<br>[2-chlorphenol] = 15 mg/L<br>[iron oxide] = 1 g/L<br>[$H_2O_2$] = 9.8 mM | E = 0.02 – 2% | Huang *et al.* [26] |
| Crushed goethite ore<br><br>R-(4-pyridyl-1-oxide)N-tertbutylnitrone (4-POBN) | pH = 5.8<br>[4-POBN] = 0.7 – 1.44 mM<br>[crushed goethite] = 50 g/L<br>[$H_2O_2$] = 150 mM | E = 1% | Huling *et al.* [51] |
| Goethite (in a mixture with sand)<br><br>Polycyclic aromatic hydrocarbons (PAH): phenanthrene, anthracene, pyrene | pH = 7<br>[PAHs] = 25 mg/kg of sand<br>[goethite] = 16.8 – 134 g/kg of sand<br>[$H_2O_2$] = 5 M | E ≈ $5\times10^{-4}$ – $10^{-3}$% | Kanel *et al.* [25] |
| Lepidocrocite (γ-FeOOH)<br><br>Benzoic acid (BA) | pH = 4.2, 5.4 and 6.8<br>[BA] = 1.44 – 1.86 mM<br>[γ-FeOOH] = 167 g/L<br>[$H_2O_2$] = 0 – 20 mM | E ≈ 1% (pH 6.8), 3% (pH 5.4) and 10-30% (pH 4.2)[b]. | Chou *et al.* [55] |
| Magnetite<br><br>Rhodamine B [RhB] | pH 7<br>[RhB] = 5 mg/L<br>[magnetite] = 1 -20 g/L<br>[$H_2O_2$] = 150 mM | E = 0.2 – 1.4% | Xue *et al.* [29] |

[a] The measured stoichiometric efficiency values are one to four orders of magnitude lower than the theoretical value calculated using equation 1.19. For example, the initial theoretical stoichiometric efficiency in the study of Huang *et al.* [26] would be:

$$E = \frac{k_{chlorophenol}[chlorophenol]}{k_{chlorophenol}[chlorophenol] + k_{H_2O_2}[H_2O_2]} \times \eta \times 100\%$$

$$= \frac{7\times10^9 \times(\frac{15}{128.5}) \times10^{-3}}{7\times10^9 \times(\frac{15}{128.5})^{-3} + 3.3\times10^7 \times 9.8 \times10^{-3}} \times 0.67 \times 100\% = 48\%$$

**[b]** There was a significant contribution from dissolved iron to the activation of $H_2O_2$ in acidic pH solutions.

### 1.4.3 The decomposition of $H_2O_2$ via non-radical mechanisms

An alternative explanation for the lower-than-expected stoichiometric efficiency invokes the ability of iron oxides to catalyze the decomposition of $H_2O_2$ into $O_2$ and $H_2O$ via mechanisms that do not produce $^{\bullet}OH$ (*i.e.*, reaction 1.4) [30, 31]. For such non-radical mechanisms to be operative, the decomposition of $H_2O_2$ on iron oxide surfaces must take place via 2-electron transfer processes. Because the ≡Fe(III)/≡Fe(II) cycling is a one-electron transfer process, this means that 2 reactive sites must participate simultaneously in this process. However, it is unclear if such a mechanism is plausible.

Alternatively, the occurrence of a 2-electron transfer process could be explained by the production of a higher-valent iron species, possibly ferryl (*i.e.*, ≡Fe[IV]). In this scenario, the decomposition of $H_2O_2$ might be initiated by the one electron reduction of ≡Fe(III) (reaction 1.5), followed by the cycling of ≡Fe(II) and ≡Fe(IV) species:

$$\equiv Fe(II) + H_2O_2 \rightarrow \equiv Fe(IV) + 2OH^- \quad (1.20)$$

$$\equiv Fe(IV) + H_2O_2 \rightarrow \equiv Fe(II) + O_2 + 2H^+ \quad (1.21)$$

The production of Fe(IV) species instead of $^{\bullet}OH$ is noteworthy because Fe(IV) is less reactive than $^{\bullet}OH$ and does not react with aromatic compounds to an appreciable extent [56]. While there is ample evidence for the production of Fe(IV) in the homogeneous Fenton system at neutral pH values [56-58], little is known about the production of surface ferryl species (*i.e.*, ≡Fe[IV]) in heterogeneous Fenton systems. Additional research is needed to address this issue.

### 1.4.4 Iron-containing catalysts for $H_2O_2$ activation

To accelerate the rate of $H_2O_2$ decomposition and increase the yield of $^{\bullet}OH$ in the heterogeneous Fenton system, investigators have put significant effort into developing better iron-containing catalysts. Among various synthesis methods, the immobilization of iron on silica supports appears to be the most promising approach because silica can alter the chemical environment of Fe and enhance the production of $^{\bullet}OH$. For example, Chou *et al.* developed a catalyst consisting of iron oxide on a ground brick support [11]. This composite catalyst was shown to result in more contaminant oxidation per mole of $H_2O_2$ consumed than goethite. In another study, Lim *et al.* immobilized iron oxide nanoparticles on alumina-coated mesoporous silica (*i.e.*, SBA-15), and examined its ability to catalyze the decomposition of $H_2O_2$ and transformation of the reactive dye, RB5, at pH 4.1 [12]. They reported that the material catalyzed RB5 degradation, with a much faster reaction rate than that seen with similar amount of iron oxides (*i.e.*, hematite and magnetite). Although the exact role of alumina and silica was not clear, it was speculated that the dispersion of iron in the silica matrix enhanced the production of $^{\bullet}OH$, while alumina, as a Lewis acid, facilitated the reduction of Fe(III) to Fe(II) by $H_2O_2$ (reaction 1.6), which is the rate limiting step in the heterogeneous Fenton system [12].

In addition to the mesoporous silica SBA-15 [59-61], other mesoporous silica supports, such as MCM-41, HMS, also have been used to prepare iron-containing catalysts [62-64]. The

use of mesoporous silica materials is attractive due to their high surface area, porosity, and unique pore structure, which allows for the synthesis of well-ordered, high surface area catalysts. Several investigators have reported that iron-containing mesoporous silica catalysts activate $H_2O_2$ more quickly than iron oxides under acidic or elevated temperature conditions [12, 62, 63, 65]. However, the ability of these catalysts toward $H_2O_2$ activation under environmentally relevant conditions (*i.e.*, 10 – 30 ºC, *circumneutral* pH values) has been largely unexplored. Additionally, the stability of such catalysts at *circumneutral* pH values might be an issue for long-term usage, since mesoporous silica materials appeared to be relatively unstable at pH values above 5 [66, 67].

In addition to silica-based supports, several researchers have synthesized iron-pillared clays as catalysts for $H_2O_2$ activation [13, 14, 64, 68, 69]. These catalysts are prepared by introducing iron into the interlayer of a 2:1 layered clay (*e.g.*, member of the smectite family) by an exchange process with an iron-containing solution, followed by a heat treatment step to dehydrate iron hydr(oxide) cluster in the interlayer. The iron-pillared clays have been shown to activate $H_2O_2$ more quickly than iron oxides under acidic conditions [13]. Moreover, because the iron that was immobilized on the clays was less susceptible to dissolution and, as a result, the catalyst could be recycled and reused multiple times [14]. However, as with iron-containing mesoporous silica catalysts, the ability of these catalysts to activate $H_2O_2$ at *circumneutral* pH values and the role of the aluminosilicates support on the reactivity of iron is not well understood.

Zeolites also have been used as supports for synthesizing iron-containing catalysts [14, 64, 70-75]. Zeolites are aluminosilicates with relatively high porosity and surface area, and are suitable for the synthesis of a high surface area catalyst. The addition of iron by a cation exchange process is a common approach for immobilizing iron onto zeolites. As with iron-pillared clays, iron-containing zeolite catalysts are stable under acidic conditions and could be reused multiple times [70, 75].

### 1.4.5 Activation of hydrogen peroxide by soil sediments and aquifer materials

Investigations of the ability of soil sediments and aquifer materials to activate $H_2O_2$ are crucial to $H_2O_2$-based for *in situ* remediation. Soils and aquifer materials are comprised of iron oxide-coated sands, silts, and clays, and are relatively heterogeneous. Their physico-chemical properties vary greatly among samples and sites. Attributes of the materials that influence rate of $H_2O_2$ decomposition and yield of $^{\bullet}OH$ remain unclear despite significant efforts of researchers to understand them.

The decomposition of $H_2O_2$ and yield of $^{\bullet}OH$ by soils, sediments and aquifer materials are likely controlled by their physico-chemical properties. These materials also often contain manganese oxides and enzymes (*e.g.*, catalase or peroxidase) – components that can decompose $H_2O_2$ via pathways that do not produce $^{\bullet}OH$ [31]. Consistent with this observation, Xu and Thomson suggested that the rate of $H_2O_2$ decomposition is proportional to the Fe and Mn content of the sediments [76]. They also observed that materials that contained more organic matter decomposed $H_2O_2$ more quickly. Petigara *et al.* measured both $H_2O_2$ decomposition rates and

•OH yields in the presence of various soils [31]. Contrary to the observation by Xu and Thomson, Petigara *et al.* observed that samples with less organic carbon reacted more quickly with $H_2O_2$. In addition, they observed that the •OH yield was inversely correlated with the rate of $H_2O_2$ decomposition. They postulated the existence of two competing $H_2O_2$ decomposition pathways: one pathway that exhibits relatively fast $H_2O_2$ decomposition rates but does not produce •OH, and another that is associated with slower reactions but higher •OH yields. Miller and Valentine speculated that the inefficient $H_2O_2$ decomposition in soil sediments is caused by the "reducible" iron and manganese oxides (*i.e.*, oxides removed when the samples were treated with strongly reducing $NH_2OH$-HCl solution), because the stoichiometric efficiency increased by approximately 50% when these "reducible" oxides were removed from the sediments [5].

In the subsurface, the rate at which $H_2O_2$ decomposes and the fraction of the $H_2O_2$ converted into •OH depends upon not only the properties of the aquifer materials but also the solution composition. For example, the presence of phosphate, bicarbonate, or metal complexing ligands, such as citrate or oxalate, enhances the stability of $H_2O_2$ because the ligands can alter the speciation of metals and decrease their reactivity [6, 15, 42]. Dissolved silica is another commonly presented solute in groundwater that can also attach to the surface of iron-containing minerals [77-79]. However, the effect of dissolved silica on the reactivity of iron minerals with $H_2O_2$ has not been investigated.

In summary, the efficacy of $H_2O_2$-based ISCO depends on the persistence of $H_2O_2$ as well as pathways through which it is decomposed, because only those pathways that produce •OH will be beneficial for oxidative contaminant removal. A thorough understanding of how different subsurface components affect the decomposition of with $H_2O_2$ will, therefore, help predict its fate and could lead to improved performance of $H_2O_2$-based ISCO systems.

## 1.5 Dissertation outline

The overall objective of this dissertation is to investigate factors affecting the activation of $H_2O_2$ on various silica- and alumina-containing iron catalysts, minerals, and aquifer materials under *circumneutral* pH conditions. Developing a better understanding of the activation of $H_2O_2$ by these solids could improve the design and operation of *ex situ* and *in situ* $H_2O_2$-based water treatment technologies.

The second chapter of this dissertation investigates the ability of silica-supported iron catalysts to activate $H_2O_2$ under *circumneutral* conditions. Two types of silica- and alumina-containing iron catalysts were synthesized by sol-gel processing techniques. The yields of $^{\bullet}OH$ during $H_2O_2$ decomposition in the presence of these catalysts and other iron oxides were measured and compared. Mechanisms of $H_2O_2$ decomposition at *circumneutral* pH values are proposed and possible roles of silica and alumina in the catalysts are discussed.

The third chapter assesses the activity of various iron oxides, iron-containing clays and sands, as well as real aquifer sediments to activate $H_2O_2$. An experimental design similar to that employed in Chapter 2 was used to assess $H_2O_2$ loss rates and $^{\bullet}OH$ yields in the presence of these solids. The surface properties of the solids were characterized and correlated with the reactivity of the solids with $H_2O_2$ to gain insight into factors affecting $H_2O_2$ activation in *in situ* treatment systems.

The fourth chapter examines the effect of dissolved silica on $H_2O_2$ activation. The rate of $H_2O_2$ decomposition and $^{\bullet}OH$ yield in the presence of various iron and manganese oxides were investigated in solutions containing dissolved silica under environmentally relevant concentrations. Adsorption of dissolved silica on iron oxides was investigated by surface characterization techniques to gain fundamental understandings of how dissolved silica affects $H_2O_2$ activation.

Chapter 5 investigates the use of an iron-containing mesoporous silica catalyst for selective oxidation of organic contaminants to improve the stoichiometric efficiency in *ex situ* treatment systems.

Chapter 6 examines the dissolution of various mesoporous silica supports and the effect of the released silica on the activity of iron-containing mesoporous silica catalyst during $H_2O_2$ activation.

The final chapter presents the key findings of this dissertation and suggests future research directions.

# Chapter 2. A Silica-Supported Iron Oxide Catalyst Capable of Activating Hydrogen Peroxide at Neutral pH Values

Reproduced with permission from Pham, A.L.T; Lee, C.; Doyle, F.M.; D.; Sedlak, D. L. A Silica-Supported Iron Oxide Catalyst Capable of Activating Hydrogen Peroxide at Neutral pH Values. *Environmental Science & Technology* **2009**, *43*, 8930-8935.

## 2.1 Introduction

The activation of hydrogen peroxide ($H_2O_2$) by iron minerals (*e.g.*, hematite, goethite, iron-containing clays and sands) and its application for contaminant oxidation has been intensively studied over the last two decades [4, 6, 7, 10, 37, 47] and the process is being applied for *in situ* contaminant oxidation [10], as well as for wastewater treatment [7]. The reaction offers significant advantages over Fenton's reagent (mixture of $Fe^{2+}$ and $H_2O_2$) because it does not generate iron sludge and is not restricted to acidic conditions. Unfortunately, the process is relatively slow and inefficient at circumneutral pH values because only a small fraction of the $H_2O_2$ is converted into oxidants that are capable of transforming recalcitrant contaminants [6, 26, 80]. As a result, very large amounts of $H_2O_2$ are needed for *in situ* treatment, or the water must be acidified prior *ex situ* treatment [7].

To overcome these limitations, heterogeneous iron-containing catalysts have been synthesized using silica supports to change the chemical environment of iron [11, 12, 65, 81]. For example, Chou *et al.*[11] developed a catalyst consisting of iron oxide on crushed brick. This composite catalyst oxidized more benzoic acid per mole of $H_2O_2$ consumed than goethite. However, the results of this study are difficult to interpret because the test solutions were unbuffered and the pH decreased substantially during the experiments (from initial pH values of 3.2, 6.0 and 10.0 to 3.0, 4.3 and 5.8 respectively), and it is unclear how much of the enhanced efficiency was attributable to acidification of the solutions. In another study, iron oxide nanoparticles immobilized on alumina-coated mesoporous silica exhibited an ability to catalyze the transformation of a dye, Reactive Black 5, by $H_2O_2$ at pH 4.1 with an efficiency that was substantially greater than that of similar amounts of hematite and magnetite [12]. Similar results have been reported for $H_2O_2$ activation by Fe and Al-pillared clay catalysts [13, 82, 83]. However, like the studies discussed above, most experiments were performed either under acidic conditions, at elevated temperatures or in the presence of ultraviolet light.

While it appears that alumina and silica supports improve the performance of heterogeneous iron-containing catalysts, the mechanism through which this occurs is not well understood. Possible explanations for the higher efficiency of iron/silica catalysts include less efficient scavenging of hydroxyl radicals by silica relative to iron oxide surfaces [11] and more oxidant production due to the better dispersion of iron on the surface [12]. In addition, alumina, as a Lewis acid, could facilitate the reduction of Fe(III) to Fe(II) by $H_2O_2$, usually the rate limiting step in the Fenton's reagent chain reaction, and thus accelerate activation of $H_2O_2$ [12].

The objective of this study was to determine how the presence of silica and alumina in an iron-containing catalyst alters $H_2O_2$ activation and contaminant oxidation at neutral pH values. For this purpose, silica- and alumina-containing iron precipitates were prepared, characterized and assessed for catalytic activity relative to iron oxides. Phenol was selected as a model target contaminant because it is not significantly adsorbed on any of the oxides in the catalysts and has a well-characterized reaction with hydroxyl radical. Understanding the role of alumina and silica on $H_2O_2$ activation may lead to the development of more efficient catalysts that could be used for *ex situ* treatment and provide a mean of harnessing the heterogeneous Fenton process using naturally occurring or modified minerals in the subsurface.

## 2.2 Materials and methods

### 2.2.1 Materials

All chemicals were reagent grade and were used without further purification. Phenol and ferric perchlorate were obtained from Aldrich. Ferric nitrate and aluminum chloride were obtained from Fisher. Tetraethyl orthosilicate (TEOS) was obtained from Alfa Aesar. All solutions were prepared using 18 MΩ Milli-Q water from a Millipore system.

Hematite was synthesized by aging freshly made ferrihydrite in a strongly alkaline solution at 90ºC for 48 hours [84]. The identity of hematite was verified by X-ray diffraction. Commercial goethite and amorphous FeOOH were obtained from Fluka and Aldrich, respectively.

### 2.2.2 FeSi-ox and FeAlSi-ox synthesis

Precipitates containing iron, silicon and aluminum were synthesized by a sol-gel process. Specifically, 100 mL of 1 M ethanol, 1 M TEOS and either 0.2 M $Fe(ClO_4)_3.9H_2O$ (*FeSi-ox* synthesis) or 0.2 M $Fe(ClO_4)_3.9H_2O$ and 0.2 M $AlCl_3$ (*FeAlSi-ox* synthesis) aqueous solution were stirred and heated at 80ºC for 2 hours in a 250-mL Pyrex flask. To initiate precipitation, 100 mL of 1.5 M ammonium hydroxide and 50 mL of water were added dropwise simultaneously (over about 15 min). After stirring at 80ºC for 2 hours, the mixture was transferred to a 500-mL beaker and then dried at 110ºC for 24 hours. The resulting particles were then washed with deionized water and separated by centrifugation at 3000g for 5 minutes. The washing step was repeated three times, and the final particles were dried at 110ºC for another 24 hours.

### 2.2.3 Characterization

The surface area of the solids was determined using $N_2$ physisorption in a Micromeretics 2000 system using the 5 point BET (Brunauer–Emmett–Teller) method. X-ray diffraction (XRD) analysis was performed with Cu Kα radiation using a Panalytical 2000 diffractometer. The morphology of *FeSi-ox* and *FeAlSi-ox* was determined using a FEI Tecnai 12 transmission electron microscope (TEM) at 100 kV and a Hitachi S-5000 scanning electron microscope (SEM) at 10 kV. The distribution of elements on the surface was determined using a LEO 439 scanning electron microscope coupled with a Princeton Gamma-Tech energy dispersive X-ray spectrometer (SEM-EDX). The composition of the catalysts was measured by first dissolving particles in a concentrated solution of HCl, then measuring Fe and Al in the liquid phase using atomic absorption spectrophotometry.

### 2.2.4 Oxidation of phenol

All oxidation experiments were carried out at room temperature (20 ± 2ºC) in the dark in 50-mL of reaction solution. All the reactors were open to the atmosphere. The initial

concentration of phenol was 0.5 mM. The initial solution pH was adjusted using 1 M NaOH or 0.5 M $H_2SO_4$. The pH of solutions was buffered with 1 mM piperazine-N,N'-bis(ethanesulfonic acid) (PIPES) for pH 7 or 1 mM borate for pH 8 – 9. Solutions with initial pH values of 5.5 were unbuffered. The pH was measured throughout each experiment, and the average pH value was calculated. The difference between the initial and final pH never exceeded 1.5 units in the experiments with pure iron oxides and 1 unit in the case of *FeSi-ox* and *FeAlSi-ox*.

The reactions were initiated by adding an aliquot of $H_2O_2$ stock solution to a pH-adjusted solution containing phenol and catalyst. In some experiments, 200 mM of *tert*-butanol (t-BuOH) was added as a hydroxyl radical scavenger. Samples were withdrawn at predetermined time intervals, filtered immediately through a 0.22-μm nylon filter and analyzed for phenol and $H_2O_2$. Experiments were carried out at least in triplicate and average values and standard deviations are presented.

### 2.2.5 Analytical methods

Filtered samples were acidified to pH 2 and analyzed for phenol by high-performance liquid chromatography (HPLC) using a Waters Alliance HPLC system equipped with a 4.6 x 150 mm Waters Symmetry C18 5 μm column. A mobile phase consisting of 50% methanol and 50% water (pH 2) was used at a flow rate of 0.8 mL/min. Phenol was detected with UV absorbance detection at 270 nm. Prior to HPLC analysis, an excess amount of methanol (*i.e.*, 50 μL) was added to 1 mL filtered aliquots to quench any additional oxidation reactions involving residual $H_2O_2$. $H_2O_2$ was analyzed spectrophotometrically by the titanium sulfate method [85]. Total dissolved iron was quantified using the 1,10-phenanthroline method after adding hydroxylamine hydrochloride to the filtered samples [86].

## 2.3 Results

### 2.3.1 Catalyst properties

SEM and TEM images, along with XRD spectra of *FeAlSi-ox* (Figure 2-1) and *FeSi-ox* (Figure 2-2) show that these materials are amorphous xerogels, a typical product from sol-gel processing [87]. The iron and aluminum content and BET surface areas of these materials are listed in Table 2-1.

**Table 2-1.** Properties of different Fe-containing materials.

| Type of material | BET surface area ($m^2/g$) | Fe content (weight %) | Al content (weight %) |
|---|---|---|---|
| Hematite | 36 | 70 [(a)] | - |
| Goethite | 13 | 35 [(b)] | - |
| Amorphous FeOOH | 166 | 62.9 [(a)] | - |
| *FeSi-ox* | 521 | 12.3 | - |
| *FeAlSi-ox* | 423 | 10.9 | 4.95 |

(a) theoretical value.
(b) value reported by the manufacturer.

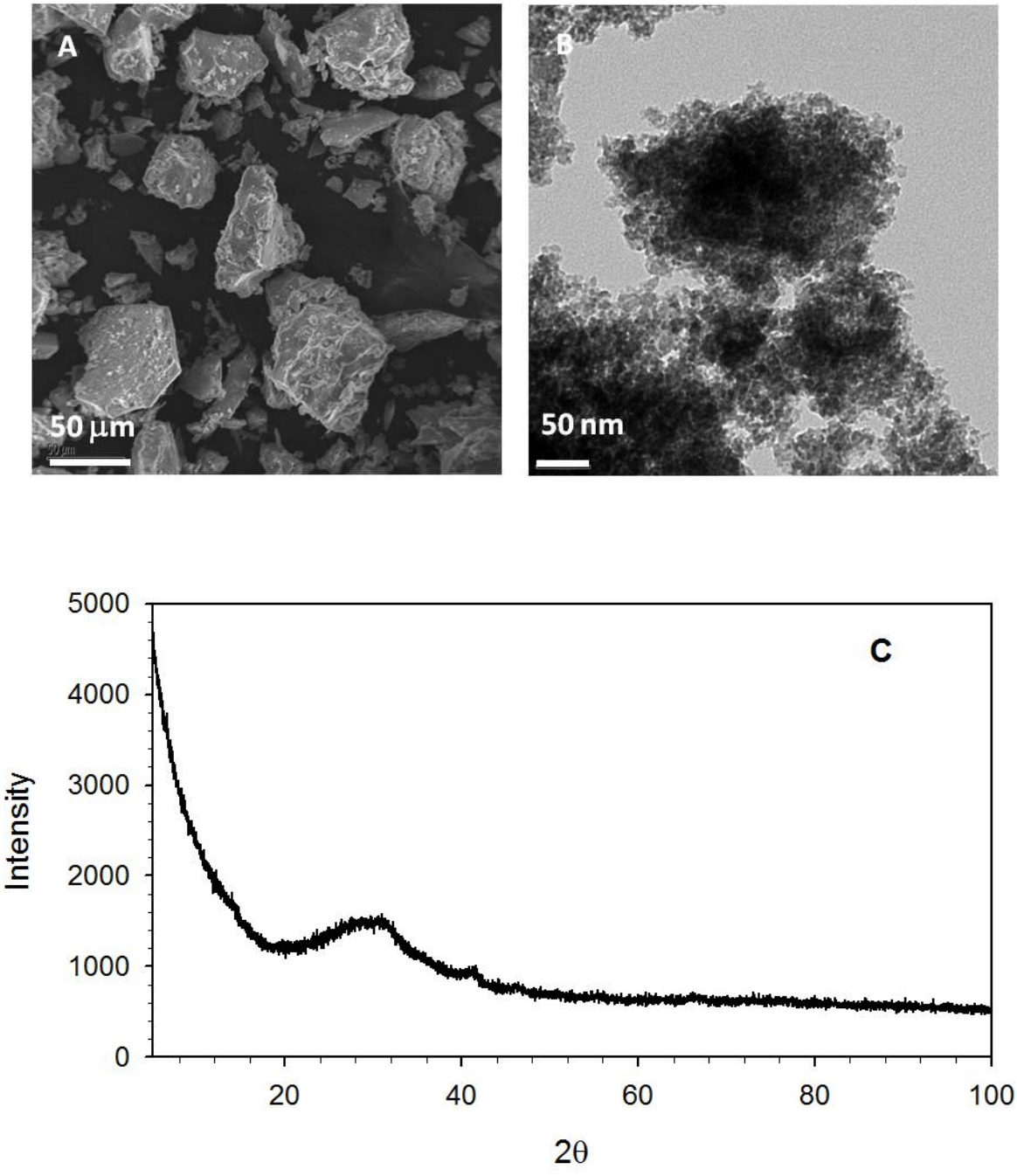


**Figure 2-1.** *FeAlSi-ox* obtained by sol – gel processing of aqueous mixture of $Fe(ClO_4)_3$, $Al(NO_3)_3$ and TEOS. (A) SEM. (B) TEM. (C) XRD.

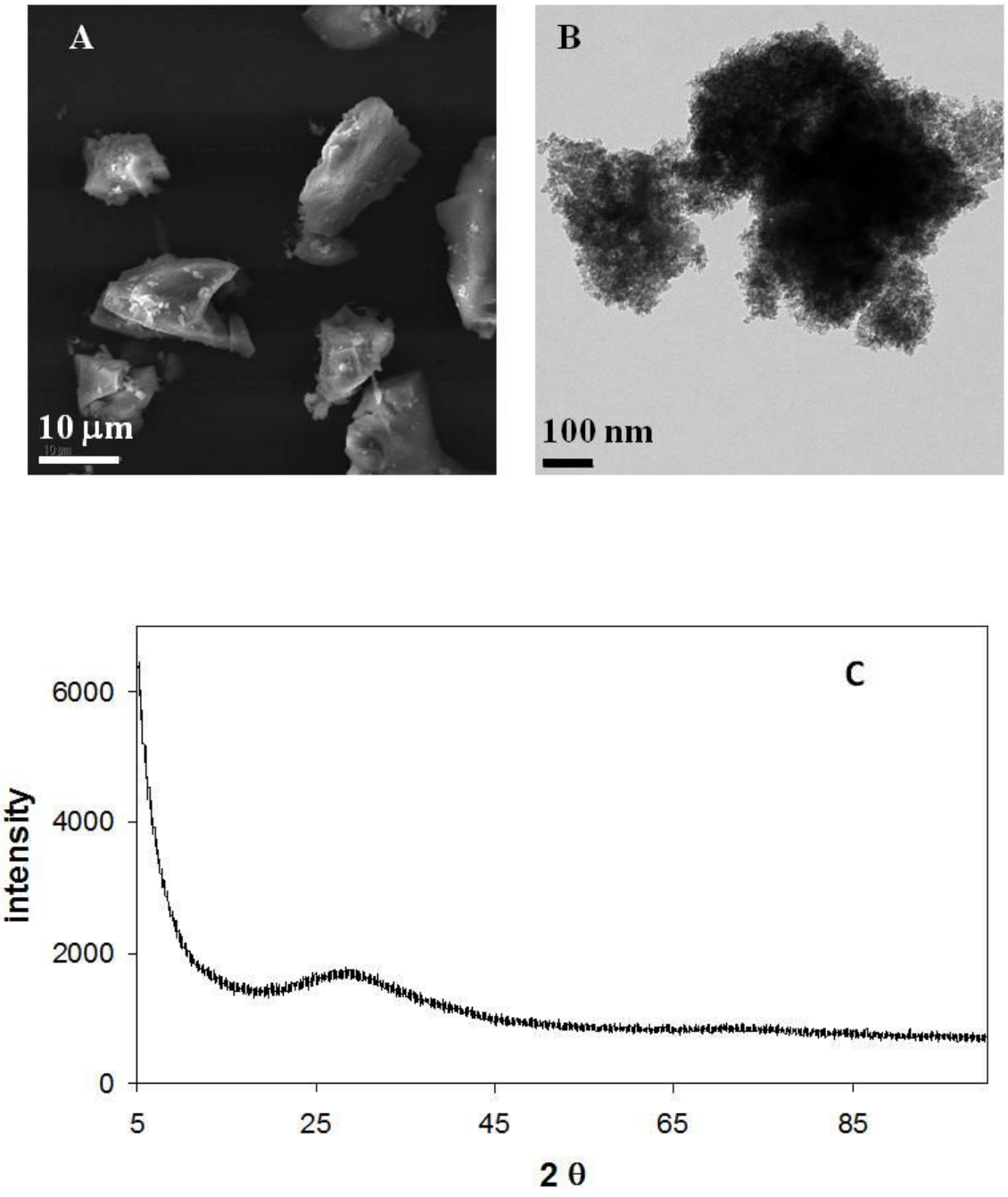


**Figure 2-2.** *FeSi-ox* obtained by sol – gel processing of aqueous mixture of $Fe(ClO_4)_3$, $Al(NO_3)_3$ and TeOS. (A) SEM. (B) TEM. (C) XRD.

### 2.3.2 Catalytic performance toward $H_2O_2$ decomposition and phenol oxidation

The oxidation of phenol catalyzed by *FeAlSi-ox* (4.9 wt % Al, 10.9 wt % Fe) is a pH dependent process, with a reaction rate that decreases with increasing pH. After 8 hours over 90% of the phenol was transformed at pH 5.3, 30%-35% at pH 6.9 and 23%-25% at pH 8.5 (Figure 2-3). The concentration of phenol decreased by less than 15% in the presence of 200 mM t-BuOH at all three pH values (Figure 2-3). Control experiments (data not shown) showed that adsorption accounted for less than 3% of the total phenol loss and thus can be neglected compared to losses due to oxidation. A gradual increase of total dissolved iron ($[Fe_{TOT}]$) was observed during the experiments conducted in the absence of t-BuOH (inset of Figure 2-3).

While t-BuOH decreased phenol loss at all pH values, $H_2O_2$ decomposition was retarded by t-BuOH only at pH 5.3 (Figure 2-4). At pH 5.3, approximately 30% of the initial $H_2O_2$ was decomposed over 8 hours in the t-BuOH-free system, while less than 5% of the $H_2O_2$ decomposed in the presence of 200 mM t-BuOH.

The catalytic performance of the *FeAlSi-ox* catalyst was compared to the alumina-free analog, *FeSi-ox* (12.3 wt % Fe) at pH 6.9. The alumina-free catalyst resulted in faster $H_2O_2$ decomposition and phenol transformation (Figure 2-5).

The rate of $H_2O_2$ decomposition and transformation of phenol catalyzed by iron oxides was also investigated over pH values ranging 5.5 – 8.8. After 8 hours, approximately 20 to 35% of the initial $H_2O_2$ was decomposed in the hematite/$H_2O_2$ system, whereas all of the $H_2O_2$ was decomposed in the presence of amorphous FeOOH and commercial goethite (Figure 2-6). However, phenol transformation catalyzed by iron oxides was very low: less than 1% phenol loss was observed for amorphous FeOOH and commercial goethite. For hematite, the concentration of phenol decreased by approximately 5% to 7% mainly due to surface adsorption.

The stoichiometric efficiency, defined as the amount of phenol decomposed per mole of $H_2O_2$ consumed (*i.e.*, $E = \frac{\Delta[phenol]}{\Delta[H_2O_2]} \times 100\%$) was used to compare the performance of the catalysts. For each experiment, we calculated the stoichiometric efficiency after 25% of the phenol was transformed to assure that the comparisons were valid. This is necessary because the products of phenol transformation (*e.g.*, hydroquinone) could react with oxidants and decrease the apparent efficiency. Conversely, measuring the stoichiometric efficiency early in the reaction (*i.e.*, when less than 10% of the phenol was transformed) could result in reduced precision due to difficulties in detecting small losses of phenol. In the iron oxide/$H_2O_2$ systems, phenol loss was always less than 25% and in these cases, $\Delta$phenol values at the end of the experiments were used to determine stoichiometric efficiency. The stoichiometric efficiency of the *FeAlSi-ox* catalyst was 3 to 4 times greater than that of the *FeSi-ox* catalyst and approximately 50 to 80 times greater than that of the iron oxides over the pH range studied (Figure 2-7).

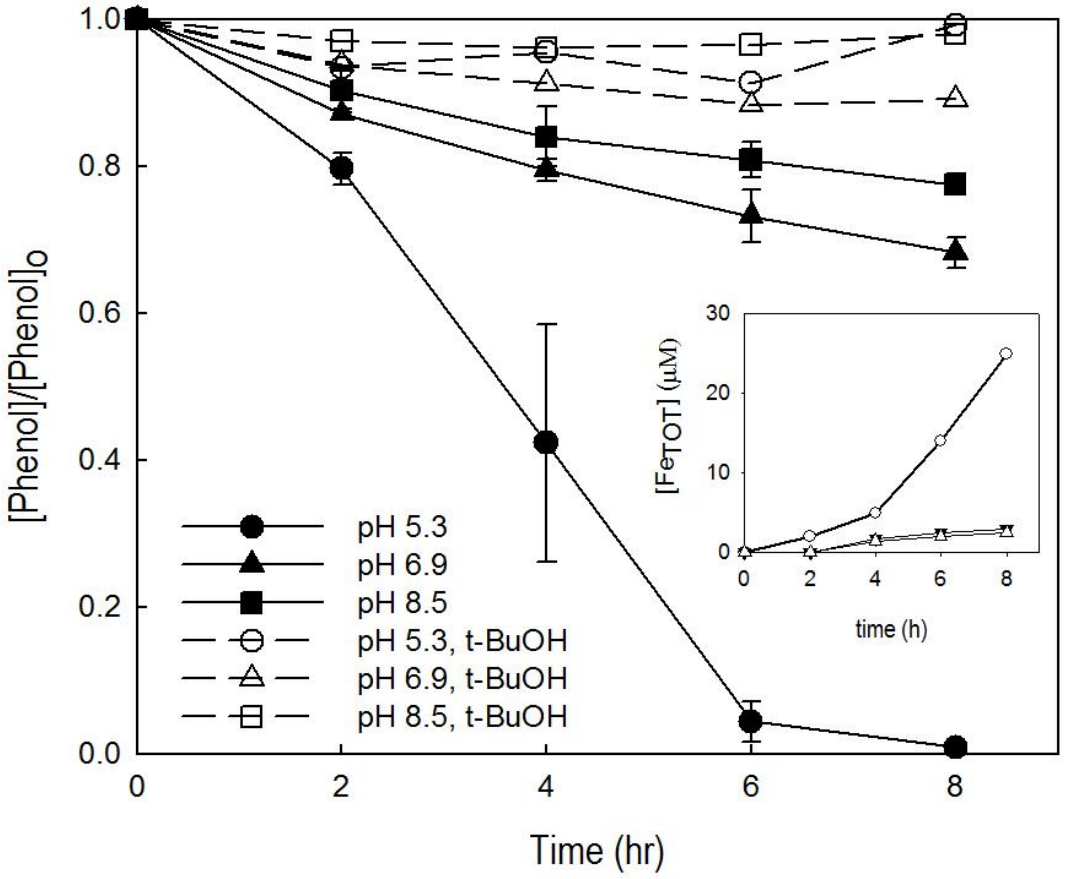


**Figure 2-3.** Effect of pH on phenol loss in the *FeAlSi-ox*/$H_2O_2$ system in the absence (solid lines) and presence (dashed lines) of t-BuOH; $[phenol]_o$ = 0.5 mM; $[H_2O_2]$ = 50 mM; [*FeAlSi-ox*] = 3 g/L; [t-BuOH] = 200 mM. $[Fe_{TOT}]$ as a function of time (inset): (●) pH 5.3; (▽) pH 6.9; (▲) pH 8.5. For the purpose of clarity, error bars were eliminated from the data in the inset. In all cases, the pH decreased by less than 1 unit during the reaction.

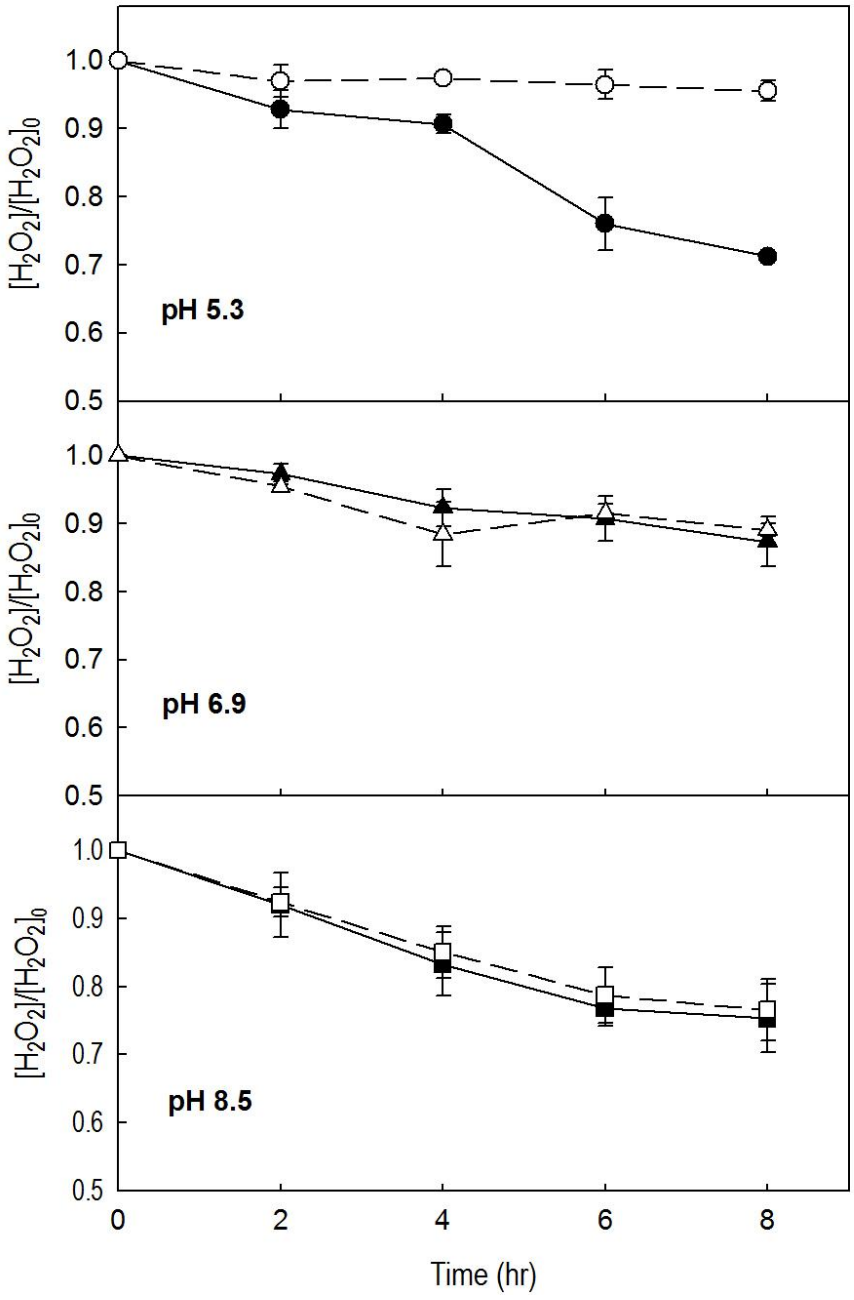


**Figure 2-4.** $H_2O_2$ loss in the *FeAlSi-ox*/$H_2O_2$ system in the absence (solid lines) and presence (dashed lines) of t-BuOH; $[phenol]_o$ = 0.5 mM; $[H_2O_2]$ = 50 mM; [*FeAlSi-ox*] = 3 g/L; [t-BuOH] = 200 mM.

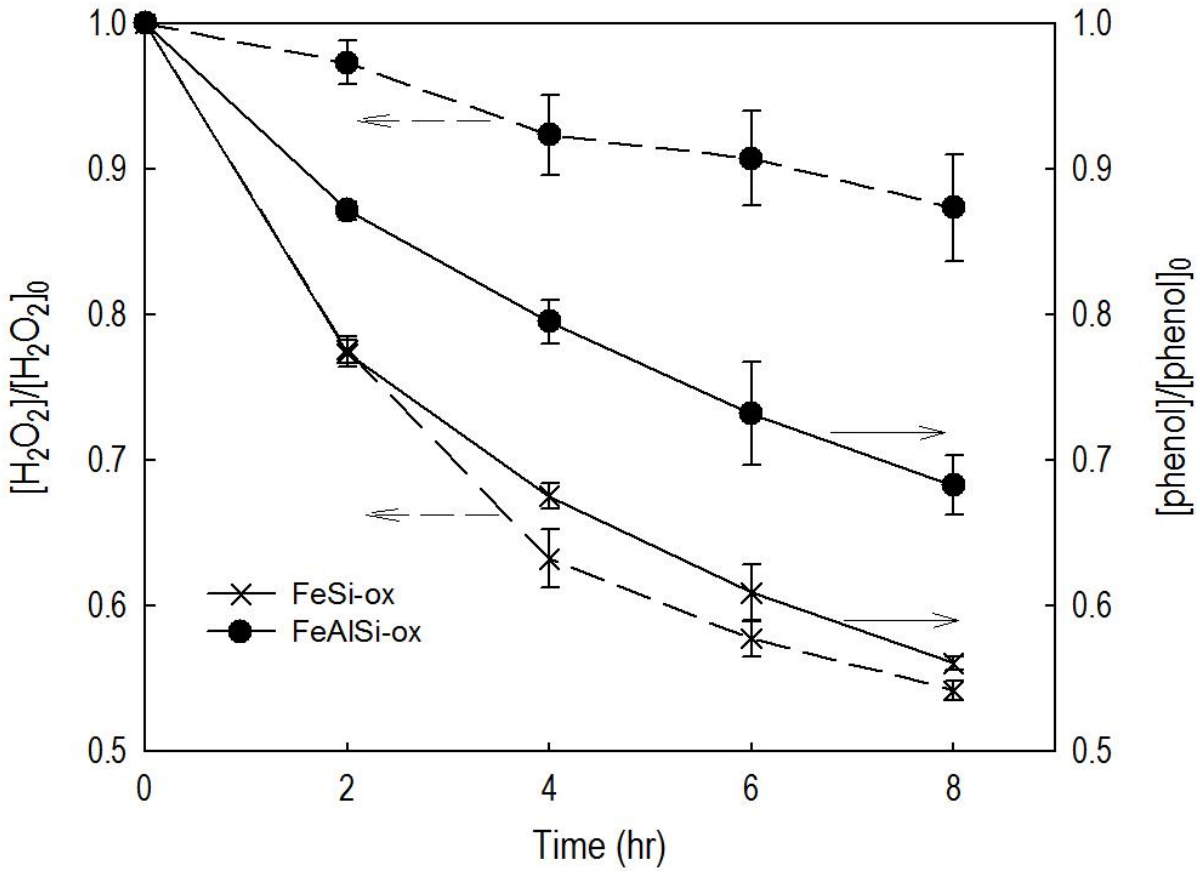


**Figure 2-5.** Phenol and $H_2O_2$ loss in the *FeSi-ox*/$H_2O_2$ and *FeAlSi-ox*/$H_2O_2$ systems; $[phenol]_o$ = 0.5 mM; $[H_2O_2]$ = 50 mM; [*FeAlSi-ox*] = [*FeSi-ox*] = 3 g/L; pH = 6.9. The pH decreased by less than 0.3 units during the reaction.

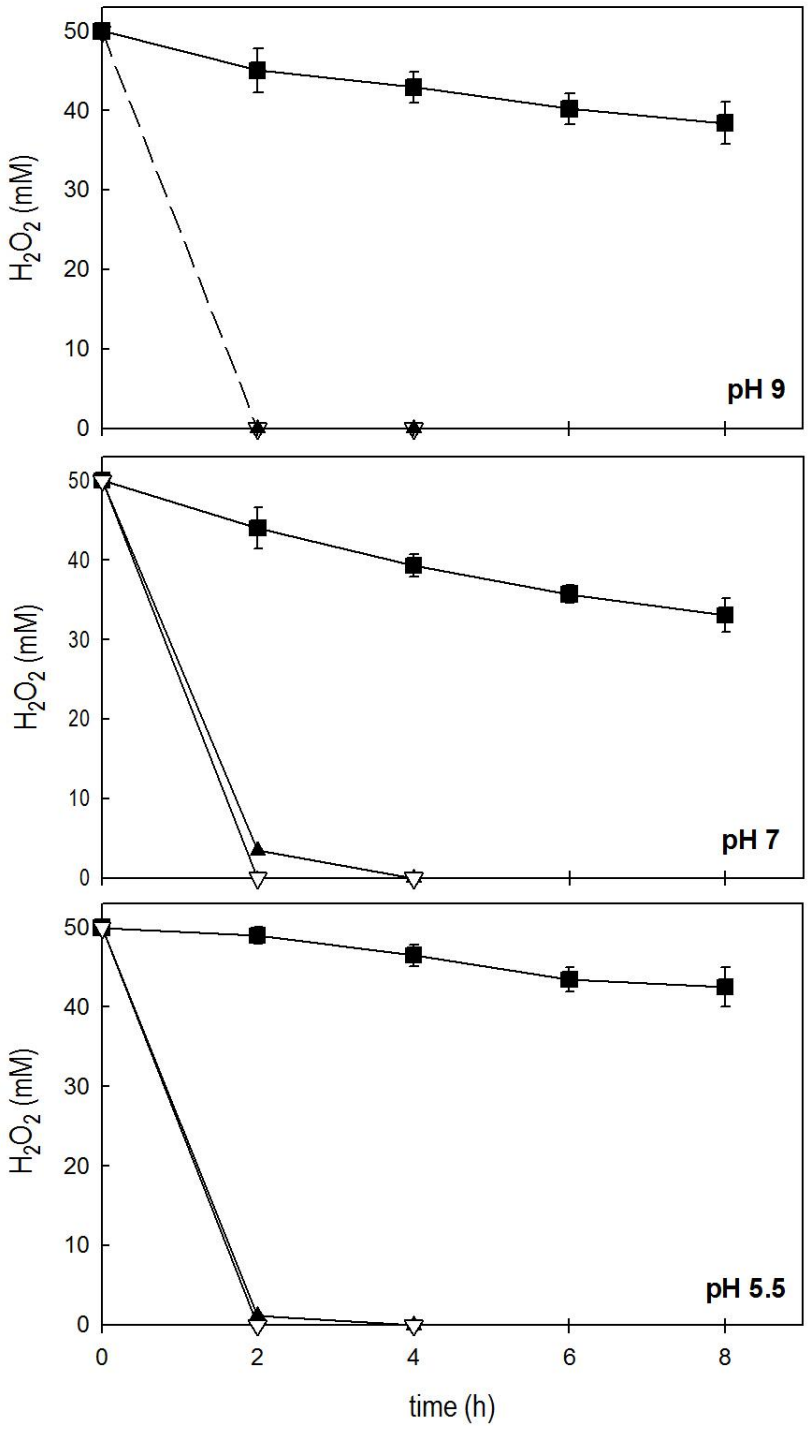


Figure 2-6. $H_2O_2$ decomposition catalyzed by iron oxides: (■) hematite; (▽) amorphous FeOOH; (▲) goethite. $[phenol]_o$ = 0.5 mM; $[H_2O_2]_o$ = 50 mM; [iron oxide] = 3 g/L.

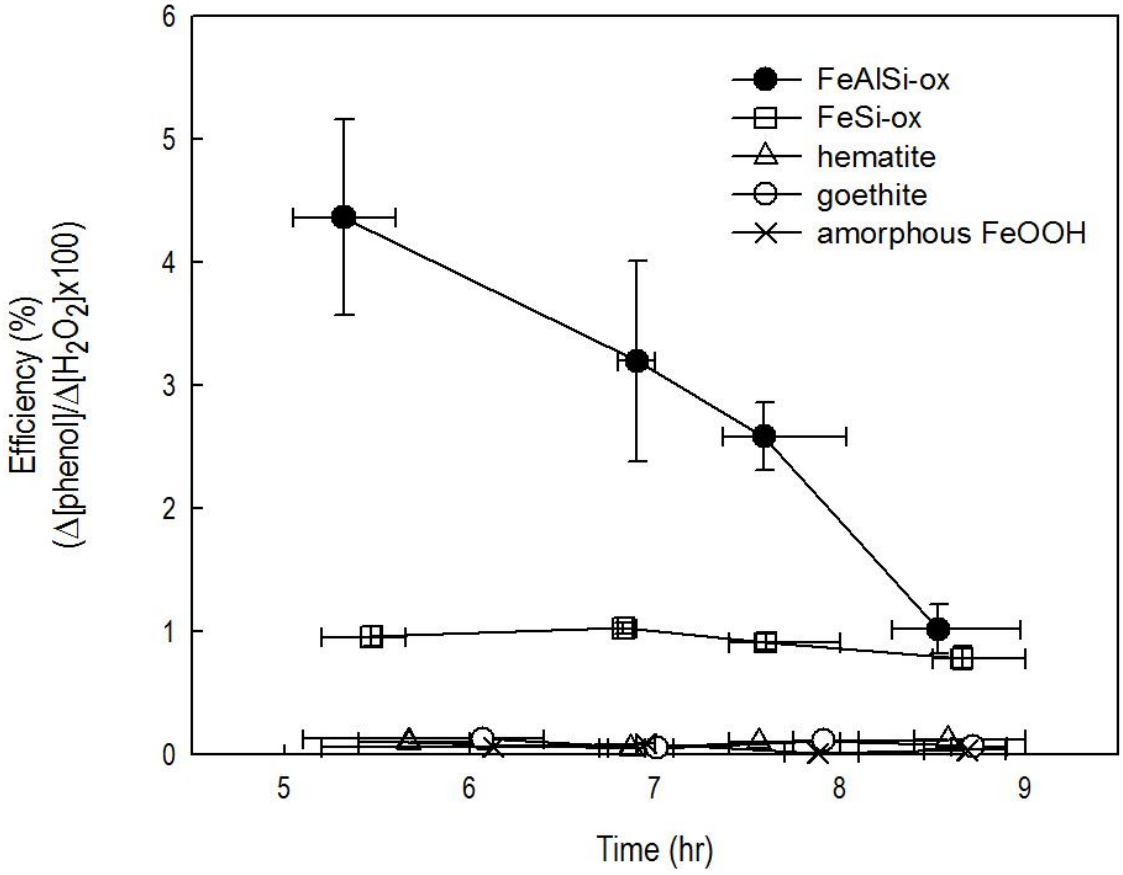


**Figure 2-7**. Stoichiometric efficiency ($\Delta[\text{phenol}]/\Delta[H_2O_2] \times 100\%$) as function of pH. Data collected when $\Delta$[phenol] = 23-27% $[\text{phenol}]_o$. $[\text{Phenol}]_o$ = 0.5 mM; $[H_2O_2]_o$ = 50 mM; [oxide] = 3 g/L.

## 2.4 Discussion

### 2.4.1 Activation of $H_2O_2$ by iron oxides

The decomposition of $H_2O_2$ by pure iron oxides (*e.g.*, goethite, hematite) has been studied over a wide pH range. Under acidic conditions, the process appears to be controlled by redox cycling of both surface and dissolved iron (*i.e.*, Fe[II]/Fe[III]), the latter resulting from dissolution of the iron oxides [30, 45]. At circumneutral pH values, the contribution of dissolved iron to $H_2O_2$ activation should be minimal because Fe(III) is sparingly soluble [46]. Therefore, the decomposition of $H_2O_2$ under circumneutral pH conditions is likely a surface-catalyzed process.

It has been suggested that the surface-initiated $H_2O_2$ decomposition proceeds through a chain reaction that is analogous to the $Fe^{3+}$-initiated decomposition of $H_2O_2$ that was initially described by Haber and Weiss under acidic conditions [22, 24, 31]. The oxidation of organic contaminants during $H_2O_2$ decomposition has been attributed to hydroxyl radical ($^{\bullet}OH$) production from the reaction of $H_2O_2$ with reduced surface iron (*i.e.*, $\equiv Fe^{II}$) (scheme 1 and reaction 2 in Table 2-2).

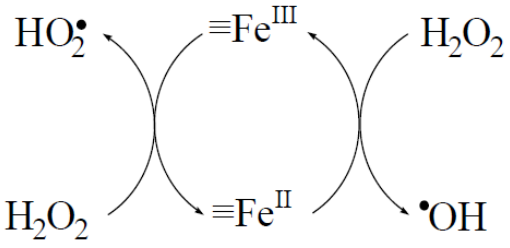


Scheme 1. Haber – Weiss mechanism

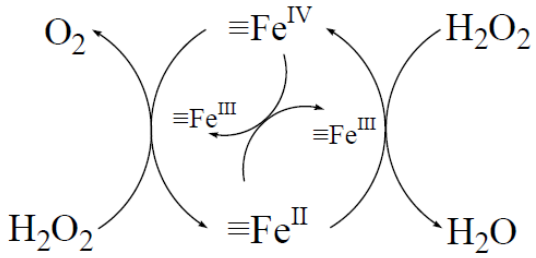


Scheme 2. Non-radical mechanism

The application of the iron oxide/$H_2O_2$ systems for oxidation of contaminants has been limited by the extremely low stoichiometric efficiency of oxidant production at neutral pH values (*e.g.*, [6, 26] and Figure 2-7). The low efficiency is often attributed to the generation of $^{\bullet}OH$ in areas on the oxide surface that are inaccessible to the contaminants (*e.g.*, $^{\bullet}OH$ is scavenged by the iron oxide surface [6]). Alternatively, the activation of $H_2O_2$ by iron oxides could produce oxidants such as high-valent iron species (*i.e.*, ≡Fe[IV]) [88]. While little is known about the exact structure and reactivity of such surface-bound oxidants, solution phase Fe(IV) species are less reactive than $^{\bullet}OH$ and do not react with aromatic compounds to an appreciable extent [56]. Some investigators also have suggested that the decomposition of $H_2O_2$ on the surface of iron oxides may proceed mainly through a non-radical mechanism that converts $H_2O_2$ directly into $O_2$ and $H_2O$ by a series of $2e^-$ transfer reactions (*e.g.*, by the presence of oxygen vacancies on the surface [89] or the cycling of ≡Fe(IV)/≡Fe(II) as proposed in scheme 2 and reactions 9 – 11 in Table 2-2). The principal net reaction in these pathways is the conversion of $H_2O_2$ into $H_2O$ and $O_2$ without the production of $^{\bullet}OH$**.**

**Table 2-2.** Mechanism of surface-initiated $H_2O_2$ decomposition.

Haber – Weiss mechanism [22, 24]

| | reaction |
|---|---|
| $\equiv Fe(III) + H_2O_2 \rightarrow \equiv Fe(II) + HO_2^{\bullet} (O_2^{\bullet -}) + H^+ (2H^+)$ | (2.1) |
| $\equiv Fe(II) + H_2O_2 \rightarrow \equiv Fe(III) + {}^{\bullet}OH + OH^-$ | (2.2) |
| $\equiv Fe(III) + HO_2^{\bullet} (O_2^{\bullet -}) \rightarrow \equiv Fe(II) + O_2 (+ H^+)$ | (2.3) |
| $HO_2^{\bullet} \Leftrightarrow H^+ + O_2^{\bullet -}$ | (2.4) |
| ${}^{\bullet}OH + H_2O_2 \rightarrow H_2O + HO_2^{\bullet}$ | (2.5) |
| ${}^{\bullet}OH + \equiv Fe(II) \rightarrow \equiv Fe(III) + HO^-$ | (2.6) |
| ${}^{\bullet}OH + HO_2^{\bullet} (O_2^{\bullet -}) \rightarrow O_2 + H_2O (+ OH^-)$ | (2.7) |
| $HO_2^{\bullet} + HO_2^{\bullet} \rightarrow H_2O_2 + O_2$ | (2.8) |

A possible non-radical mechanism

| | reaction |
|---|---|
| $\equiv Fe(III) + H_2O_2 \rightarrow \equiv Fe(II) + HO_2^{\bullet} + H^+$ | (2.1) |
| $\equiv Fe(II) + H_2O_2 \rightarrow \equiv Fe(IV) + 2OH^-$ | (2.9) |
| $\equiv Fe(IV) + H_2O_2 \rightarrow \equiv Fe(II) + O_2 + 2H^+$ | (2.10) |
| $\equiv Fe(IV) + \equiv Fe(II) \rightarrow 2\equiv Fe(III)$ | (2.11) |
| $\equiv Fe(III) + HO_2^{\bullet} (O_2^{\bullet -}) \rightarrow \equiv Fe(II) + O_2 (+ H^+)$ | (2.3) |
| $HO_2^{\bullet} + HO_2^{\bullet} \rightarrow H_2O_2 + O_2$ | (2.8) |

### 2.4.2 Efficiency enhancement with *FeAlSi-ox* and *FeSi-ox*

The stoichiometric efficiency of *FeSi-ox* and *FeAlSi-ox* is much higher than that of iron oxides (Figure 2-7). In the *FeAlSi-ox*/$H_2O_2$ system, the rate of phenol transformation decreases dramatically with increasing pH (Figure 2-3) while the rate of $H_2O_2$ loss only varies by about 15% with a minimum at pH 6.9 (Figure 2-4). The decreased rate of phenol loss at higher pH values appears to be attributable to a decrease in the production of oxidants capable of reacting with phenol. The oxidation of phenol in this system is most likely due to $^{\bullet}OH$ because upon addition of t-BuOH phenol transformation rate decreased significantly (Figure 2-3).

As mentioned previously, Fe(III) is sparingly soluble at circumneutral pH values. The concentration of soluble Fe(III) is expected to range from 0.001 μM to 0.1 μM over pH values ranging from 5.5 to 9, assuming that the system is at equilibrium with 2-line ferrihydrite [46]. As the reaction proceeded, however, the concentration of dissolved iron increased to 20 ± 10 μM at pH 5.3 and 2 ± 1 μM at pH 6.9 – 8.5 (inset of Figure 2-3). This dissolution of Fe(III) was attributable to the interaction of surface iron and intermediate oxidation products of phenol (*e.g.*, hydroquinones, organic acids) that enhance iron solubility via complexation and reductive dissolution [45]. This hypothesis was supported by the fact that iron leaching and phenol oxidation were not observed upon addition of t-BuOH, as little intermediates were formed.

In a previous study [30], the activation of $H_2O_2$ by dissolved iron was observed at [Fe(III)] as low as 0.42 μM. Consequently, to determine whether the higher stoichiometric efficiency of *FeAlSi-ox*/$H_2O_2$ system was due to better $H_2O_2$ activation by the *FeAlSi-ox* surface or to activation of $H_2O_2$ by dissolved iron, we investigated the proportions of homogeneous and heterogeneous reaction using filtration to isolate the solution-phase reaction (Figure 2-8). Following filtration, at pH 6.9 and 8.5, the phenol concentration decreased by less than 3% during a 16-hour period, indicating that dissolved iron is unimportant to phenol transformation compared to surface catalyzed reactions. At pH 5.3, the phenol concentration decreased significantly after filtration (Figure 2-9), albeit less than in the presence of *FeAlSi-ox*. Phenol transformation at this pH value therefore was attributable to the production of oxidants from both homogeneous and surface-catalyzed reaction.

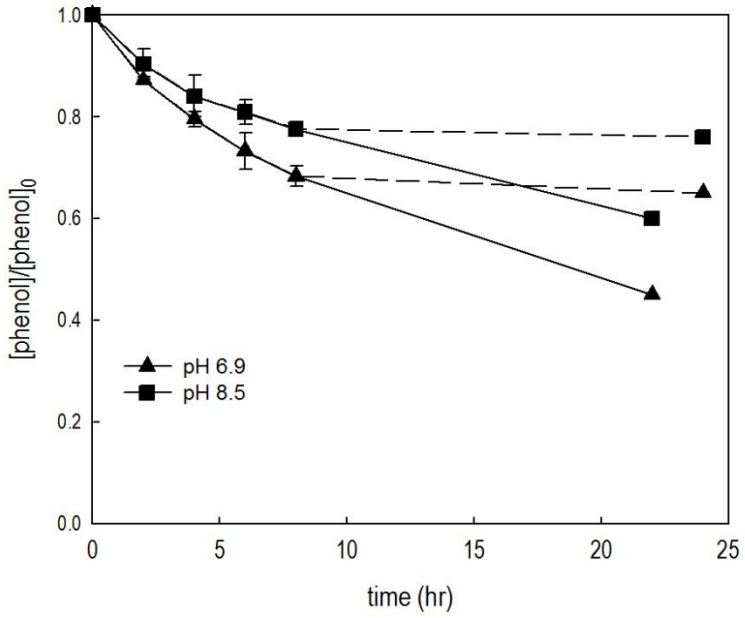


**Figure 2-8.** Phenol concentration as a function of time. $[phenol]_o$ = 0.5 mM; $[H_2O_2]$ = 50 mM; [*FeAlSi-ox*] = 3 g/L. At t = 8hours, *FeAlSi-ox* was removed from the reactor and phenol concentration was followed (dashed lines).

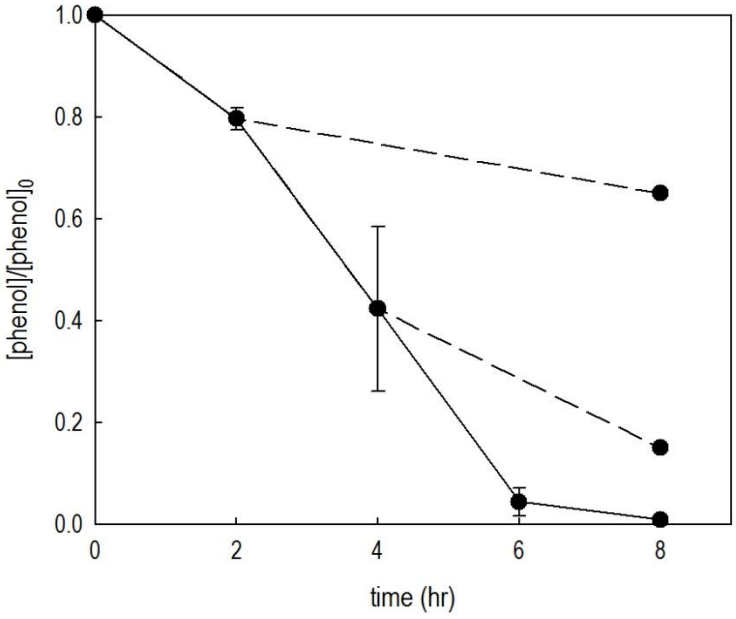


**Figure 2-9.** Phenol concentration as a function of time at pH 5.3. $[phenol]_o$ = 0.5 mM; $[H_2O_2]$ = 50 mM; [*FeAlSi-ox*] = 3 g/L. Phenol concentration was followed in the filtered samples (dashed lines).

### 2.4.3 Role of silica and alumina

$SiO_2$ and $Al_2O_3$ do not catalyze the decomposition of $H_2O_2$ at circumneutral pH values (less than 1% of the initial $H_2O_2$ was lost in the presence of just either $SiO_2$ or $Al_2O_3$). Therefore, the significant enhancement in $H_2O_2$ activation by *FeSi-ox* and *FeAlSi-ox* at circumneutral pH values relative to pure iron oxides is attributable to the interaction of iron with alumina and silica in the mixed catalyst. There are several possible explanations for this phenomenon. First, the dispersion of the iron oxide phase within the silica and alumina matrix might prevent the iron from aggregating into clusters, resulting in changes in the number and properties of the reactive surface sites. These structural differences can alter the relative proximity of reactive sites, which in turn may affect the reactions between the surface and the reactant (*i.e.*, $H_2O_2$). The role of steric position of reactive sites on redox processes has been speculated to be important in the reduction of carbon tetrachloride by Fe(II) associated with goethite, where the steric position of the latter can enhance multiple electron transfer reactions [90]. In a similar way, iron dispersion within the silica and alumina matrix might favor the radical mechanism (series of $1e^-$ transfer steps) over the non-radical mechanisms ($2e^-$ transfer step), leading to more $^{\bullet}OH$ production during the decomposition of $H_2O_2$.

The higher efficacy of *FeAlSi-ox* and *FeSi-ox* compared with iron oxides may also arise from the difference in electronic properties of iron because silica, alumina and iron oxides exhibit different points of zero charge (pzc) values. The pzc of $SiO_2$ (*i.e.*, 2 – 5) is much lower than that of iron oxides and alumina (*i.e.*, 7.5 – 9) [91]. At circumneutral pH values, it is expected that the surface of *FeSi-ox* and *FeAlSi-ox* will be negatively charged because $SiO_2$ is the predominant component in these materials (Figure 2-10) whereas iron oxide surfaces will be positively charged, or will have a much less negative charge. In addition to altering the electronic properties of reactive sites, the negative surface charge of *FeAlSi-ox* may also affect the sorption of $H_2O_2$ on the surface, which was suggested to be the rate limiting step in $H_2O_2$ decomposition [30]. While the mechanism and kinetics of $H_2O_2$ interactions with surfaces have not been well studied, $H_2O_2$ forms strong hydrogen bonds with the oxygen in siloxane bridges, Si-O-Si [92]. It is possible that such interactions with the silica-containing catalyst may alter the reactions of $H_2O_2$ with iron on the catalyst surface.

It is interesting to note that although the decomposition of phenol and $H_2O_2$ occurred at a faster rate when catalyzed by *FeSi-ox*, a higher stoichiometric efficiency was obtained with *FeAlSi-ox*. The mechanism through which alumina alters the efficiency is unclear. Lim *et al.* [12] postulated that alumina facilitates the reduction of Fe(III) by $H_2O_2$ because alumina, a Lewis acid, can attract electron density from iron and thus raise the oxidation potential of the Fe(III) center. This explanation seems unlikely because the reactions were slower for the Al-containing catalyst (*i.e.*, *FeAlSi-ox*). On the basis of the iron content and surface area (Table 2-1), we hypothesize that faster reactions observed with *FeSi-ox* are related to its higher surface and iron content. However, this cannot explain the higher $H_2O_2$ utilization efficiency of the *FeAlSi-ox* catalyst. Additional research is needed to characterize the role that Al plays in the catalyst.

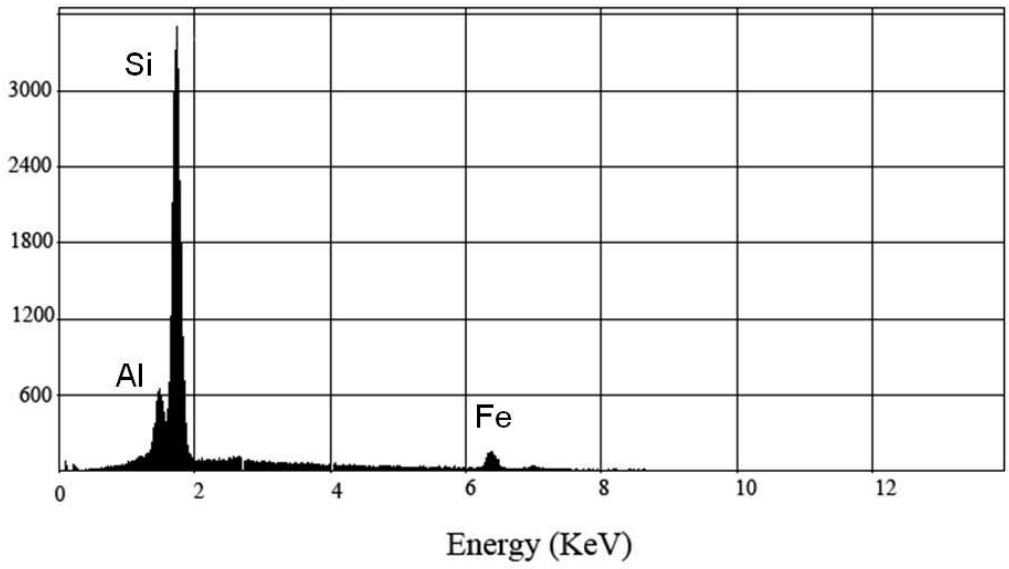


**Figure 2-10.** EDX spectra of *FeAlSi-ox.*

## 2.5 Environmental implications

The silica- and alumina-containing iron oxide catalyst has the potential to be more effective in the oxidative treatment of industrial waste and contaminated water at circumneutral pH values than iron oxides studied previously for this application. While over 90% of the $H_2O_2$ that was lost in the presence of the catalyst does not produce oxidants capable of transforming aromatic compounds, the absence of a pH adjustment step, minimal waste production and low potential for production of toxic byproducts may provide advantages over other approaches. Additional research is needed to further enhance the efficiency of the catalyst and assess the scale up of the treatment systems employing the catalyst.

This study also has important implications for the design and operation of *in situ* remediation systems that use $H_2O_2$ for oxidation of contaminants. Previous studies on the mechanism of $H_2O_2$ reduction by pure iron oxides indicated that iron oxides can activate $H_2O_2$ into species capable of oxidizing contaminants. Researchers studying pure iron oxides suggested that iron-containing minerals in the subsurface could be exploited to activate $H_2O_2$ for *in situ* remediation. The present study suggests that iron oxides associated with alumina and silica may behave differently from pure iron oxides. The activity of iron associated with aluminosilicates and silica-containing minerals may help to explain differences in the production of oxidants observed during $H_2O_2$ decomposition in soils [31]. Additional research on the stoichiometric efficiency of aquifer materials may lead to better predictions of the efficacy of $H_2O_2$-based *in situ* remediation systems.

# Chapter 3. Kinetics and Efficiency of $H_2O_2$ Activation by Iron-Containing Minerals and Aquifer Materials

(Under consideration for publication in *Water Research*)

## 3.1 Introduction

Over the past two decades, hydrogen peroxide-based *in situ* Chemical Oxidation (ISCO) has become increasingly popular as a means of remediating contaminated soil and groundwater [10, 38]. In this practice, concentrated solutions of $H_2O_2$ are injected into groundwater or added to soils. Upon contacting iron-containing minerals, some of the $H_2O_2$ is converted into $^{\bullet}OH$ (reaction 3.1 and 3.2 [24, 31]), which subsequently oxidizes contaminants. The technology is simple, easy to deploy, and effective against many of the most recalcitrant organic contaminants typically encountered at contaminated sites (*e.g.*, benzene, phenol, trichloroethylene, polycyclic aromatic hydrocarbons). The use of $H_2O_2$ is also attractive because it is relatively inexpensive and its byproducts, namely $O_2$ and $H_2O$, are benign.

$$\equiv Fe(III) + H_2O_2 \rightarrow \equiv Fe(II) + HO_2^{\bullet} + H^+ \quad (3.1)$$

$$\equiv Fe(II) + H_2O_2 \rightarrow \equiv Fe(III) + {}^{\bullet}OH + OH^- \quad (3.2)$$

$$2H_2O_2 \xrightarrow{\text{Fe- and Mn-oxides, enzymes}} 2H_2O + O_2 \quad (3.3)$$

The cost and efficiency of $H_2O_2$-based ISCO systems depend largely upon the distance that $H_2O_2$ travels in the subsurface, as well as the fraction of the $H_2O_2$ that is converted into $^{\bullet}OH$. Due to the slow rate at which groundwater moves relative to the rate of $H_2O_2$ decomposition, conditions that maximize $H_2O_2$ persistence are usually desirable, because they minimize both the amount of $H_2O_2$ and the number of injection wells needed to decontaminate a given site. As $H_2O_2$ also can be decomposed by non-radical pathways (*i.e.*, the pathways that do not produce $^{\bullet}OH$, which are represented collectively by reaction 3.3) [31, 93], the amount of $H_2O_2$ required also depends upon the yield of $^{\bullet}OH$ (*i.e.*, the relative amount of $H_2O_2$ decomposed by reaction 3.1 and 3.2 to the total amount of $H_2O_2$ decomposed by reaction 3.1 – 3.3).

To gain insight into factors that influence $H_2O_2$ persistence and $^{\bullet}OH$ yield, previous investigators have studied $H_2O_2$ decomposition and contaminant transformation in systems consisting of pure iron oxides (*e.g.*, ferrihydrite, hematite and goethite [6, 26, 30]), iron minerals (*e.g.*, pyrite [27]), iron-containing aluminosilicates (*e.g.*, [13]), and aquifer materials and soils ([4, 31, 37, 42, 76]). Although these studies help explain the trends in the rates of removal of contaminants in groundwater and sediments upon addition of $H_2O_2$, it is still difficult to predict the rates of these processes under conditions encountered at hazardous waste sites.

Studies conducted with pure minerals have suggested that the crystallinity of the oxide, the coordination of Fe, and the mineral surface area affect $H_2O_2$ decomposition rates and $^{\bullet}OH$ yields [6, 26]. Nevertheless, these studies are of limited utility because iron in aquifer materials usually exists as a mixture of different phases and/or is associated with other oxides (*e.g.*, silica, alumina or manganese oxides). The reactivity of oxides in mixed oxides and silicates is different from that of the constituent end-member minerals (see chapter 2 and references [12, 93, 94]).

Moreover, in addition to iron minerals, other components in soils, such as manganese oxides, organic matter, and enzymes (*e.g.*, catalase or peroxidase), also serve as $H_2O_2$ sinks [31, 76]. Thus, results obtained with iron oxides and iron minerals do not capture the heterogeneity and complexity of sediment systems, and could overestimate the production $^{\bullet}OH$ in remediation systems. Although studies conducted with aquifer materials and soils have the potential to capture some of this heterogeneity, most previous studies have not related rates of $H_2O_2$ decomposition and $^{\bullet}OH$ yields to the surface properties of the sediments. For example, Xu and Thomson [76] attempted to correlate the rate of $H_2O_2$ decomposition with aquifer materials' properties. Their results suggested that the $H_2O_2$ decomposition rate is correlated with the Fe and Mn content of the aquifer materials. However, they did not quantify $^{\bullet}OH$ yields. Thus, it is currently difficult to predict the performance of $H_2O_2$-based ISCO treatment systems without conducting extensive site-specific scoping studies. Hence, more research is needed to predict and optimize contaminant removal in $H_2O_2$-based ISCO treatment system.

To address these needs, the reactivity of various iron-containing minerals and aquifer materials has been investigated. By studying $H_2O_2$ activation in materials from ten different aquifers under similar conditions (*i.e.*, well-buffered solution pH and identical initial concentration of $H_2O_2$ and target contaminant) and correlating results with data on physical properties, new insight has been gained about the factors affecting the $H_2O_2$ decomposition rates and $^{\bullet}OH$ yields. To assess the role of *free* iron and manganese oxides (*i.e.*, pure oxides that exist as discrete particles or as surface coatings), aquifer materials were leached with citrate-bicarbonate-dithionite (CBD) solution prior to $H_2O_2$ addition. In addition, the effect of dissolved $SiO_2$, a solute that is ubiquitous in groundwater, on the reactivity of aquifer materials was also studied.

## 3.2 Materials and methods

### 3.2.1 Chemicals

All chemicals were reagent grade and were used without further purification. Solutions were prepared using 18 MΩ Milli-Q water from a Millipore system.

### 3.2.2 Iron-containing minerals

Amorphous iron oxyhydroxide 50 – 80 mesh (*i.e.*, amorphous Fe-oxide, obtained from Adrich) was ground using a mortar and pestle prior to sieving through a 150-μm sieve. Goethite and hematite were synthesized by aging freshly made ferrihydrite in a concentrated NaOH solution at 70ºC for 60 hours (goethite synthesis) or at pH 8 to 8.5 in the presence of $NaHCO_3$ at 90 °C for 48 h (hematite synthesis) [84]. Two types of 2:1 iron-containing clay, namely Wyoming Montmorillonite (Swy-2, 2.59% Fe by weight) and Australian Nontronite (NAu-2, 26.04% Fe by weight), were obtained from the Source Clays Repository (The Clay Minerals Society). Fine powder Swy-2 was used as received, while large chunks of NAu-2 were ground

using a shatter box prior to sieving through a 150-μm sieve. Iron oxide-coated sand (1% Fe by weight, 4.8 $m^2/g$) was kindly provided by Peter Nico (Lawrence Berkeley National Laboratory). The synthesis and characterization of iron oxide-coated sand have been reported elsewhere [95]. FeSi-ox and FeAlSi-ox catalysts were synthesized following the procedure reported previously [93]. The surface area of these minerals, determined using the 5-point BET (Brunauer–Emmett–Teller) nitrogen physisorption method, is reported in Table 3-1.

### 3.2.3 Aquifer materials

Aquifer materials were obtained from 10 aquifers located in California (CADIR, CADOU, CADMS, CAROL), Arizona (AWBPH, AFTCS, AMTAL), Wyoming (WYSAN, WYLAM), and Kentucky (KENTK). Samples were dried, homogenized, and sieved through a 600-μm sieve. The 600-μm fractions were used in the phenol oxidation experiments (section 2.5). Their physico-chemical properties are reported in Table 3-2.

### 3.2.4 Treatment of aquifer materials with citrate-bicarbonate-dithionite solution

Samples of six selected aquifer materials (*i.e.*, CADIR, CADOU, AFTCS, AWBPH, WYLAM, and WYSAN) were treated with citrate-bicarbonate-dithionite (CBD) solution prior to the phenol oxidation experiment. The CBD treatment removes primarily pure iron and manganese oxides that exist as discrete particles or as coatings on the surface of aquifer materials, but not structural iron and manganese incorporated in silicates or aluminosilicates [96]. Briefly, citrate-bicarbonate-dithionite (CBD) solution was prepared by dissolving 3.53 gram of sodium citrate and 0.21 gram of sodium bicarbonate in 45 mL MiliQ water. The solution was then heated to 77$^{o}$C using a water bath. 2 gram of sample and 1 gram of sodium dithionite ($Na_2S_2O_4$) were added to the pre-heated solution and the suspension was stirred constantly for 1 minute, and occasionally afterward for 15 minutes. The CBD-treated sample was recovered by centrifugation, washed 5 times with Mili-Q water, dried and homogenized. The amount of CBD-extractable Fe and Mn in the aquifer materials is reported in Table 3-2.

**Table 3-1.** Properties of iron-containing minerals and observed-first order rate constants for mineral-catalyzed $H_2O_2$ decomposition.

| Minerals | Surface area ($m^2/g$) | Iron content (wt. %) | $k_{obs}/m^{2}$ [(b) (c)] ($hr^{-1}\times m^{-2}$) |
|---|---|---|---|
| Goethite | 19 | 62.9[(a)] | 0.015 |
| Hematite | 30 | 70.0 | 0.032 |
| Amorphous Fe-oxide | 166 | 62.9[(a)] | 0.097 |
| Swy-2 | 32 | 2.6 | 0.022 |
| NAu-2 | 69 | 26.2 | 0.012 |
| Iron oxide-coated sand | 5 | 1.0 | 0.199 |
| FeSi-ox | 521 | 12.3 | 0.007 |
| FeAlSi-ox | 423 | 10.9 | 0.003 |

(a) Values were calculated based on the FeOOH formula.
(b) The observed-first order rate constants ($k_{obs}$) were obtained by fitting the experimental data to the first order decay reaction rate law. The $r^2$ values of the fittings were always $r^2 > 0.99$.
(c) Rate constants were normalized by the total surface area of the solid used in the experiment.

**Table 3-2**. Properties of aquifer materials. Surface area was measured in our laboratory while the other properties were analyzed by the Analytical Laboratory at the University of California, Davis. Details on the analytical protocols are available at http://anlab.ucdavis.edu/analyses/soil/

| Soil ID | Sand (wt. %) | Silt (wt. %) | Clay (wt. %) | pH | $pH_{av}$[a] | BET surface area[b] ($m^2/g$) | Total Fe (mg/kg) | Total Mn (mg/kg) | Fe-CBD (mg/kg) | Mn-CBD (mg/kg) | TC (%) | TOC (%) |
|---|---|---|---|---|---|---|---|---|---|---|---|---|
| CADIR | 80 | 16 | 4 | 8.4 | 8.4 | 4.7 | 9600 | 96 | 2460 | 28 | 0.22 | 0.1 |
| CADOU | 84 | 10 | 6 | 9.2 | 8.7 | 3.9 | 7700 | 106 | 3020 | 54 | 0.32 | 0.2 |
| CADMS | 90 | 5 | 5 | 8.8 | 8.5 | 3.2 | 6840 | 90 | 2400 | 44 | 0.23 | 0.11 |
| CAROL | 63 | 18 | 19 | 7.6 | 8.2 | 39.8 | 24880 | 156 | 4800 | 76 | 0.08 | 0.08 |
| AWBPH | 82 | 10 | 8 | 7.8 | 8.5 | 14.3 | 16700 | 287 | 8010 | 191 | 0.03* | 0.04* |
| AFTCS | 60 | 22 | 18 | 7.7 | 8.3 | 27.7 | 14400 | 321 | 4470 | 185 | 0.36 | 0.05 |
| AMTAL | 64 | 22 | 14 | 7.2 | 8.2 | 16.2 | 18490 | 1162 | 10500 | 943 | 0.04* | 0.06* |
| WYSAN | 86 | 8 | 6 | 7.8 | 8.5 | 9.0 | 11500 | 193 | 4170 | 142 | 0.19 | 0.04 |
| WYLAM | 42 | 32 | 26 | 7.7 | 8.3 | 34.6 | 13900 | 294 | 2580 | 189 | 0.34 | 0.04 |
| KENTK | 87 | 5 | 8 | 4.6 | 7.2 | 5.1 | 12400 | 67 | 10950 | 57 | 0.02* | 0.05* |

* TOC (Total Organic Carbon) was greater than TC (Total Carbon) because these values were within the uncertainty range of the analysis methods.

[a] The average pH of the solution during the course of phenol degradation experiment. Solutions were buffered with 10 mM borate and the initial pH was 8.5.

[b] BET surface area was measured in duplicate, and the average results are reported.

### 3.2.5 Hydrogen peroxide decomposition and phenol transformation

$H_2O_2$ decomposition and phenol transformation experiments were conducted in the dark in a 150-mL Pyrex flask that was shaken at 200 rpm. Phenol was selected as a model target contaminant because it is not significantly adsorbed by any of the solids and reacts with $^{\bullet}OH$ at a near-diffusion controlled rate. Each flask contained 10 mL of a solution consisting of 250 mM $H_2O_2$ and 0.5 mM phenol, with 1 – 10 g/L of iron-containing minerals or 50 – 150 g/L of aquifer materials. Suspensions were buffered with 2 – 10 mM borate. The initial pH of the suspensions was 8.4 and did not vary by more than 0.3 pH unit over the course of the experiment, with the exception of the KENTK materials, where the pH dropped quickly to 7.2 and remained stable during the experiment. Reactors were open to the atmosphere but were covered with parafilm to minimize evaporation.

Samples were withdrawn at predetermined time intervals and divided into two aliquots. The first aliquot was centrifuged to separate the solids, then the supernatant was filtered immediately through a 0.2-μm nylon filter prior to analysis for $H_2O_2$. Acetonitrile was added to the second aliquot (acetonitrile:sample = 1:1) and the mixture was agitated vigorously for 2 minutes with a vortex mixer to extract phenol from the solids. The solids were then separated by centrifugation and filtration, and the solution was analyzed for phenol. Phenol recovery by acetonitrile extraction was always above 98% in $H_2O_2$-free controls. The stoichiometric efficiency, E, defined as the amount of phenol transformed per mole of hydrogen peroxide decomposed (*i.e.*, $E = \frac{\Delta[phenol]}{\Delta[H_2O_2]} \times 100\%$), was used to compare the $H_2O_2$ activation efficiency for different solids [93]. All experiments were carried out at 22 ± 2ºC and at least in triplicate, and the average results were reported together with one standard deviation.

### 3.2.6 Analytical methods

Phenol was analyzed using HPLC as described previously [93]. $H_2O_2$ was analyzed spectrophotometrically by the titanium sulfate method [85]. Total dissolved iron was quantified using the 1,10-phenanthroline method after adding hydroxylamine hydrochloride to the filtered samples [86]. The concentration of dissolved iron was always below the detection limit (*i.e.*, less than 5 μM).

## 3.3 Results and discussions

### 3.3.1 $H_2O_2$ decomposition, phenol oxidation, and stoichiometric efficiency

*a. Iron-containing minerals*

Under the conditions employed in the experiments, $H_2O_2$ and phenol disappeared from the suspensions over a period of several days (Figure 3-1A). No phenol loss was observed in the absence of $H_2O_2$ or in the presence of 100 mM tert-butanol (an $^{\bullet}OH$ scavenger). These results collectively suggested that phenol was lost from systems containing minerals and $H_2O_2$ through the reaction with $^{\bullet}OH$. Furthermore, $^{\bullet}OH$ production in these systems was mainly attributable to surface-catalyzed reactions because the concentration of dissolved iron was always below the detection limit (*i.e.*, less than 5 μM).

The stoichiometric efficiency in the iron-containing mineral/$H_2O_2$ systems varied over an order of magnitude, from 0.02% with amorphous Fe-oxide to 0.25% with FeAlSi-ox (Figure 3-1B). The low stoichiometric efficiency suggests that the majority of the $H_2O_2$ (*i.e.*, more than 99%) was decomposed via reactions that do not produce $^{\bullet}OH$ [31, 93]. Consistent with our previous study [93], the stoichiometric efficiency was higher for the iron silicates and aluminosilicates (FeSi-ox, FeAlSi-ox, NAu-2 and Swy-2) than for the pure iron oxides. This was most likely attributable to the Fe coordination environment in the silicates and aluminosilicates, which favored $H_2O_2$ decomposition via the radical mechanisms (reaction 3.1 and 3.2) over the non-radical mechanisms (reaction 3.3) [93]. The stoichiometric efficiency also appeared to be inversely correlated with the rate of $H_2O_2$ decomposition, with lower stoichiometric efficiency occurring mainly in systems with faster $H_2O_2$ decomposition (Figure 3-1B and Table 3-1).

Both FeSi-ox and iron oxide-coated sand contained Fe and Si. Under the experimental conditions employed in this study, however, FeSi-ox was approximately 5 times more effective than iron oxide-coated sand in $H_2O_2$ activation (stoichiometric efficiency of 0.24 and 0.045% for FeSi-ox and iron oxide-coated sand, respectively (Figure 3-1B)). The higher efficiency of the FeSi-ox catalyst might also have been attributable to the difference in Fe coordination environment in each solid. In the case of iron oxide-coated sand, sand particles were coated with ferrihydrite slurry [95] whereas the FeSi-ox was synthesized by a sol-gel process, in which a mixture of tetraethyl orthosilicate (a silica precursor) and dissolved $Fe^{3+}$ was coprecipitated in a strong alkaline solution [93]. For FeSi-ox, the coordination of Fe by silicate and/or close interaction between Fe and Si might have created surface conditions that were more favorable for $^{\bullet}OH$ production during $H_2O_2$ decomposition [93].

While NAu-2 and Swy-2 are both 2:1 layered smectites, the stoichiometric efficiency with NAu-2 (0.21%) was almost double that with Swy-2 (0.12%). Compared with other 2:1 clays, NAu-2 contains a significantly higher concentration of Fe in the octahedral layer [97]. The potential for structural iron to produce higher $^{\bullet}OH$ yields when used as a heterogeneous catalyst warrants further investigation. Additionally, detailed study on the correlation between the structure of well-characterized clays and their potential to produce $^{\bullet}OH$ from $H_2O_2$ might provide further insight into the reaction mechanism, as well as a basis for synthesizing more effective catalysts for $H_2O_2$-based *ex situ* oxidative treatment.

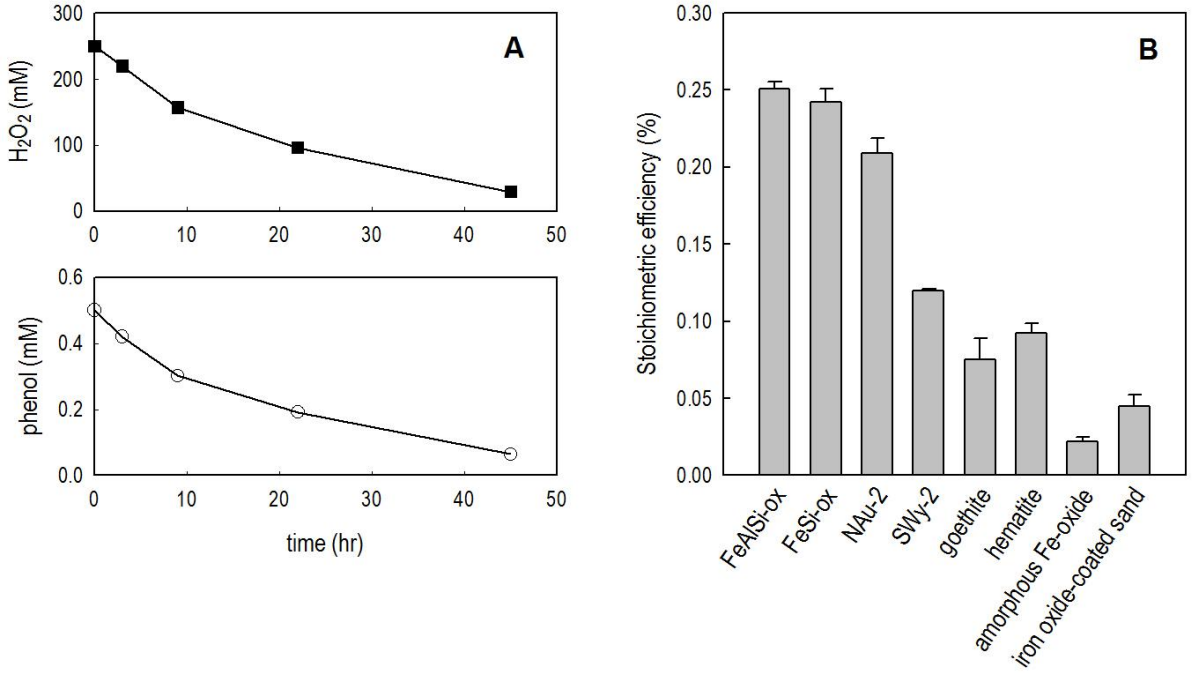


**Figure 3-1**. **(A)**: A representative example of $H_2O_2$ decomposition and phenol transformation. [NAu-2] = 5 g/L, pH = 8.4 ± 0.1, [borate] = 2 mM. **(B)**: Stoichiometric efficiency ($\Delta$[phenol]/$\Delta[H_2O_2]$ × 100%) with different iron-containing minerals. $[H_2O_2]_0$ = 250 mM, $[phenol]_0$ = 0.5 mM, [FeSi-ox] = [FeAlSi-ox] = 10 g/L, [NAu-2] = 5 g/L, [Swy-2] = 10 g/L, [hematite] = [goethite] = 10 g/L, [FeOOH] = 1 g/L, [Fe-coated sand] = 10 g/L, pH = 8.4 ± 0.1.

*b. Aquifer materials*

The catalytic activity of aquifer materials with respect to $H_2O_2$ activation was investigated using an approach similar to that employed for iron-containing minerals. In the aquifer materials/$H_2O_2$ systems, phenol and $H_2O_2$ loss by dissolved metal-catalyzed reactions were negligible compared with those catalyzed by the surface of the materials[1]. Phenol loss was attributable mainly to oxidation by $^{\bullet}OH$, as no phenol loss was observed in the presence of 100 mM tert-butanol or in the absence of $H_2O_2$. This also suggests that phenol loss in the presence of

[1] In experiments with aquifer materials, metals can be released into solution by the dissolution of minerals or exchange process. Therefore, control experiments were performed to evaluate the contribution of dissolved metals to the decomposition of $H_2O_2$ and the transformation of phenol. In brief, a sample was suspended in pH 8.5 solution (buffered with 10 mM borate) for 24 hrs. The solid was then separated by centrifugation and the supernatant was filtered through a 0.2 micron filter. To this filtered supernatant, aliquots of $H_2O_2$ and phenol were added, resulting in a solution containing 5 mM $H_2O_2$ and 0.05 mM phenol. Phenol and $H_2O_2$ loss in this solution were then monitored for 48 hrs. In all experiments, phenol and $H_2O_2$ loss were always less than 5%, indicating that the $H_2O_2$ and phenol loss observed in the presence of aquifer materials were catalyzed mainly by materials surface and not by dissolved metals.

$H_2O_2$ was not due to a biological transformation reaction. Note that aquifer materials were not sterilized and, therefore, it is possible that some of the $H_2O_2$ was decomposed by enzymes.

The stoichiometric efficiency of phenol oxidation for aquifer materials (Figure 3-2B) spanned the range observed with iron minerals (Figure 3-1B), with a stoichiometric efficiency of 0.28% with the KENTK sample and 0.005% with the WYLAM sample (Figure 3-2B). The KENTK sample was tested at a pH value of 7.2, which was lower than the pH values used for the other materials. Previous experiments have shown that the stoichiometric efficiency increases as pH decreases [93].

As observed for the iron-containing minerals, the stoichiometric efficiency was in general inversely correlated with the rate of $H_2O_2$ decomposition (Figure 3-2A and 3-2B), with samples that were more reactive toward $H_2O_2$ decomposition exhibiting lower stoichiometric efficiencies. A similar relationship between $H_2O_2$ decomposition rates and $^{\bullet}OH$ yields was reported by Petigara *et al.* [31], who postulated the existence of two competing $H_2O_2$ decomposition pathways, with the pathway that does not produce $^{\bullet}OH$ being more important in soils with higher $H_2O_2$ decomposition rates.

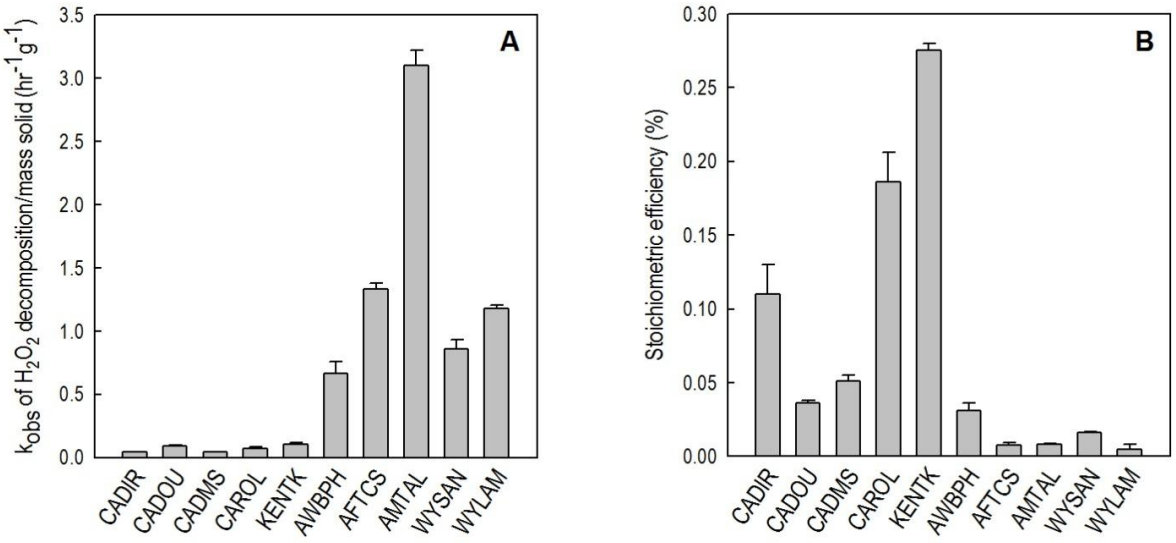


**Figure 3-2.** Mass-normalized observed-first order rate constants for $H_2O_2$ decomposition (A) and stoichiometric efficiency (B) with aquifer materials. $[H_2O_2]_0$ = 250 mM, $[phenol]_0$ = 0.5 mM, [solid] was either 150 g/L (for CADIR, CADOU and CADMS) or 50 g/L (for all other aquifer materials), [borate] = 10 mM, pH = 8.2 – 8.7, except in experiments with KENTK, in which the pH was 7.2 (see Table 3-2). The observed-first order rate constants ($k_{obs}$) were obtained by fitting the experimental data to the first order decay reaction rate law. The $r^2$ values of the fittings were always $r^2 > 0.99$.

The reactivity of aquifer materials with $H_2O_2$ is likely related to their physico-chemical properties, especially the iron and manganese oxide content. To provide insight into the relative importance of iron and manganese oxides in $H_2O_2$ activation, we investigated the relationship between the amount of these oxides in the samples and the rates of $H_2O_2$ loss and yields of $^{\bullet}OH$. The decomposition of $H_2O_2$ on iron and manganese oxides has been widely reported to exhibit a first order dependence on both $H_2O_2$ and the surface area of oxides (for example, the results of Lin and Gurol [24], Valentine and Wang [6], Teel *et al.* [98]). In the current study, a first order dependence of the $H_2O_2$ loss rate on $[H_2O_2]$ was also observed in all experiments (Table 3-1 and Figure 3-2A). As such, the rate of $H_2O_2$ loss in the aquifer materials systems can be described as:

$$\frac{d[H_2O_2]}{dt} = - k_{obs} \times [H_2O_2] = - (k_{Fe\text{-}ox} \times [Fe\text{-}ox] + k_{Mn\text{-}ox} \times [Mn\text{-}ox]) \times [H_2O_2] \qquad (3.4)$$

In this expression, the rate constants for the reactions between $H_2O_2$ and iron and manganese oxides (*i.e.*, Fe-ox and Mn-ox) are $k_{Fe\text{-}ox}$ and $k_{Mn\text{-}ox}$, respectively. Because $H_2O_2$ decomposition is a surface-catalyzed process, [Fe-ox] and [Mn-ox] in equation (3.4) should represent the concentration of Fe and Mn accessible at the surface. This is not necessary the same as the bulk concentration of Fe and Mn that would be measured by digesting aquifer materials sample with a strong acid.

A least-square multiple regression was performed on the mass-normalized value of $k_{obs}$ ($hr^{-1}g^{-1}$), [total-Mn] and [total-Fe] (mg/g) to obtain $k_{Fe\text{-}ox}$ and $k_{Mn\text{-}ox}$ in equation (3.4). (The bulk concentrations of Fe and Mn were used instead of the surface concentrations, because it is expected that there would be no unique surface concentration of Fe and Mn in a heterogeneous aquifer materials sample). This regression yielded $k_{Fe\text{-}ox} = - 0.005 \pm 0.010$ ($hr^{-1}mg^{-1}$), $k_{Mn\text{-}ox} = 2.900 \pm 0.335$ ($hr^{-1}mg^{-1}$), and an $r^2$ value for the regression of 0.95.

Independent linear regressions between the mass-normalized $k_{obs}$ and either [total-Fe] or [total-Mn] were also performed. The results of the regressions showed a weak correlation between $k_{obs}$ and [total-Fe] (*i.e.*, $k_{obs} = (0.056 \pm 0.02) \times$ [total-Fe], $r^2 = 0.47$), and a relatively strong correlation between $k_{obs}$ and [total-Mn] (*i.e.*, $k_{obs} = (2.780 \pm 0.218) \times$ [total-Mn], $r^2 = 0.95$) (Figure 3-3A and 3-3B). Furthermore, the $k_{Mn\text{-}ox}$ value obtained from the linear regression (*i.e.*, $2.780 \pm 0.218$ $hr^{-1}mg^{-1}$) was nearly identical to the value obtained from the least-square multiple regression (*i.e.*, $2.900 \pm 0.335$ $hr^{-1}mg^{-1}$), indicating that the $H_2O_2$ loss rate in aquifer materials systems could be described without including loss of $H_2O_2$ on the iron oxides. This result suggests that the manganese oxides are much more important than the iron oxides to $H_2O_2$ decomposition in aquifer materials systems, despite the fact that the aquifer materials contained 16 to 185 times more Fe than Mn (Table 3-2).

No clear correlation was observed between the stoichiometric efficiency (E) and [total-Fe] (Figure 3-3C). In contrast, the efficiency was inversely proportional to [total-Mn], with samples having [total-Mn] above 200 mg/kg exhibiting efficiencies lower than 0.03%, while those having [total-Mn] less than 200 mg/kg exhibiting efficiencies that ranged from 0.036% to 0.28% (Figure 3-3D). The trend between E and [total-Mn] is consistent with the fact that $^{\bullet}OH$ is not produced when $H_2O_2$ is decomposed on manganese oxides.

In brief, the above analysis indicated that in aquifer materials systems, both the rates of $H_2O_2$ decomposition and stoichiometric efficiency are correlated with [total-Mn]. Therefore, the Mn content of aquifer samples might be used to make a preliminary comparison of the kinetics and efficiency of $H_2O_2$-based ISCO systems for different for aquifer materials.

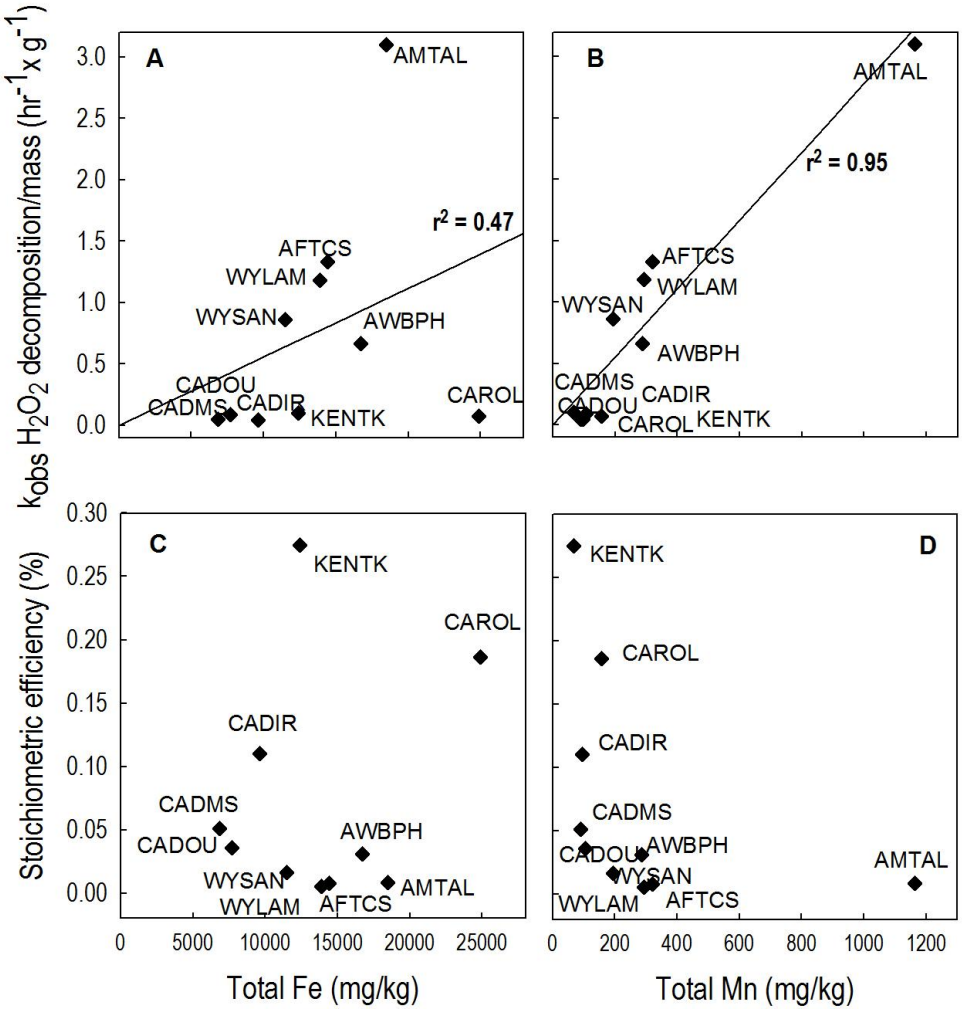


**Figure 3-3.** Correlation between $H_2O_2$ decomposition rate (A and B), stoichiometric efficiency (C and D) and the total Fe and Mn of aquifer samples. The top and bottom figures share the same x-axis.

Previous research indicated that, in addition to manganese and iron oxides, natural organic matter could also affect $H_2O_2$ decomposition, because natural organic matter associates with the surface of aquifer materials and directly affects their reactivity toward $H_2O_2$ decomposition. The presence of natural organic matter has the potential to decreases stoichiometric efficiency because it can act either as an $^{\bullet}OH$ scavenger or as an absorptive phase that slows contaminant oxidation by preventing the $^{\bullet}OH$ from reacting with the contaminant. There is, however, no consensus observation on the effect of natural organic matter on the rate of $H_2O_2$ decomposition in soils. Valentine and Wang [6], Crimi and Siegrist [99] and Bissey *et al.* [100] reported that the rate of $H_2O_2$ decomposition was inversely correlated with the amount of organic matter. In contrast, Xu and Thomson [76] observed that materials with high organic carbon content were more reactive with $H_2O_2$. Regarding stoichiometric efficiency, Valentine and Wang [6] showed that addition of humic acid to the goethite/$H_2O_2$ system resulted in an overall increase in stoichiometric efficiency. A similar efficiency enhancement was reported by Huling *et al.* [28], who observed that a soil slurry that had been amended with peat was more effective than the original counterpart in activating $H_2O_2$. In contrast, Petigara *et al.* [31] reported that low $^{\bullet}OH$ yields were associated with soils that contained more organic matter. In our study, there was no clear correlation between organic carbon content (TOC in Table 3-2) and $k_{obs}$ or E (Figure 3-4).

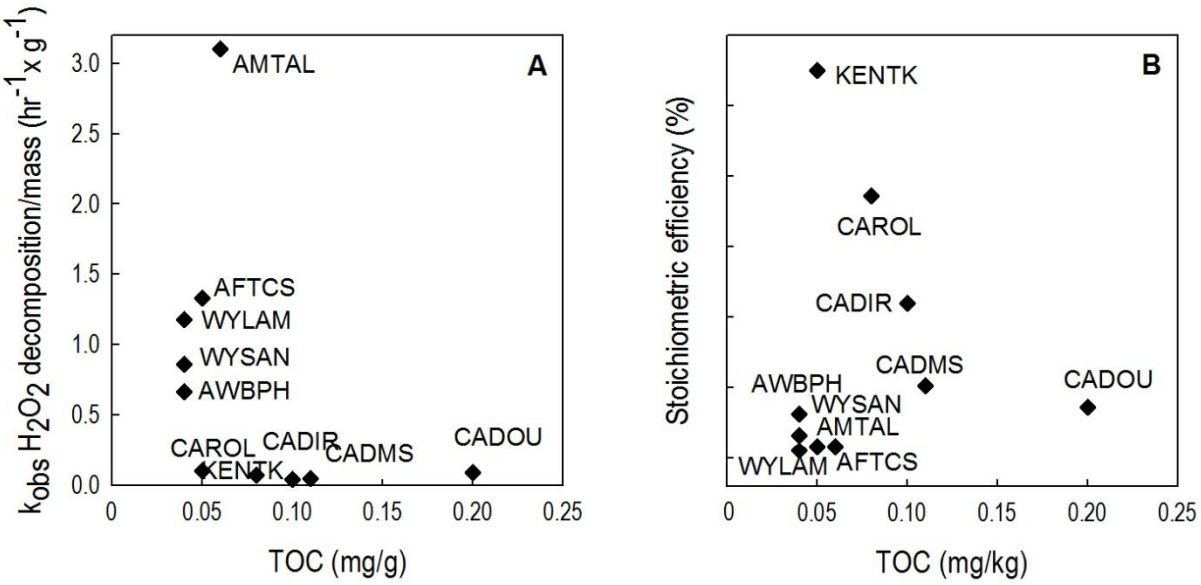


**Figure 3-4.** Correlation between $H_2O_2$ decomposition rate (A), stoichiometric efficiency (B) and the TOC content of aquifer samples.

### 3.3.2 Stoichiometric efficiency enhancement by citrate-bicarbonate-dithionite extraction

Relatively low stoichiometric efficiencies were observed with iron oxides (especially amorphous iron oxide, section 3.3.1.a) and with aquifer materials that contained high concentrations of manganese oxides (section 3.3.1.b). We hypothesized that removing these oxides would improve $^{\bullet}OH$ yield in the aquifer material systems. To test this hypothesis, 6 aquifer samples (CADIR, CADOU, AWBPH, AFTCS, WYLAM, and WYSAN) were treated with citrate-bicarbonate-dithionite (CBD) solution to remove iron and manganese oxide coatings and discrete particles attached to the surface of aquifer materials. The amount of CBD-extractable Fe and Mn in these materials is reported in Table 3-2 as CBD-Fe and CBD-Mn.

The rates of $H_2O_2$ loss were much slower on the CBD-treated samples than on the original counterparts (Figure 3-5A). Moreover, CBD-treated samples were more effective in converting $H_2O_2$ into $^{\bullet}OH$ (Figure 3-5B). The extent of the improvement in stoichiometric efficiency varied among samples. For example, the CBD-treated SDIR9 sample ($E = 0.15 \pm 0.01\%$) was only 1.3 times more effective than the original SDIR9 sample ($E = 0.11 \pm 0.02\%$). In contrast, the CBD-treated AFTCS, WYSAN and WYLAM samples were 10 to 40 times more effective. The extent of improvement in $^{\bullet}OH$ yield appeared to correlate with the fraction of Mn removed by CBD treatment (over 50% of the total Mn in AFTCS, WYSAN and WYLAM was CBD-extractable Mn, Table 3-2). A previous study [37] demonstrated that removing Mn-oxide by treating a sediment sample with $NH_2OH/HCl$ also increased the stoichiometric efficiency by over 3 times. Although injecting CBD or $NH_2OH/HCl$ solution into the subsurface is unlikely to be practical, employing conditions that favor the release of iron and manganese oxides, such as adjusting redox conditions to favor reductive dissolution or adding a strong chelating agent during soil washing, could enhance $^{\bullet}OH$ yield in $H_2O_2$-based ISCO treatment systems.

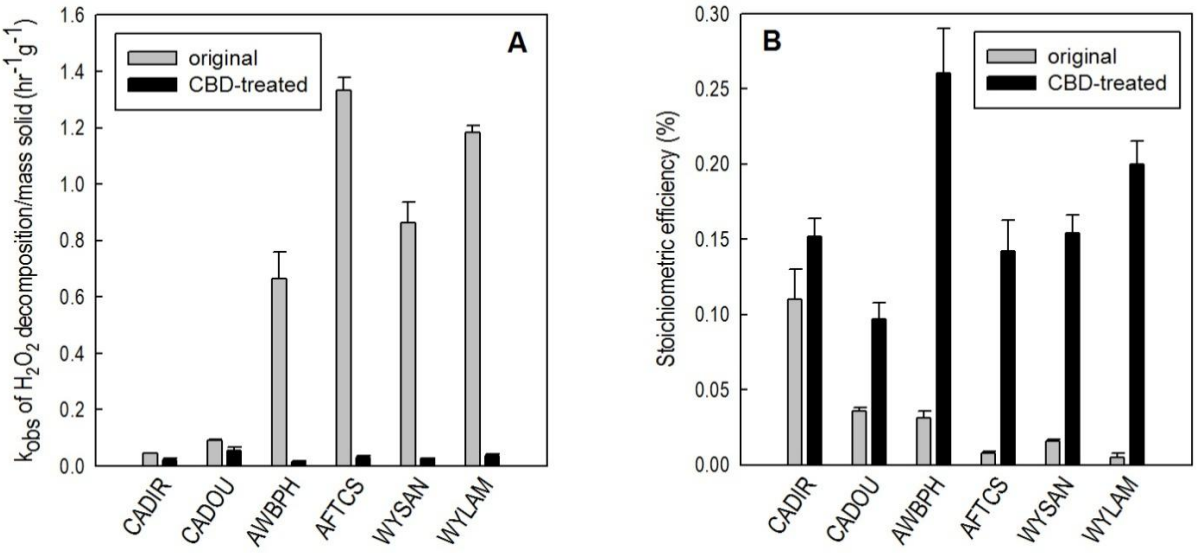


**Figure 3-5.** Mass-normalized observed-first order rate constants for $H_2O_2$ decomposition (A) and stoichiometric efficiency (B) with original and CBD-treated aquifer materials. Experimental conditions were similar to those described in the capture of Figure 3-2.

### 3.3.3 Effect of dissolved silica on the rate of $H_2O_2$ decomposition and stoichiometric efficiency with aquifer materials

In $H_2O_2$-based ISCO, the rate of $H_2O_2$ decomposition and the yield of $^{\bullet}OH$ are controlled by both the properties of the aquifer minerals and the groundwater composition (*e.g.*, pH, the presence of naturally occurring solutes, such as dissolved silica, bicarbonate or phosphate). In our study (to be reported in Chapter 4) [101], we observed that dissolved $SiO_2$ slows the rate of $H_2O_2$ decomposition on iron- and manganese-containing minerals, because dissolved $SiO_2$ adsorbs onto mineral surfaces and decreases their catalytic reactivity. To determine whether dissolved $SiO_2$ has a similar effect on $H_2O_2$ activation in ISCO systems, we measured the rate of $H_2O_2$ decomposition and $^{\bullet}OH$ yield for aquifer minerals in the presence and absence of dissolved $SiO_2$. Our results indicated that 2 mM of dissolved $SiO_2$ slowed $H_2O_2$ decomposition by approximately 25 to 60% (Figure 3-6). For the three samples exhibiting the highest stoichiometric efficiencies (*i.e.*, CADIR, CAROL and KENTK), the presence of dissolved $SiO_2$ did not affect the efficiency (inset of Figure 3-6). These results suggest that dissolved $SiO_2$ in groundwater is beneficial for $H_2O_2$-based ISCO because it can increase $H_2O_2$ persistence in the subsurface. Furthermore, injecting dissolved $SiO_2$ together with $H_2O_2$ could further improve $H_2O_2$ persistence, without compromising $^{\bullet}OH$ yield.

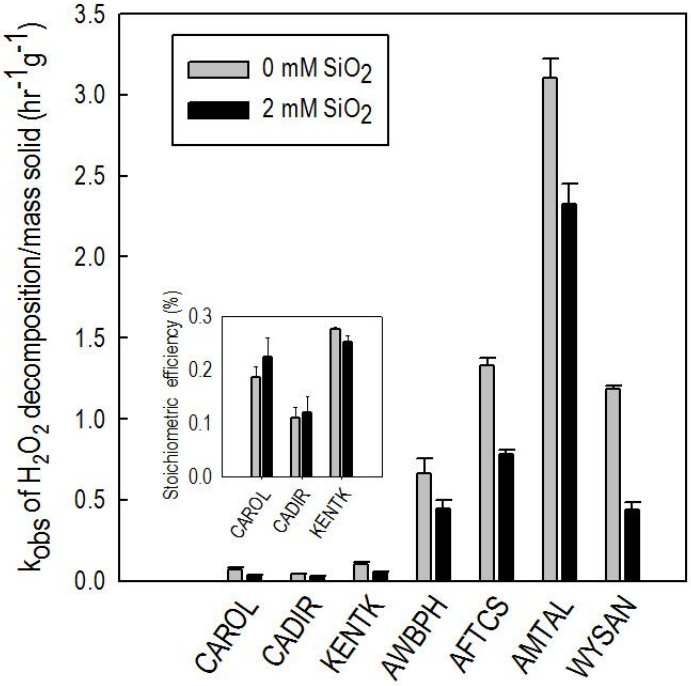


**Figure 3-6.** Effect of dissolved $SiO_2$ on the rate of $H_2O_2$ decomposition by aquifer materials and stoichiometric efficiency (inset). $[SiO_2]$ = 2 mM, $[H_2O_2]_0$ = 250 mM, $[phenol]_0$ = 0.5 mM, [solid] was either 150 g/L (SDIR9) or 50 g/L (all other aquifer materials), [borate] = 10 mM, pH = 8.2 – 8.5.

## 3.4 Conclusions

The findings presented in this study have important implications for the design and operation of $H_2O_2$-based *in situ* chemical oxidation systems employed for soil and groundwater remediation. They also provide insights into the design of better iron catalysts for *ex situ* waste treatment systems. Major findings and their implications are summarized below:

1. The coordination of iron in the solid affects its reactivity with respect to $H_2O_2$ activation. Due to the coordination between Fe and Al and/or Si, surfaces comprising mixed phases of Fe, Al and Si oxides (*e.g.*, iron-containing aluminosilicate minerals, FeSi-ox and FeAlSi-ox catalysts) were more effective in converting $H_2O_2$ into $^{\bullet}OH$ than the surfaces of pure iron oxides. Therefore, silica- and alumina-containing iron oxides have the potential to be more effective than iron oxides in *ex situ* treatment systems.

2. Surfaces that were more reactive with $H_2O_2$ tend to be less effective in producing $^{\bullet}OH$. Although fast $H_2O_2$ decomposition expedites contaminant removal, this might compromise $^{\bullet}OH$ yield which, in turn, requires disproportionately more $H_2O_2$. This should be considered in the design of catalysts for *ex situ* treatment systems.

3. Aquifer materials that contain high concentrations of manganese oxides decomposed $H_2O_2$ at a faster rate but generated less $^{\bullet}OH$ (*i.e.*, they had a lower stoichiometric efficiency). The strong correlation between Mn content and $H_2O_2$ loss rate and $^{\bullet}OH$ yield suggests that the amount of Mn in aquifer materials could serve as a proxy for predicting $H_2O_2$ activation rates and contaminant oxidation efficiency. Additional research with more aquifer materials is needed to assess the predictive strength of this correlation.

4. Removing free iron and manganese oxides from aquifer materials slows $H_2O_2$ decomposition and increases $^{\bullet}OH$ yield. Although the addition of citrate-bicarbonate-dithionite solution into soil and groundwater is unlikely to be practical, other approaches that remove manganese and iron oxides could enhance the efficiency of $H_2O_2$-based ISCO.

5. In aquifer materials systems, dissolved $SiO_2$ slows the $H_2O_2$ decomposition rate without affecting $^{\bullet}OH$ yields. Therefore, during ISCO remediation, dissolved $SiO_2$ could be injected into the subsurface to increase the persistence of $H_2O_2$. Dissolved $SiO_2$ is inexpensive and benign and could replace phosphate as a $H_2O_2$ stabilizing reagent. In *ex situ* treatment systems that employ iron catalysts, dissolved silica might result in gradual loss in catalyst reactivity.

# Chapter 4. Inhibitory Effect of Dissolved Silica on $H_2O_2$ Decomposition by Iron(III) and Manganese(IV) Oxides: Implications for $H_2O_2$-based In Situ Chemical Oxidation

Reproduced with permission from Pham, A.L.T; Doyle, F.M.; Sedlak, D. L. Inhibitory Effect of Dissolved Silica on the $H_2O_2$ Decomposition by Iron(III) and Manganese(IV) Oxides: Implications for $H_2O_2$-based In Situ Chemical Oxidation. *Environmental Science & Technology* **2012**, *46*, 1055-1062.

## 4.1 Introduction

The injection of oxidants into the subsurface is a widely used approach for remediating soils and groundwater contaminated with organic compounds. This method, known as *In Situ* Chemical Oxidation (ISCO), is attractive because it requires less infrastructure investment and has lower maintenance and operation cost than pump-and-treat remediation [10]. Furthermore, the relatively fast production of oxidants expedites completion of site remediation.

Among various oxidants employed in ISCO (*i.e.*, permanganate, hydrogen peroxide, ozone and persulfate) [10], hydrogen peroxide ($H_2O_2$) is probably the most widely used, because it is relatively inexpensive, easy to transport and introduce into the subsurface, and the byproducts of $H_2O_2$ decomposition, namely $O_2$ and $H_2O$, are benign. $H_2O_2$-based ISCO technologies rely on the conversion of $H_2O_2$ into hydroxyl radical ($^{\bullet}OH$), either by reactions with subsurface materials (*e.g.*, iron-containing clays and minerals) or by reactions with dissolved ferrous ions that are sometimes co-injected with $H_2O_2$ [7, 10]. However, the rapid loss of $H_2O_2$ upon injection is often problematic because $H_2O_2$ may decompose before it reaches contaminated zones [10, 41]. Consequently, a large excess of $H_2O_2$ is often used and injection wells have to be constructed immediately proximate to contaminated areas.

The rate at which $H_2O_2$ decomposes and the fraction of the $H_2O_2$ converted into $^{\bullet}OH$ depends upon the composition of the aquifer materials and groundwater. Iron oxides (*e.g.*, ferrihydrite or goethite) convert $H_2O_2$ into $^{\bullet}OH$ through a surface-initiated chain reaction analogous to the Haber-Weiss mechanism [7, 30, 93]. Iron oxides also can convert $H_2O_2$ directly into $O_2$ and $H_2O$ via two-electron transfer mechanisms [31, 93]. In contrast, manganese oxides do not generate $^{\bullet}OH$ when they decompose $H_2O_2$ [31, 44]. In the subsurface, $H_2O_2$ can also be decomposed by enzymes (*e.g.*, catalases and peroxidases) via pathways that also do not produce $^{\bullet}OH$ [31]. Conversely, the presence of phosphate [102] or metal-complexing ligands, such as citrate and phytate [42], enhance the stability of $H_2O_2$ because they can bind metals and decrease their reactivity. The efficacy of $H_2O_2$-based ISCO, therefore, depends on the $H_2O_2$ persistence as well as the pathways through which it is decomposed, because only those that produce $^{\bullet}OH$ will be beneficial for oxidative contaminant removal. A thorough understanding of how different subsurface components affect the decomposition of $H_2O_2$ will, therefore, help to predict its fate and could lead to an ability to improve the performance of $H_2O_2$-based ISCO.

The aim of this research was to investigate the effect of dissolved $SiO_2$ on the rate of $H_2O_2$ decomposition catalyzed by different types of iron- and manganese- containing materials. Depending on local geology, groundwater can contain dissolved $SiO_2$ at concentrations ranging from 5 mg/L to 85 mg/L (*i.e.*, 0.08 – 1.42mM $SiO_2$) [103]. Although dissolved $SiO_2$ adsorbs on the surface of iron oxides [77, 104] and $SiO_2$ is known to act as a corrosion inhibitor, its effect on $H_2O_2$ decomposition in the subsurface, to the best of our knowledge, has not been investigated previously. Therefore, the rate of $H_2O_2$ decomposition on goethite, hematite, amorphous iron oxyhydroxide, iron-coated sand, montmorillonite and pyrolusite was studied in solutions containing various amount of dissolved $SiO_2$ (*i.e.*, 0 – 1.5 mM $SiO_2$). The effect of dissolved $SiO_2$ on the overall $^{\bullet}OH$ yield, defined as the percentage of decomposed $H_2O_2$ producing $^{\bullet}OH$, was also investigated. The implications of our study toward $H_2O_2$-based ISCO are discussed.

## 4.2 Materials and methods

### 4.2.1 Chemicals

Amorphous iron oxyhydroxide (*i.e.*, FeOOH) was obtained from Aldrich, while pyrolusite (β-$MnO_2$) was obtained from Fisher. Wyoming montmorillonite (Swy-2, 31.8 $m^2/g$, 2.59 wt% Fe) was obtained from the Source Clays Repository (The Clay Minerals Society). All other chemicals were reagent grade from Fisher Scientific and were used without further purification.

Goethite and hematite were synthesized following procedures reported in the literature [84] and their identity was verified by X-ray diffraction. Briefly, goethite was synthesized by aging freshly made ferrihydrite in a strong alkaline solution (NaOH) at 70ºC for 60 hours. Hematite was synthesized using the same method except that the aging was conducted at pH 8 – 8.5 in the presence of $NaHCO_3$ at 90ºC for 48 hours. Amorphous FeOOH 50 – 80 mesh was ground using a mortar and pestle prior to sieving through a 150 micron sieve.

The surface area of these solids, determined using the 5 point BET (Brunauer–Emmett–Teller) nitrogen physisorption method, was 22 $m^2/g$ for hematite, 19 $m^2/g$ for goethite, 166 $m^2/g$ for FeOOH, and less than 1 $m^2/g$ for $MnO_2$. Iron-coated sand (1 wt% Fe, 4.8 $m^2/g$) was kindly provided by Peter Nico (Lawrence Berkeley National Laboratory). Synthesis and characterization of iron-coated sand are reported elsewhere [95].

A stock solution of 15 mM silica was prepared daily from $Na_2SiO_3.9H_2O$. For simplicity, all species of dissolved silica (*e.g.*, $H_4SiO_4$, $H_3SiO_4^-$ and polymeric silica) are denoted as $SiO_2$. All solutions were prepared using 18 MΩ Milli-Q water from a Millipore system.

### 4.2.2 Experimental setup

All experiments were carried out at 25 ± 1ºC in the dark in a 50-mL polypropylene flask open to the atmosphere. The temperature was controlled with a water bath. The pH of solutions was buffered with 1 mM piperazine-N,N'-bis(ethanesulfonic acid) (PIPES) for pH 7 or 4 mM borate for pH 8 – 9. The ionic strength of the solutions was maintained with 0.1 M $NaNO_3$. The pH was measured throughout each experiment and was adjusted when it deviated from the initial value by more than 0.1 unit. Experiments were conducted at least in triplicate and average values along with one standard deviation are presented.

*Adsorption of dissolved $SiO_2$ by the solids.* Silica was added from a 15 mM stock solution to the buffered solutions and the pH was adjusted with 1 M NaOH or 0.5 M $H_2SO_4$. To minimize the polymerization and avoid $SiO_{2(s)}$ precipitation, $SiO_2$ concentrations never exceeded 1.5 mM [105]. Next, a solid (*i.e.*, iron oxide, iron coated sand, Swy-2 or pyrolusite) was added to the solution and the pH again was adjusted if necessary. Samples were withdrawn at pre-determined time intervals. Within 5 minutes, the solid was separated by centrifugation, then the

supernatant was filtered immediately through a 0.2-μm nylon filter and analyzed for dissolved $SiO_2$.

*$H_2O_2$ decomposition and phenol oxidation.* The decomposition of $H_2O_2$ catalyzed by the solids was investigated in the absence and presence of dissolved $SiO_2$. Prior to the addition of $H_2O_2$, suspensions were mixed for 24 hours to equilibrate the solids with $SiO_2$. All experiments with iron-containing minerals were performed in pH 7 ± 0.1 solutions. Experiments with β-$MnO_2$ were conducted at pH 8.4 because the 1 mM PIPES buffer was ineffective at pH 7.0. At pH 8.4, the pH never changed by more than 0.1 units during the experiments.

To investigate the effect of dissolved $SiO_2$ on $^{\bullet}OH$ production, the transformation of 0.2 mM phenol in the goethite/$H_2O_2$ system was studied. Phenol was chosen as a model target contaminant because it is not significantly adsorbed by any of the solids and reacts with $^{\bullet}OH$ at a near-diffusion controlled rate. Samples were withdrawn at predetermined time intervals and divided into two parts. In the first aliquot, the solids were separated by centrifugation followed by filtration and the solution was analyzed for $H_2O_2$. Acetonitrile was added to the second aliquot (acetonitrile:sample = 1:1) and the mixture was agitated vigorously for 2 minutes with a vortex mixer to extract any adsorbed phenol from the solids. The solids were then separated by centrifugation and filtration and the solution was analyzed for phenol. Phenol recovery by acetonitrile extraction was always above 98% in $H_2O_2$-free controls. The stoichiometric efficiency, defined as the amount of phenol transformed per mole of hydrogen peroxide decomposed (*i.e.*, $E = \frac{\Delta[phenol]}{\Delta[H_2O_2]} \times 100\%$) [93], was used to evaluate the effect of dissolved $SiO_2$ on $^{\bullet}OH$ production.

### 4.2.3 Analytical methods

Phenol was analyzed using HPLC as described previously [93]. $H_2O_2$ was analyzed spectrophotometrically by the titanium sulfate method [85]. An inductively coupled plasma optical emission spectrometer (ICP-OES) was used to measure dissolved $SiO_2$; all results are reported in molar based on the $SiO_2$ formula. Total dissolved iron was quantified using the 1,10-phenanthroline method [86] after adding hydroxylamine hydrochloride to the filtered samples. The concentration of dissolved iron was always below the detection limit (*i.e.*, 5 μM).

Goethite surfaces, pre-equilibrated with $SiO_2$ solutions, were examined with a Philips CM200/FEG transmission electron microscope coupled with an energy dispersive X-ray (EDX). The instrument was operated in scanning mode (STEM/EDX) with a probe size of 1.4 nm. Samples for STEM/EDX analysis were prepared as follows: after the adsorption experiment, the solid was collected by centrifugation and then resuspended in 2 mL fresh Milli-Q water. An aliquot of this suspension was spread on the copper grid, the excess water was gently removed with a Kimwipe tissue and the grid was dried under air at room temperature.

## 4.3 Results

### 4.3.1 Silica adsorption

The rate of silica adsorption onto goethite, hematite and Swy-2 in pH 7 solutions with different $[SiO_2]_{initial}$ was investigated. In all cases, $SiO_2$ adsorption approached equilibrium within 24 hours (inset of Figure 4-1 and Figure 4-2). Therefore, $SiO_2$ adsorption as a function of $[SiO_2]_{initial}$ was measured after a 24-hour equilibration period. This equilibration period was also employed in the study of $H_2O_2$ decomposition and phenol transformation.

Higher initial $SiO_2$ concentrations resulted in more $SiO_2$ adsorption onto goethite (Figure 4-1). Except for the last data point in Figure 4-1 ($[SiO_2]_{equilibrium}$ = 1.14 mM), the adsorption isotherm followed a Langmuir-type isotherm, with a maximum adsorption density ($\Gamma_{SiO2}$) of approximately 0.062 mmol $SiO_2$/g goethite (Figure 4-1). At $[SiO_2]_{equilibrium}$ = 1.14 mM, the amount $SiO_2$ sorbed was significantly higher (0.09 mmol $SiO_2$/g goethite).

STEM/EDX analysis indicated that $SiO_2$ was not uniformly adsorbed on the goethite surface. For example, EDX spectra of a goethite sample that was pre-equilibrated with 0.5 mM $SiO_2$ for 24 hours showed that the surface elemental composition varied among locations (Figure 4-3), with Si peaks not observed in some locations (Figure 4-3a), co-occurring with iron in others (Figure 4-3b) and existing in the absence of an iron peak in others (Figure 4-3c). The fraction of sites that were fully coated with Si (*i.e.*, sites having EDX spectra similar to that of Figure 4-3c) increased as the $[SiO_2]_{initial}$ increased.

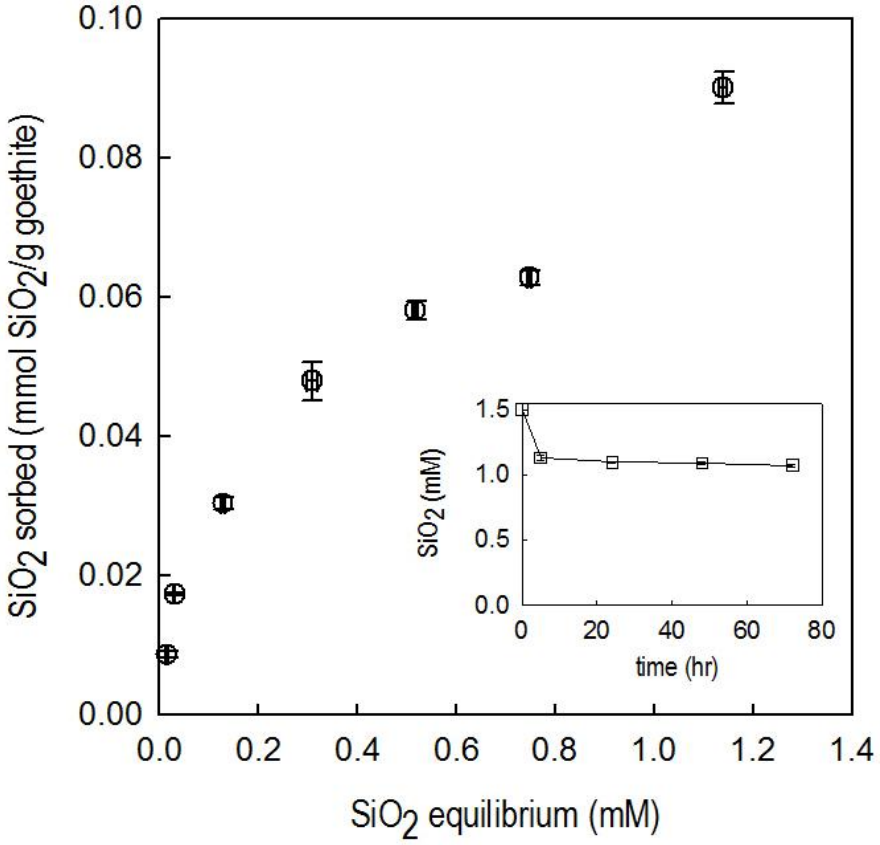


**Figure 4-1**. Adsorption isotherm (24 hour equilibration) of dissolved $SiO_2$ on goethite. [goethite] = 4 g/L, [PIPES] = 1 mM, [$NaNO_3$] = 0.1 M, pH = 7. $[SiO_2]_{initial}$ = 0 – 1.5 mM (inset: adsorption kinetics).

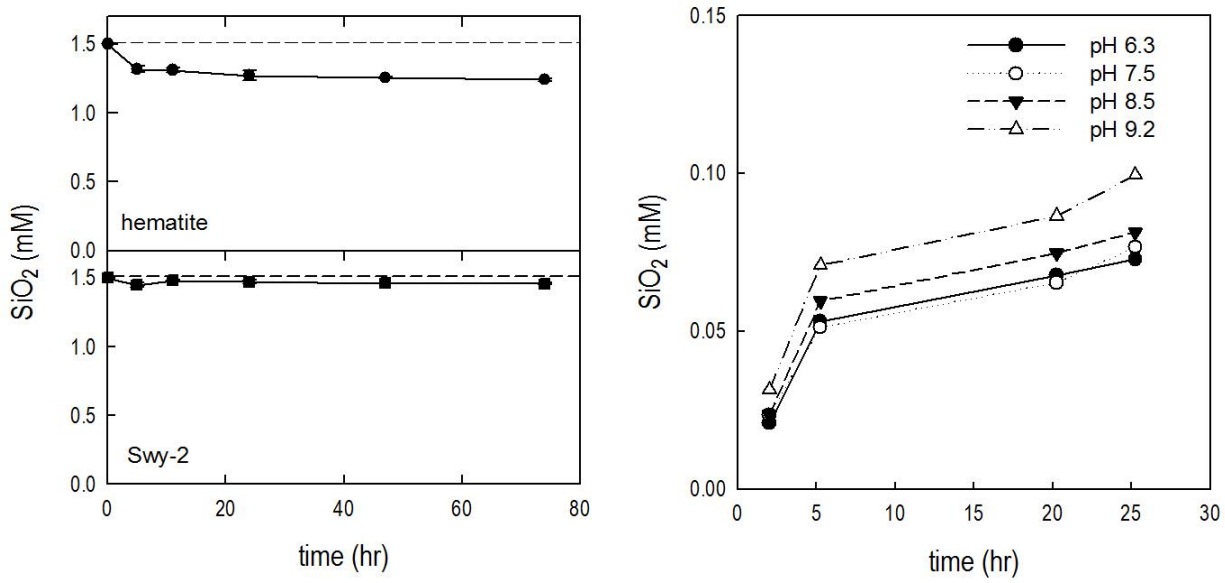


**Figure 4-2. (Left):** Silica adsorption on hematite and Swy-2 montmorillonite. pH = 7, buffered by [PIPES] = 1 mM; [$NaNO_3$] = 0.1 M; [hematite] = 3 g/L, [Swy-2] = 4 g/L; [ [$SiO_2$] = 1.5 mM. Note: The results with Swy-2 may underrepresent the $SiO_2$ adsorption capacity of Swy-2 because this aluminosilicate mineral contains 62.9 wt. % of $SiO_2$, which introduces additional dissolved $SiO_2$ into the solution. For example, control experiments indicated that up to 0.07 mM $SiO_2$ was released when 4 g/L Swy-2 was suspended in a pH 7.5 solution for 24 hours (**Right**). Therefore, measuring $SiO_2$ in the supernatant could underestimate the actual amount of $SiO_2$ associated with the mineral surface. The results presented here, however, indicate that dissolved $SiO_2$ is adsorbed onto Swy-2, as the $SiO_2$ concentration decreased upon contacting with Swy-2.

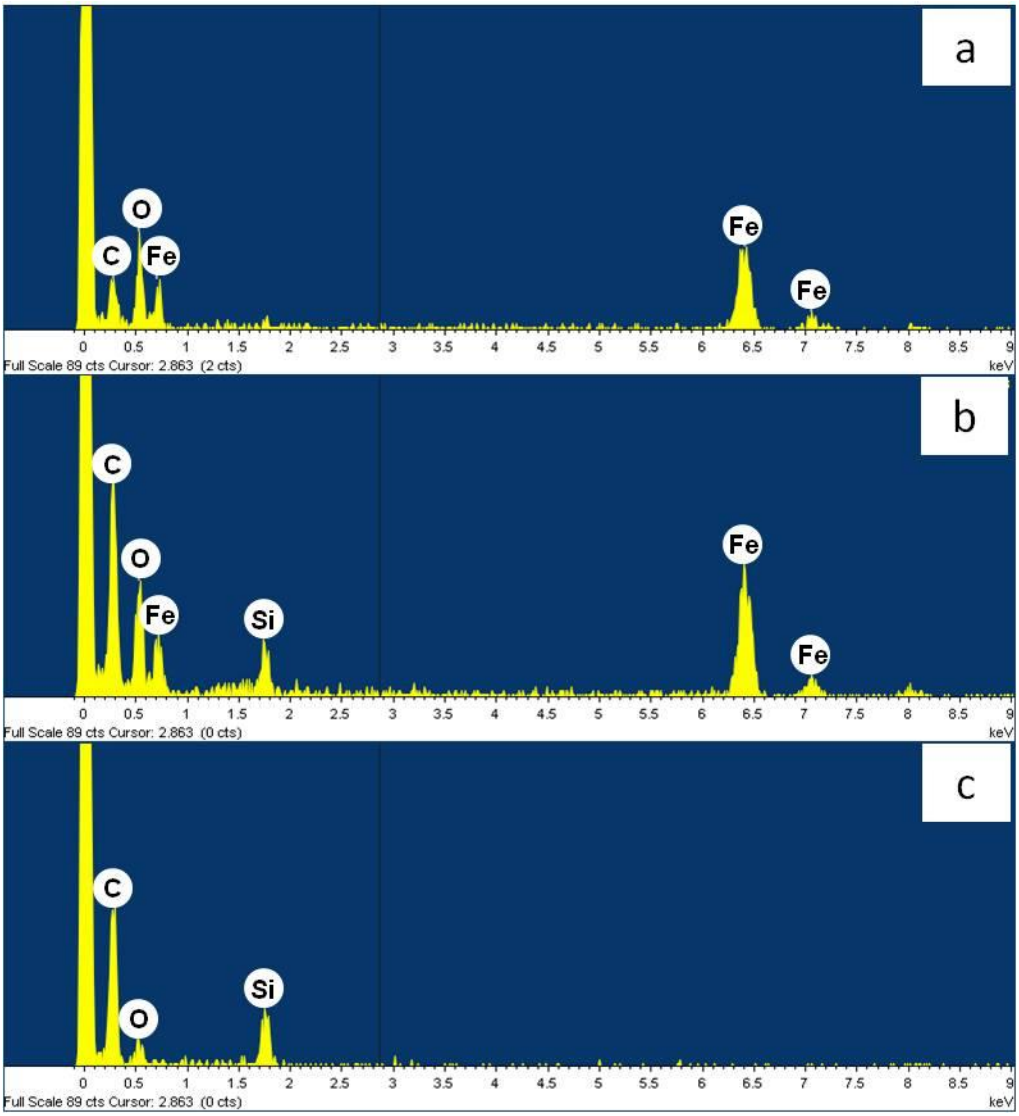


**Figure 4-3**. EDX spectra from three different locations on a goethite surface that was pre-equilibrated with 0.5 mM dissolved silica solution for 24 hours. Carbon peaks come from the grid support.

### 4.3.2 $H_2O_2$ decomposition and phenol transformation

In the $SiO_2$-free system, the half-life of 5 mM $H_2O_2$ in the presence of 4 g/L goethite was 7.77 ± 0.34 hr (Table 4-1). Addition of dissolved $SiO_2$ slowed the rate of $H_2O_2$ decomposition, increasing the $H_2O_2$ half-life to 21.7 ± 1.2 hr and 28.2 ± 1.8 hr at an $[SiO_2]_{initial}$ of 0.5 mM and 1.5 mM, respectively (Table 4-1 and Figure 4-4a). The half-life of $H_2O_2$ in the presence of $[SiO_2]_{initial}$ = 1.5 mM was comparable to that observed in a solution containing 2 mM phosphate ($t_{1/2}$ = 31.6 ± 1.4 hr, Table 4-1). Under the experimental conditions employed in this study, the $H_2O_2$ decomposition rate was limited by the intrinsic chemical reactivity of the solids and not by diffusion of $H_2O_2$ to the surface or the number of sites available for $H_2O_2$ adsorption (see Figure 4-5, 4-6, and the caption of figure 4-5 for detailed discussion). The observed-first order rate constant of $H_2O_2$ decomposition ($k_{obs}$) was inversely proportional to the amount of $SiO_2$ in the solution (Figure 4-4b). At adsorption densities below 0.04 mmol/g goethite, $k_{obs}$ decreased linearly with the $SiO_2$ adsorption density, with a slope of -0.303 $hr^{-1}.mmol^{-1}.gram$. At adsorption densities above 0.04 mmol/g goethite, $k_{obs}$ was much less sensitive to increasing adsorption density (the slope of the regression line was -0.036 $hr^{-1}.mmol^{-1}.gram$). The presence of dissolved $SiO_2$ also diminished the rate of $H_2O_2$ loss catalyzed by other iron-containing minerals (Table 4-1). In the presence of $[SiO_2]_{initial}$ = 0.5 mM, the half-life of $H_2O_2$ increased by at least a factor of two compared with the $SiO_2$-free system in all cases.

To understand the effect of dissolved $SiO_2$ on the efficiency of the conversion of $H_2O_2$ into $^{\bullet}OH$ by iron-containing minerals, the oxidation of phenol in the goethite/$H_2O_2$ system was investigated. Typical phenol transformation data are presented in Figure 4-7a, which shows that silica slowed the rate of both $H_2O_2$ decomposition and phenol transformation. A control experiment indicated no phenol loss in the absence of $H_2O_2$. Addition of 100 mM tert-butanol, a $^{\bullet}OH$ scavenger, completely eliminated phenol degradation (data not shown), confirming that the loss of phenol observed was due to reaction with $^{\bullet}OH$. In the absence of dissolved $SiO_2$, the stoichiometric efficiency throughout the course of the experiment ranged from 0.25 to 0.3%. The stoichiometric efficiency was slightly lower in the presence of $[SiO_2]_{initial}$ = 0.5 mM, while at $[SiO_2]_{initial}$ = 1.5 mM the efficiency ranged from 0.14 to 0.2% (Figure 4-7b).

**Table 4-1**. Observed-first order rate constants ($k_{obs}$) for $H_2O_2$ decomposition catalyzed by iron-containing minerals under various conditions. Unless otherwise noted, $[H_2O_2]_{initial}$ = 5 mM, pH = 7, $[NaNO_3]$ = 0.1 M. The rate constants were obtained by fitting the experimental data to the first order decay reaction rate law. The $r^2$ values of the fittings were always $r^2 > 0.99$.

| | Experiment condition | $H_2O_2$ $k_{obs}$ ($h^{-1}$) | $H_2O_2$ half-life (h) |
|---|---|---|---|
| 1 | 4g/L goethite, 0 mM $SiO_2$ | 0.089 ± 0.003 | 7.77 ± 0.34 |
| 2 | 4g/L goethite, 0.5 mM $SiO_2$ | 0.032 ± 0.002 | 21.7 ± 1.2 |
| 3 | 4g/L goethite, 1.5 mM $SiO_2$ | 0.025 ± 0.002 | 28.2 ± 1.8 |
| 4 | 4g/L goethite, 2 mM phosphate | 0.022 ± 0.001 | 31.6 ± 1.4 |
| 5 | 4g/L goethite, 0.5 mM $SiO_2$ and 2 mM phosphate | 0.021 ± 0.001 | 33.5 ± 1.3 |
| 6 | 4g/L hematite, 0 mM $SiO_2$ | 0.018 ± 0.002 | 39.4 ± 3.5 |
| 7 | 4g/L hematite, 0.5 mM $SiO_2$ | 0.009 ± 0.001 | 77.7 ± 8.7 |
| 8 | 1 g/L FeOOH, 0 mM $SiO_2$ | 0.562 ± 0.005 | 1.23 ± 0.01 |
| 9 | 1 g/L FeOOH, 0.5 mM $SiO_2$ | 0.165 ± 0.015 | 4.22 ± 0.37 |
| 10 | 1 g/L FeOOH, 100 mM $H_2O_2$ | 0.539 ± 0.014 | 1.29 ± 0.03 |
| 11 | 1 g/L FeOOH, 100 mM $H_2O_2$, 0.5 mM $SiO_2$ | 0.15 ± 0.02 | 4.81 ± 0.69 |
| 12 | 5 g/L iron coated sand, 0 mM $SiO_2$ | 0.134 ± 0.012 | 5.21 ± 0.45 |
| 13 | 5 g/L iron coated sand, 0.5 mM $SiO_2$ | 0.036 ± 0.010 | 20.3 ± 6.5 |
| 14 | 4 g/L montmorillonite, 0 mM $SiO_2$, $[H_2O_2]_{initial}$ = 50 mM. | 0.0094 ± 0.0008 | 74.4 ± 6.6 |
| 15 | 4 g/L montmorillonite, 0.5 mM $SiO_2$, $[H_2O_2]_{initial}$ = 50 mM. | 0.00283 ± 0.00005 | 244.7 ± 4.9 |

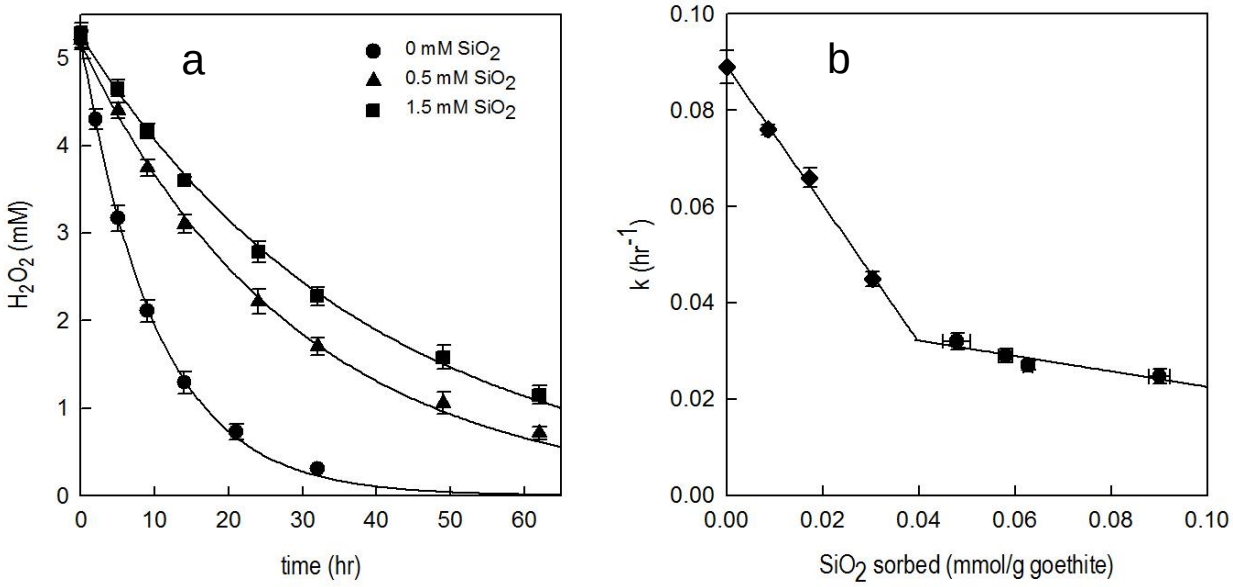


**Figure 4-4.** Effect of dissolved $SiO_2$ on $H_2O_2$ decomposition by goethite. [goethite] = 4 g/L, $[H_2O_2]_{initial}$ = 5.1 ± 0.1 mM, pH = 6.9 ± 0.1, [PIPES] = 1 mM, $[NaNO_3]$ = 0.1 M. Solid lines are first-order fit of $H_2O_2$ decomposition (**a**) and linear fits of first order rate constant $k_{obs}$ vs. $SiO_2$ sorbed (**b**).

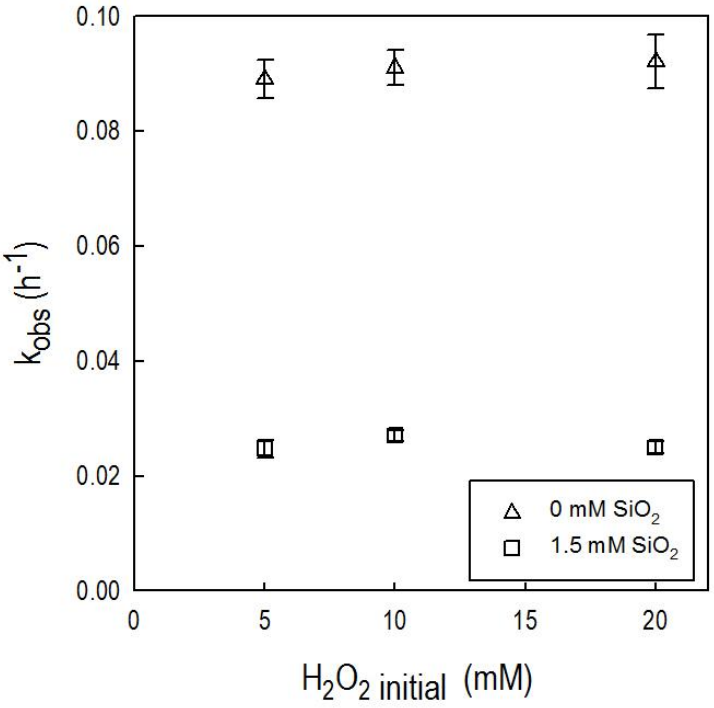


**Figure 4-5.** Observed-first order rate constant for the decomposition of $H_2O_2$ catalyzed by goethite. [goethite] = 4 g/L, pH = 7 (buffered by 1 mM PIPES), [$NaNO_3$] = 0.1 M. Under the experimental conditions employed in this study, $H_2O_2$ decomposition appears to be limited only by the intrinsic chemical reactivity of the solid and not by either diffusion of $H_2O_2$ to the surface or the number of site available for $H_2O_2$ adsorption. The observed-first order rate constant ($k_{obs}$) for the $H_2O_2$ decomposition remained constant under wide range of $[H_2O_2]_{initial}$, indicating that number of surface sites available for $H_2O_2$ adsorption was not limited under these conditions. To evaluate the role of $H_2O_2$ diffusion on the decomposition rate, we performed the Thiele modulus calculation similar to that employed by Lin and Gurol [24]. The Thiele modulus, $\phi$:

$$\phi = [\frac{k}{(D/L^2)}]^{0.5}$$

k ($s^{-1}$): reaction rate constant; D ($cm^2/s$): diffusion coefficient of solutes in water, typically has a value of $10^{-5}$ $cm^2/s$; L (cm): thickness of the stagnant liquid film (external mass transfer resistance) or the pore length (internal mass transfer resistance).

If the Thiele modulus is less than 0.5, the overall rate is dominated by the reaction rate. Alternatively, if $\phi > 5$, the rate is dominated by diffusion. Using an L value of $10^{-3}$ cm in the case of external mass transfer resistance, the Thiele modulus for the fastest rate of $H_2O_2$ decomposition ($k_{obs}$ = 0.089 $h^{-1}$) was calculated as $\phi = 1.57 \times 10^{-3} << 0.5$. Regarding internal mass transfer resistance, based on the shape of goethite particles (Figure 4-6) we assume L = 1000 nm = $10^{-4}$ cm so the Thiele modulus was $\phi = 1.57 \times 10^{-4} << 0.5$.

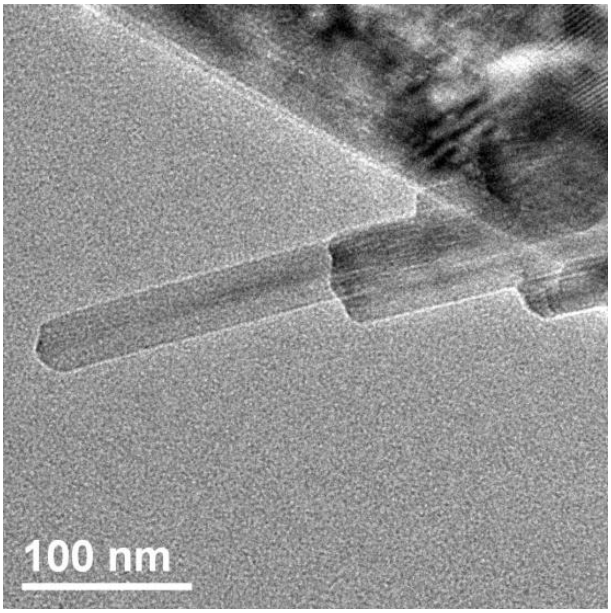


**Figure 4-6.** TEM micrograph of goethite employed in this study. The crystals have a needle-like morphology.

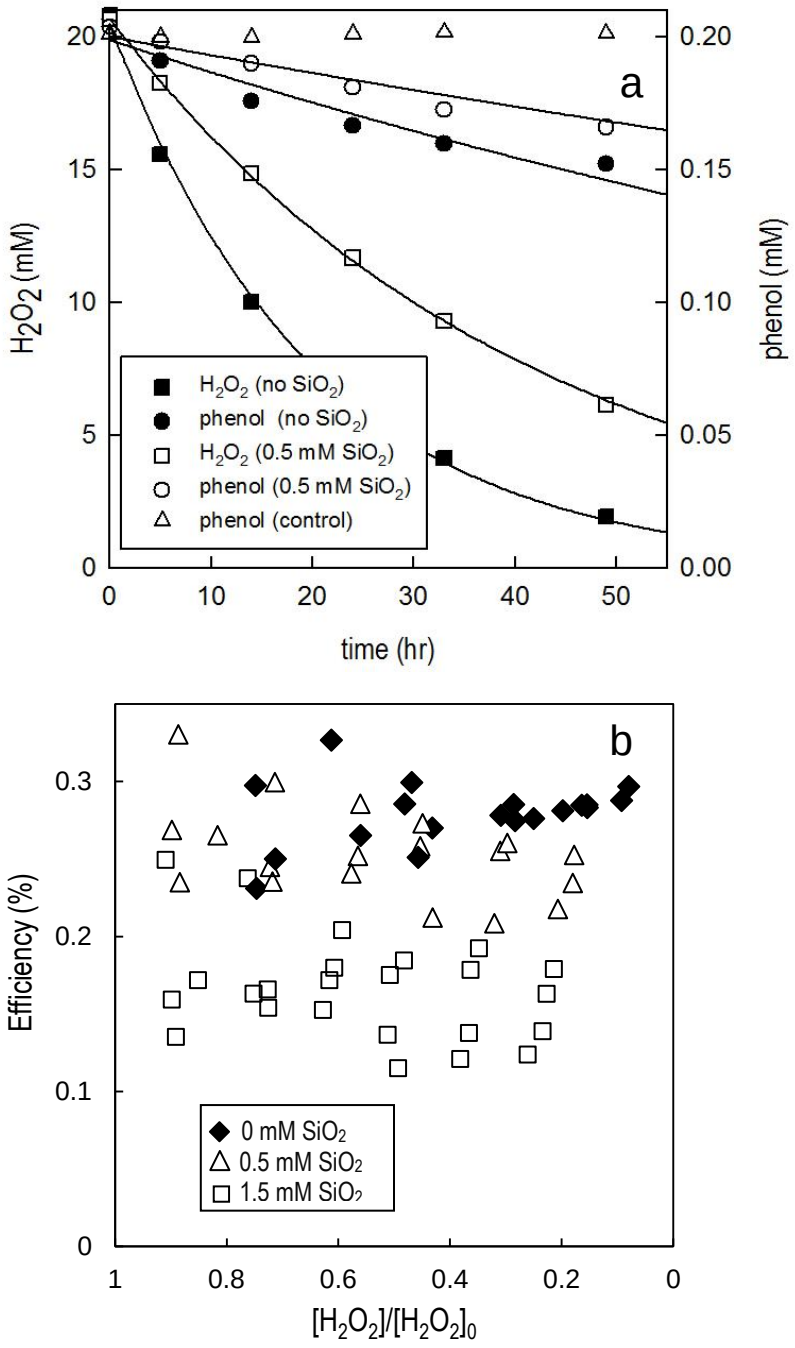


**Figure 4-7. (a):** $H_2O_2$ decomposition (left axis) and phenol transformation (right axis) catalyzed by goethite. Solid line: first order fit to the data. **(b)**: stoichiometric efficiency in the presence of dissolved silica. Experiments were conducted at least triplicate and, instead of presenting the average value and standard deviation, all results were presented. [goethite] = 4 g/L, pH = 7, [PIPES] = 1 mM, [$NaNO_3$] = 0.1 M. Except for the control experiment (inversed triangle), the $H_2O_2$ initial concentration in all experiments was $[H_2O_2]_0$ = 20 mM.

**Pyrolusite.** The adsorption of dissolved silica onto β-$MnO_2$ and its effect on the catalytic activity of β-$MnO_2$ toward $H_2O_2$ decomposition were also investigated (Figure 4-8). In the $SiO_2$-free system, 50 mM $H_2O_2$ was decomposed within 2 hours. As with iron-containing materials, addition of dissolved $SiO_2$ slowed the rate of $H_2O_2$ decomposition in proportion to the concentration of added $SiO_2$. The half-life of $H_2O_2$ was approximately 0.15 hr for the $SiO_2$-free system and 0.5 hr for the experiment with 1.5 mM $SiO_2$. Unlike the case with iron oxides, the adsorption of $SiO_2$ was not measurable even at a β-$MnO_2$ concentration of 20 g/L (inset of Figure 4-8).

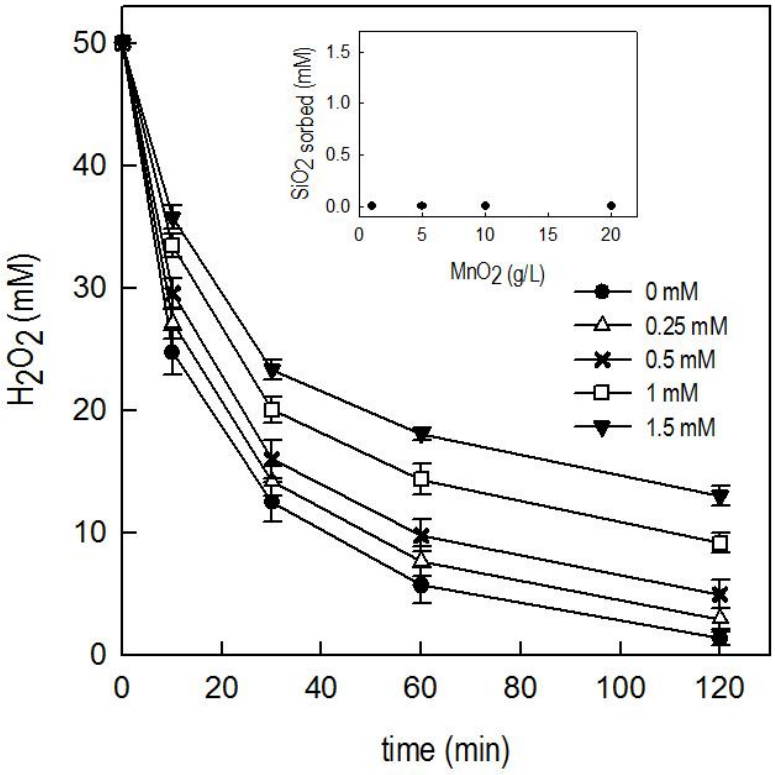


**Figure 4-8**. Decomposition of $H_2O_2$ catalyzed by pyrolusite (β-$MnO_2$) in the presence of various concentrations of dissolved $SiO_2$. [β-$MnO_2$] = 1 g/L, pH = 8.4, [$NaNO_3$] = 0.1 M, [borate] = 4 mM. Inset: [$SiO_2$] remaining in the solution after 24 hr equilibration with various amount of $MnO_2$. $[SiO_2]_{initial}$ = 1.5 mM, [$MnO_2$] = 1 – 20 g/L, other conditions were similar to those above.

## 4.4 Discussion

Adsorption of $SiO_2$ affects the surface properties and reactivity of metal oxides and clays in natural and engineered processes. For example, the presence of dissolved $SiO_2$ inhibits the nucleation and growth of iron precipitates[17] as well as the transformation of amorphous iron (hydr)oxide into more stable phases (*e.g.*, goethite) [18]. Dissolved $SiO_2$ also appears to stabilize iron oxide colloids, enhancing their mobility in natural waters and decreasing the efficiency of iron-based coagulation processes employed in drinking and wastewater treatment operation [19, 106, 107]. Adsorption of $SiO_2$ also alters the surface area, charge and surface complexation sites on iron oxides, thereby affecting the adsorption of various solutes [18, 108-110]. The presence of $SiO_2$ in water also affects the corrosion of iron, with sorbed $SiO_2$ forming a protective layer that inhibits corrosion [111, 112] or an impurity that destabilizes protective iron oxide scale layers [112].

In our experimental system, silica slowed the rate of $H_2O_2$ decomposition on iron and manganese mineral surfaces (Figure 4-4 and 4-8). To understand how $SiO_2$ affects the reactivity of minerals in this process, it is necessary to understand how $SiO_2$ and $H_2O_2$ interact with metal-containing surfaces. The adsorption behavior of $SiO_2$ on iron minerals is discussed below, followed by a discussion of $H_2O_2$ decomposition mechanisms and the possible effects of $SiO_2$. As the mechanism through which $H_2O_2$ is decomposed on $MnO_2$ differs from that of iron minerals, the $MnO_2$ system is discussed separately.

### 4.4.1 Iron minerals

$SiO_2$ adsorption often exhibits a fast and a slow stage, with more than 90% of adsorption taking place within the first few hours and the remaining 10% of adsorption occurring over several weeks (Figure 4-1 and 4-2) [78, 104]. Solution conditions such as pH and $SiO_2$-to-iron oxide ratio strongly affect this process [78, 107]. In addition to the bulk solution measurements, spectroscopic techniques such as ATR-IR [113] and XAFS [17], as well as surface modeling tools, have been used to infer the bonding of sorbed $SiO_2$ and the mechanism through which adsorption occurs. The adsorption process generally has been described as a complexation reaction between surface hydroxyl groups and $SiO_2$. However, no consensus has been reached on the exact nature of this interaction at a molecular level. Some investigators argued that the process involves the reaction between a monomeric $SiO_2$ species and one hydroxyl group (reaction (4.1) and (4.2) in Table 4-2) [77, 79]. However, Davis *et al*. invoked $SiO_2$ adsorption by both monomeric and dimeric species (reaction (4.3) and (4.4)) to explain adsorption data along with the zeta potential data [104]. It also has been suggested that adsorption can involve a bidentate complex between a $SiO_2$ monomer and 2 hydroxyl groups (reaction (4.5)) [17, 78] and that the siloxane linkages could form between two adjacent sorbed $SiO_2$ monomers or/and between sorbed monomers and dissolved $SiO_2$ (reaction (4.6)) [113, 114]. The latter scenario might lead to the formation of oligomeric silica species (*e.g.*, a linear trimer [113], or cyclic tetramer [115]) on the surface. The difference in the behavior of surface-adsorbed $SiO_2$ could be attributable to differences in solution conditions that were employed in these studies. Polymeric silica species tend to be important at high pH and high $SiO_2$ concentrations [104] while a high

$SiO_2$-to- iron oxide ratio could result in a high density of sorbed $SiO_2$ ($\Gamma_{Si}$), leading to the formation of oligomeric species.

**Table 4-2.** Possible surface complexation reactions between iron oxides and dissolved $SiO_2$

| | Reaction | Reference |
|---|---|---|
| $\equiv FeOH + Si(OH)_4 \rightarrow \equiv FeSiO(OH)_3 + H_2O$ | (4.1) | [77, 79, 104] |
| $\equiv FeOH + Si(OH)_4 \rightarrow \equiv FeSiO_2(OH)_2^- + H_2O + H^+$ | (4.2) | [77, 79, 104] |
| $\equiv FeOH + Si_2O_2(OH)_5^- + H^+ \rightarrow \equiv FeSi_2O_2(OH)_5 + H_2O$ | (4.3) | [104] |
| $\equiv FeOH + Si_2O_2(OH)_5^- \rightarrow \equiv FeSi_2O_3(OH)_4^- + H_2O$ | (4.4) | [104] |
| $2 \equiv FeOH + Si(OH)_4 \rightarrow \equiv Fe_2O_2Si(OH)_2 + 2\ H_2O$ | (4.5) | [17, 78] |
| $2 \equiv FeOH + 3\ Si(OH)_4 \rightarrow \equiv Fe_2H_{6-n}Si_3O_{10}^{n-} + n\ H^+ + 4\ H_2O$ | (4.6) | [113] |

In the present study, we used STEM/EDX to investigate the distribution of Si on the surface of goethite that had been pre-equilibrated with solutions containing varying amounts of dissolved $SiO_2$. With a nano-sized probe (1.4 nm in this study), STEM/EDX is capable of providing a high resolution elemental distribution map that cannot be obtained by other techniques (*e.g.*, scanning electron microscopy/EDX or X-ray photoelectron spectroscopy). A nano-sized probe technique is also needed to evaluate heterogeneity of the small goethite particles employed in this study (less than 100 nm, Figure 4-6). The relatively heterogeneous distribution of Si on the goethite surface and the presence of regions that were fully coated with Si (Figure 4-3) suggest that the adsorption did not take place in a "layer-by-layer" mode, presumably because adsorption is more favorable on some crystallographic faces than on others. The presence of more regions that were fully coated with Si at higher $[SiO_2]_{initial}$ supports the hypothesis that a high $SiO_2$-to-iron oxide ratio leads to the formation of oligomeric species.

*Hydrogen peroxide decomposition*. Iron oxides and iron-containing minerals (*e.g.*, ferrihydrite, goethite, iron-containing clays and iron-coated sand) can catalyze the decomposition of $H_2O_2$. This process can generate hydroxyl radical ($^{\bullet}OH$), presumably through a Haber – Weiss mechanism analogous to that observed in the homogeneous Fenton system [7, 24, 30, 31]:

$$\equiv Fe\text{-}OH^{3+} + H_2O_2 \rightarrow \equiv Fe\text{-}OH^{2+} + HO_2^{\bullet} + H^+ \quad (4.7)$$

$$\equiv Fe\text{-}OH^{2+} + H_2O_2 \rightarrow \equiv Fe\text{-}OH^{3+} + {}^{\bullet}OH + OH^- \quad (4.8)$$

$$HO_2^{\bullet} \Leftrightarrow H^+ + O_2^{\bullet -} \quad (4.9)$$

Some investigators have postulated that, as in the homogeneous Fenton system, reaction (4.7) actually consists of a series of reactions, beginning with the formation of a complex between the surface and $H_2O_2$ [24, 47]:

$$\equiv Fe\text{-}OH^{3+} + H_2O_2 \Leftrightarrow \equiv Fe\text{-}OH^{3+}(H_2O_2)_{(s)} \quad (4.10)$$

$$\equiv Fe\text{-}OH^{3+}(H_2O_2)_{(s)} \rightarrow \equiv Fe\text{-}OH^{2+}(HO_2^{\bullet})_{(s)} + H^+ \quad (4.11)$$

$$\equiv Fe\text{-}OH^{2+}(HO_2^{\bullet})_{(s)} \rightarrow \equiv Fe\text{-}OH^{2+} + HO_2^{\bullet} \quad (4.12)$$

Assuming that reaction (4.10) is the first step in $H_2O_2$ decomposition, sorbed $SiO_2$ may alter the reactivity of iron minerals by occupying iron surface hydroxyl groups, thereby preventing the formation of $\equiv Fe\text{-}OH^{3+}(H_2O_2)_{(s)}$.As mentioned above, the $SiO_2$ adsorption mechanism is not totally understood. Therefore, we did not try to estimate the number of hydroxyl groups that were occupied by $SiO_2$ and consequently, no correlation between the number of available hydroxyl groups with $k_{obs}$ has been made. However, the $\Gamma_{Si} - k_{obs}$ profile (Figure 4-4b) supports the hypothesis that the slower decomposition of $H_2O_2$ was due to occupation of surface sites by $SiO_2$. At a $\Gamma_{Si} < 0.04$ mmol/g goethite, where regions that were fully covered with Si were negligible, $k_{obs}$ drastically decreased as $\Gamma_{Si}$ increased. Due to the formation of oligomer species at higher $\Gamma_{Si}$, the number of iron sites that were occupied by $SiO_2$ only increased slightly, resulting in a much slower $k_{obs}$ decrease in this range. The higher $\Gamma_{Si}$ observed at $[SiO_2]_{equilibrium} = 1.14$ mM (Figure 4-1) also could be attributable to the formation of oligomer species. Finally, the presence of sites that were not occupied with Si (Figure 4-3a) could help to explain why $H_2O_2$ decomposition in all experiments was still observed at high $SiO_2$ concentration.

It was previously observed that under circumneutral pH conditions, $H_2O_2$ decomposes mainly through pathways that do not produce $^{\bullet}OH$ [31, 101]. Consequently, understanding the branching between different pathways is important because only those that produce $^{\bullet}OH$ will be beneficial for contaminant oxidation. Our data (Figure 4-7) indicate that dissolved $SiO_2$ has a detrimental effect on the overall stoichiometric efficiency. A possible explanation might be that surface sites have different reactivity toward $^{\bullet}OH$ production and the preferential adsorption of $SiO_2$ on "more $^{\bullet}OH$ productive" sites would lower the stoichiometric efficiency. Although assigning surface sites with different affinities is used widely in describing adsorption on iron oxides [116], the above hypothesis is speculative and further research is needed to address this issue.

### 4.4.2 Pyrolusite

Manganese oxides (such as birnessite and pyrolusite) are very reactive in catalyzing $H_2O_2$ decomposition. Although the mechanism of this process remains unclear, our data (Figure 4-9) and those of other investigators [10, 31, 44] indicate that this process does not produce $^{\bullet}OH$. Consequently, the presence of $MnO_2$ in aquifer materials is detrimental for $H_2O_2$-based ISCO.

$H_2O_2$ decomposition by β-$MnO_2$ also slowed in the presence of dissolved $SiO_2$, although the mechanism through which the loss of $H_2O_2$ was inhibited is unclear. In a batch experiment with β-$MnO_2$, $SiO_2$ adsorption was not measurable (inset of Figure 4-8). We were also unable to find any reports of adsorption of $SiO_2$ onto $MnO_2$, suggesting that $SiO_2$ does not adsorb on $MnO_2$ to an appreciable extent. However, it would be difficult to measure minor adsorption in the batch tests, even with the highest solids density tested. A column experiment was used to assess the potential for $SiO_2$ adsorption at higher β-$MnO_2$ concentrations (refer to the caption of Figure 4-10 for experimental setup). The results show that there was, indeed, a modest degree of silica uptake onto the β-$MnO_2$ from the solution during the first few minutes of the test, the uptake being proportional to the amount of $MnO_2$ in the column (Figure 4-10). This modest uptake of silica is likely to be responsible for the lower reactivity of $MnO_2$ observed experimentally. However, further research is needed to address this issue.

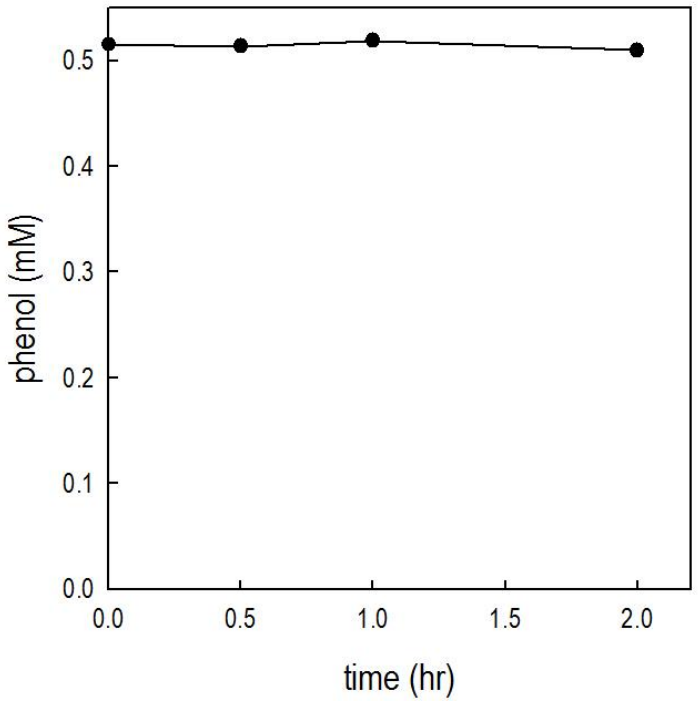


**Figure 4-9.** Concentration of phenol as a function of time in the presence of pyrolusite and $H_2O_2$. [β-$MnO_2$] = 1 g/L, $[H_2O_2]_0$ = 50 mM, pH = 8.4, [$NaNO_3$] = 0.1 M, [borate] = 4 mM, $[phenol]_0$ = 0.5 mM.

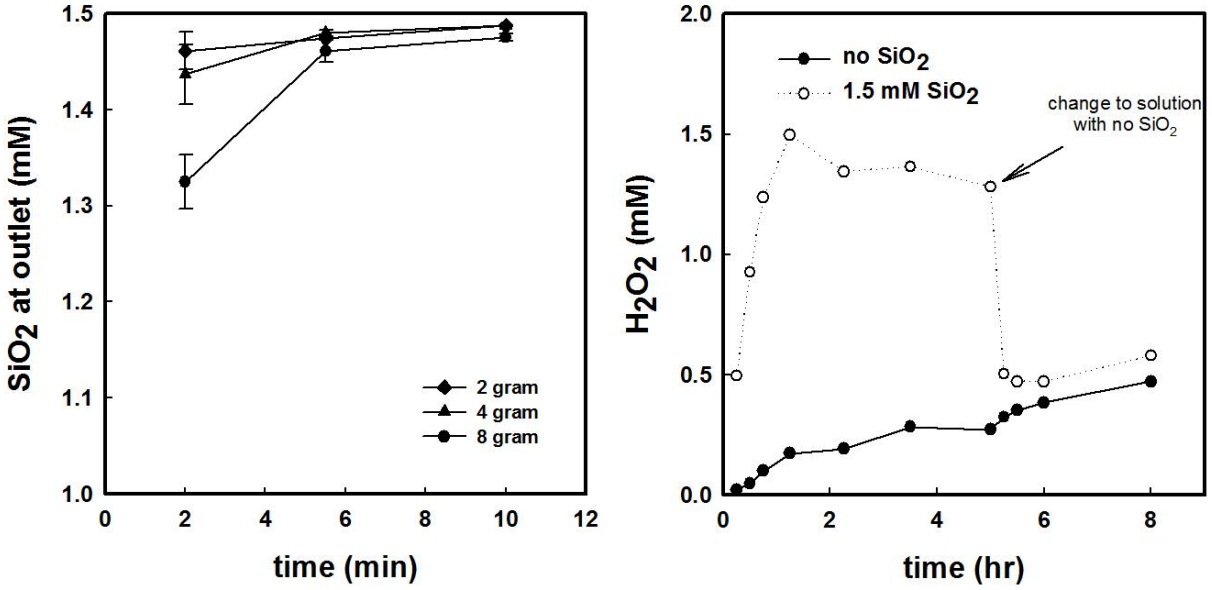


**Figure 4-10**. **Column experiments with β-$MnO_2$.** The effect of $SiO_2$ on β-$MnO_2$ reactivity toward $H_2O_2$ decomposition was studied using a column experiment in which a pH 8.5 solution was passed continuously at 0.4 mL/min through the **β-$MnO_2$** packed in an i.d. = 10 mm diameter column. Hydrogen peroxide and dissolved silica concentration in the solution coming out of the column was continuously measured. **Left:** Concentration of dissolved $SiO_2$ in the eluate. The column was packed with different amount of β-$MnO_2$. pH = 8.4, [$NaNO_3$] = 0.1 M, [borate] = 4 mM, $[SiO_2]_0$ = 1.5 mM. During the first 5 minutes, the amount of $SiO_2$ removed due to adsorption is proportional to the amount of β-$MnO_2$ in the column. After this period, the β-$MnO_2$ surface became saturated with $SiO_2$ and the concentration of dissolved $SiO_2$ at the outlet approached that at the inlet. **Right:** the decomposition of $H_2O_2$ by 1g β-$MnO_2$ in the column experiment. $[H_2O_2]_{inlet}$ = 10 mM, pH = 8.4, [$NaNO_3$] = 0.1 M, [borate] = 4 mM. In the column that was fed with 1.5 mM $SiO_2$ and 10 mM $H_2O_2$, less $H_2O_2$ was decomposed (dashed line). At t = 5hr, the solution was changed to one containing no $SiO_2$; the $H_2O_2$ concentration at the outlet quickly decreased.

## 4.5 Environmental implications

The results of this study suggest that in $H_2O_2$-based ISCO systems, $H_2O_2$ should last longer if groundwater contains a significant amount of dissolved $SiO_2$. In systems where the subsurface is deficient in $SiO_2$, dissolved silica could be injected together with $H_2O_2$ to increase the persistence of $H_2O_2$ to assure remediation of areas further from the injection well. Dissolved $SiO_2$ has a potential to be a better $H_2O_2$-stabilizing agent than phosphate because $SiO_2$ is inexpensive and does not stimulate bacterial growth. Although $SiO_2$ decreased the stoichiometric yield of $^{\bullet}OH$ from iron minerals, this effect was relatively modest, and would be outweighed in *in situ* applications by the greater longevity of $H_2O_2$ in the presence of $SiO_2$. The effect of $SiO_2$, however, will vary among aquifers with different compositions (*e.g.*, iron and manganese content and crystalinity, soil organic matter content and groundwater composition) and should be considered in the design and operation of $H_2O_2$-based ISCO. Additionally, because silica adsorption is a reversible process (Figure 4-11), it is advisable to inject dissolved $SiO_2$ and $H_2O_2$ simultaneously to assure the $H_2O_2$ lifetime enhancement.

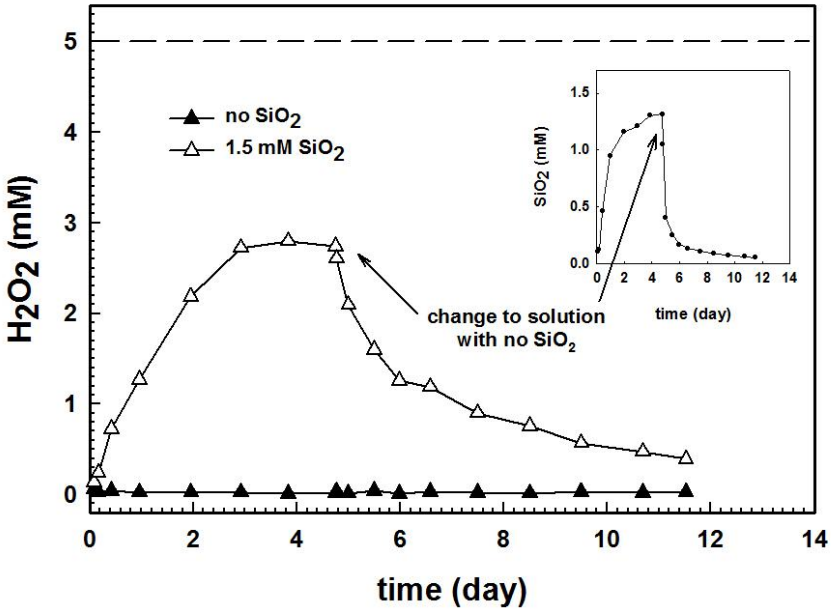


**Figure 4-11.** The decomposition of $H_2O_2$ by 1g FeOOH in the column experiment. Flow rate: 0.5 mL/min. $[H_2O_2]_{inlet}$ = 5 mM, pH = 8.4, $[NaNO_3]$ = 0.1 M, [borate] = 4 mM. In the column that was fed with 1.5 mM $SiO_2$ and 5 mM $H_2O_2$, less $H_2O_2$ was decomposed (white triangles). At t = 5hr, the solution was changed to one containing no $SiO_2$; the $H_2O_2$ concentration at the outlet quickly decreased. Inset: Concentration of dissolved $SiO_2$ in the eluate.

Our study also indicates that many bench-scale studies performed in the absence of dissolved $SiO_2$ may have underestimated the lifetime of $H_2O_2$ or overestimated the effect of stabilizing agents. For example, in the $SiO_2$-free system ($H_2O_2$ half-life of 7.77 hr, Table 4-1), 2 mM phosphate increased the $H_2O_2$ half-life by approximately a factor of four ($t_{1/2}$ = 31.6 hr). In the presence of 0.5 mM $SiO_2$, however, phosphate provided much less of an effect, increasing the half-life of $H_2O_2$ by about only 50% ($t_{1/2}$ = 21.7 hr and 33.5 hr in the absence and presence of phosphate, respectively).

$SiO_2$ also suppressed $H_2O_2$ decomposition by $MnO_2$. Depending on the relative amount of iron- and manganese-containing solids, $SiO_2$ could enhance the overall efficiency of the remediation process, especially in soils with high Mn content. Additional research is needed to assess the contribution of different iron- and manganese-containing solids to $H_2O_2$ loss in soils and aquifer materials.

Finally, our data also suggest that dissolved silica can affect the reactivity of iron-containing catalysts used in $H_2O_2$-based advanced oxidation processes. Although the $SiO_2$ concentrations in surface waters and industrial wastes are often lower than those observed in groundwater, a gradual loss in catalyst activity due to $SiO_2$ adsorption will likely occur during long-term catalyst use.

# Chapter 5. Size Exclusion and Oxidation of Organic Compounds in an Iron Oxide-Containing SBA15 – Hydrogen Peroxide System: Minimizing Hydroxyl Radical Consumption by Non-Target Compounds

Hydrogen peroxide-based Advanced Oxidation Processes (AOPs) are being used increasingly to treat water contaminated with organic compounds [7, 28, 117]. These processes involve the conversion of hydrogen peroxide ($H_2O_2$) into hydroxyl radical ($^{\bullet}OH$), a highly reactive and unselective oxidant capable of oxidizing most recalcitrant organic contaminants (*e.g.*, solvents, aromatic compounds). Oxidation by $^{\bullet}OH$ often converts contaminants into forms that are less toxic and more biodegradable than the parent compound.

One common approach for converting $H_2O_2$ into $^{\bullet}OH$ uses iron-containing minerals, such as iron oxides and iron-containing clays and sands, to catalyze the decomposition of $H_2O_2$ [6, 26]:

$$\equiv Fe(III) + H_2O_2 \rightarrow \equiv Fe(II) + HO_2^{\bullet} + H^+ \quad (5.1)$$

$$\equiv Fe(II) + H_2O_2 \rightarrow \equiv Fe(III) + {}^{\bullet}OH + OH^- \quad (5.2)$$

$$HO_2^{\bullet} \Leftrightarrow H^+ + O_2^{\bullet -} \ (pK_a = 4.8) \quad (5.3)$$

This approach, also known as the heterogeneous Fenton process, offers several advantages over the homogeneous Fenton analog (*i.e.*, dissolved $Fe^{2+}$ and $H_2O_2$ under acidic pH conditions). Specifically, the catalysts can be easily recovered and recycled, the system does not precipitate iron oxide waste and the process may be operated at less acidic pH values. However, heterogeneous Fenton systems tend to be slower than the homogeneous Fenton process and catalyst reactivity may decrease over time due to iron leaching [93]. Furthermore, heterogeneous Fenton processes are often very inefficient, with most of the $H_2O_2$ decomposing to species other than hydroxyl radical [6, 26, 31, 93].

To overcome these limitations, investigators have modified catalysts by immobilizing iron into various types of silica supports, including silica-alumina gels [93], zeolites [65], clays [13], and mesoporous silica SBA15 [12]. While supported catalysts often perform better than iron oxides, the role of the support material on the reactivity of the catalyst and the importance of reactions on the support are still unclear.

When hydroxyl radical-based oxidation is used to treat water that contains high concentrations of non-target compounds (*e.g.*, natural organic matter, proteins, carbohydrates), a significant fraction of the $^{\bullet}OH$ may be lost in side reactions that at best are unnecessary, and at times undesirable. Not only does the consumption of $^{\bullet}OH$ by non-target organic substances waste reagents such as $H_2O_2$ and $O_3$, but the partial oxidation of complex organic compounds may stimulate adverse microbial activity after treatment.

The selective reaction of $^{\bullet}OH$ with target compounds has been promoted by means such as molecular recognition [118] and production of $^{\bullet}OH$ in a microenviroment from which the non-target compounds are excluded [119, 120]. Previous efforts to employ size exclusion to enhance reaction efficiency have been limited to the $TiO_2$/UV system; to the best of our knowledge the selective reaction of $^{\bullet}OH$ with target compounds has not been studied in the Fenton system. Here

we propose and test a novel approach for minimizing $^{\bullet}OH$ scavenging by non-target compounds in heterogeneous Fenton systems using a mesoporous silica SBA15 support containing iron oxide within narrow pores. More efficient utilization of $^{\bullet}OH$ should be possible if the $^{\bullet}OH$ generated in these pores is able to react with small target compounds (phenol in this study) that enter the pores, while macromolecules, such as proteins or humic substances, are too large to enter the pore. Because the $^{\bullet}OH$ radicals are short-lived compared to the time required for them to diffuse out of the pores, little of the $^{\bullet}OH$ would be expected to react with compounds outside of the pores. Here we report our effort to identify: (a) whether oxidation of small model contaminants occurs within a mesoporous support and (b) whether large molecules are, indeed, excluded from such a catalyst.

The synthesis of mesoporous SBA15 silica is reported elsewhere [121]. Iron-containing SBA15 (SBA15-$Fe_2O_3$) was synthesized by grafting an iron precursor on the surface of SBA15 as described by Gervasini *et al.* [122]. Briefly, 1 g of SBA15 was suspended in a mixture of 60 mL water and 60 mL 1-propanol. The solution pH was adjusted to 10 with ammonium hydroxide while maintaining the temperature at 0 ºC in an ice bath (suspension A). 5.3 g Fe(III)-acetylacetonate was dissolved in a mixture of 250 mL water and 250 mL 1-propanol, and the resulting solution was added to suspension A over a period of approximately 10 minutes, maintaining the pH at 10. The resulting suspension was vigorously stirred at room temperature for 24 hr. During this period, Fe(III)-acetylacetonate adsorbed on the internal and external surfaces of the SBA15 support. Finally, the iron-containing SBA15 was filtered, dried at 90 ºC for 20 hr and calcined at 500 ºC for 4 hr to decompose adsorbed iron complexes to iron oxide.

TEM images of SBA15 and calcined SBA15-$Fe_2O_3$ (Figure 5-1) show that $Fe_2O_3$ was uniformly dispersed inside of the pore space of SBA15 but did not completely fill the pores. The low angle XRD pattern (Figure 5-2a) and the TEM image indicate that the original hexagonal pore structure of SBA15 was retained after deposition and calcining. Only one broad peak was evident in the high angle XRD pattern, at around $2\theta = 25^{\circ}$, with no peaks corresponding to $\alpha$– or $\gamma$–$Fe_2O_3$ (Figure 5-2b). As discussed by Gervasini *et al.*, who observed a similar pattern, this is representative of amorphous $Fe_2O_3$ [122]. After the iron oxide had been deposited in the SBA-15, the surface area and pore volume decreased by 20 to 30%, while the diameter of the pores was only slightly reduced (Table 5-1).

The SBA15-$Fe_2O_3$ catalyzed $H_2O_2$ decomposition and phenol transformation at pH 6.8 (Figure 5-3). The stoichiometric efficiency, defined as the amount of phenol decomposed per mole of $H_2O_2$ consumed (*i.e.*, $\Delta[\text{phenol}]\times 100\%/\Delta[H_2O_2]$) was approximately 0.9%, which is 10 times higher than that of iron oxides and comparable to that of the composite iron-silicon oxide reported previously [93]. The addition of 100 mM *tert*-butanol (t-BuOH), an uncharged compound that reacts with $^{\bullet}OH$, decreased the rate of phenol transformation but did not affect the rate of $H_2O_2$ decomposion. In contrast, the addition of 0.33 mM Bovine Serum Albumin (BSA), a macromolecule that also reacts with $^{\bullet}OH$, did not decrease the rate of phenol transformation. Calculated pseudo-first order rate constants based on bulk concentrations of t-BuOH and BSA and reaction rate constants (k) for the homogeneous reaction of the compounds with $^{\bullet}OH$ suggest that without the effect of size exclusion BSA and t-BuOH should have had a similar effect on the transformation rate of phenol (Table 5-2). The slower phenol transformation

was unlikely to be due to slower •OH generation because the rate of $H_2O_2$ decomposition in the presence of BSA remains unchanged (Figure 5-3).

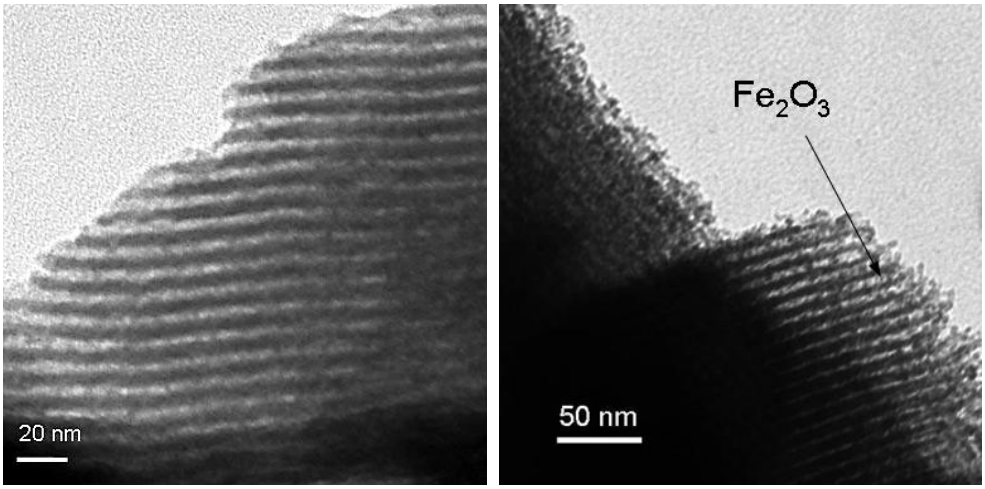


**Figure 5-1.** TEM image of SBA15 (left) and SBA15-$Fe_2O_3$ (right)

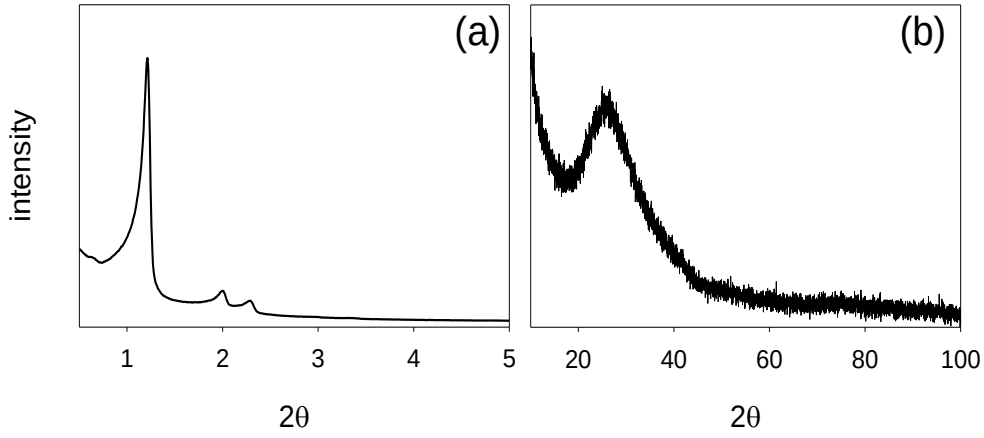


**Figure 5-2.** Low angle (a) and high angle (b) X-ray diffraction patterns of SBA15-$Fe_2O_3$ (Cu Kα radiation)

**Table 5-1.** Properties of SBA15 and SBA15-$Fe_2O_3$.

| Sample name | Surface area [a] ($m^2/g$) | Pore volume [b] ($cm^3/g$) | Pore size [c] (Å) | Fe (wt. %) |
|---|---|---|---|---|
| SBA15 | 636 | 0.82 | 52 | - |
| SBA15-$Fe_2O_3$ | 447 | 0.68 | 49 | 8.6 |

[a] BET surface area
[b] Calculated by BJH method

**Table 5-2.** Rate constants (k) for the reaction between $^{\bullet}OH$ and analytes present in the solution; initial pseudo-first order rate constant $k' = k \times$ [initial concentration] and the fraction of $^{\bullet}OH$ consumed by analytes in the presence of either t-BuOH or BSA.

| | Initial concentration (M) | k ($M^{-1}s^{-1}$) | $k'$ ($s^{-1}$) | fraction of $^{\bullet}OH$ consumed** |
|---|---|---|---|---|
| Phenol | $5\times10^{-4}$ | $6.6\times10^{9}$ | $3.3\times10^{6}$ | 5-10% |
| $H_2O_2$ | 0.05 | $2.7\times10^{7}$ | $1.3\times10^{6}$ | 2-4% |
| Bovine serum albumin | $3.3\times10^{-4}$ | $7.8\times10^{10}$ | $2.57\times10^{7}$ | 82-85% |
| t-BuOH | 0.1 | $6.6\times10^{8}$ | $6.6\times10^{7}$ | 92-93% |
| PIPES | $1\times10^{-3}$ | $\sim10^{8}$-$10^{9}$* | $\sim10^{5}$-$10^{6}$* | <3% |

* Reaction rate constant between $^{\bullet}OH$ and PIPES is unknown. The value used here is typical for many organic compounds.
** The fraction of $^{\bullet}OH$ react with the analyte (i) can be calculated based on the following equation:
$f_{^{\bullet}OH,(i)} = k_{^{\bullet}OH,(i)}[i]/(k_{^{\bullet}OH,phenol}[phenol] + k_{^{\bullet}OH,H_2O_2}[H_2O_2] + k_{^{\bullet}OH,scavenger}[scavenger]^{***} + k_{^{\bullet}OH,PIPES}[PIPES])$
***scavenger: either t-BuOH or BSA

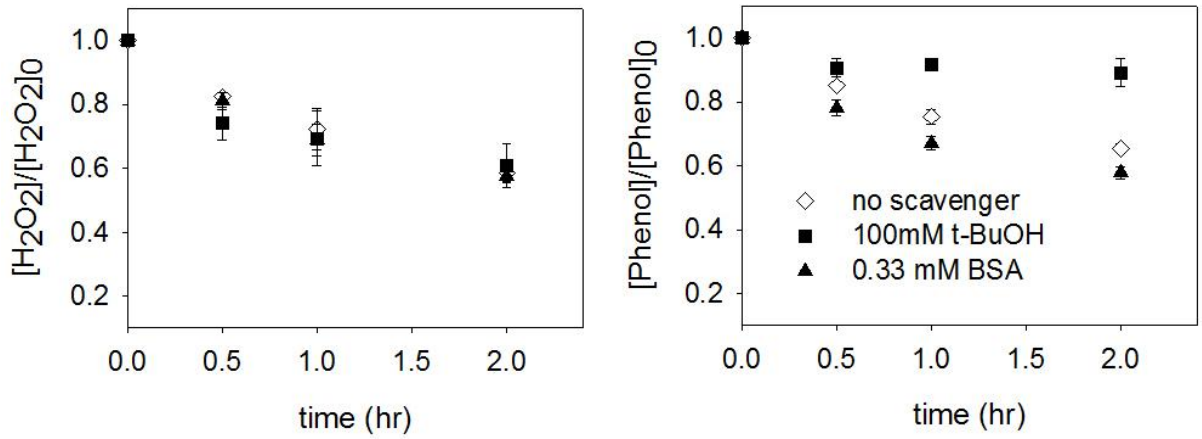


**Figure 5-3.** Hydrogen peroxide decomposition and phenol transformation. $[Phenol]_{ini}$ = 0.5 mM, [SBA15-$Fe_2O_3$] = 25g/L, [$H_2O_2$] = 50 mM. Solutions were buffered with 1 mM piperazine-*N,N'*-bis(ethanesulfonic acid) (PIPES). $pH_{average}$ =6.8.

The inability of BSA to slow the rate of phenol transformation appears to be due to the inability of the BSA to reach most of the sites where $^{\bullet}OH$ was produced. Indeed, comparing the hydraulic diameter (70 Å) and the steric size (40 Å × 40 Å × 140 Å) of BSA with the pore size of SBA15-$Fe_2O_3$ (49 Å) indicates that BSA is too large to enter the pores, which has been corroborated in previous research [123]. In contrast, both phenol and t-BuOH are much smaller than the pores (*i.e.*, these small molecules have a steric size below 10 Å) and thus can enter the pore to react with $^{\bullet}OH$.

To confirm that the inability of BSA to curtail phenol transformation in the SBA15-$Fe_2O_3$/$H_2O_2$ system was due to size exclusion rather than to some unanticipated chemical effect, we repeated the experiment in a homogeneous Fenton system under comparable conditions using phosphotungstate ($PW_{12}O_{40}^{3-}$) to prevent precipitation of Fe(III) (under these conditions, BSA does not form a complex with Fe(III) as shown in Figure 5-4). Under these conditions, the Fe(III)-$PW_{12}O_{40}^{3-}$ complex catalyzes the conversion of $H_2O_2$ into $^{\bullet}OH$ through a mechanism similar to that observed for the heterogeneous system [124]. In this homogeneous system, it is expected that BSA has access to $^{\bullet}OH$. Figure 5-5 shows that the phenol transformation rate in the presence of BSA is comparable with the transformation rate in the presence of t-BuOH, and much slower than that observed in the absence of scavengers. The fact that BSA did not slow the rate of phenol transformation in the SBA-$Fe_2O_3$ system demonstrates that (a) the majority of the $^{\bullet}OH$ was produced within the pores, and (b) the BSA was excluded from the sites where it was generated.

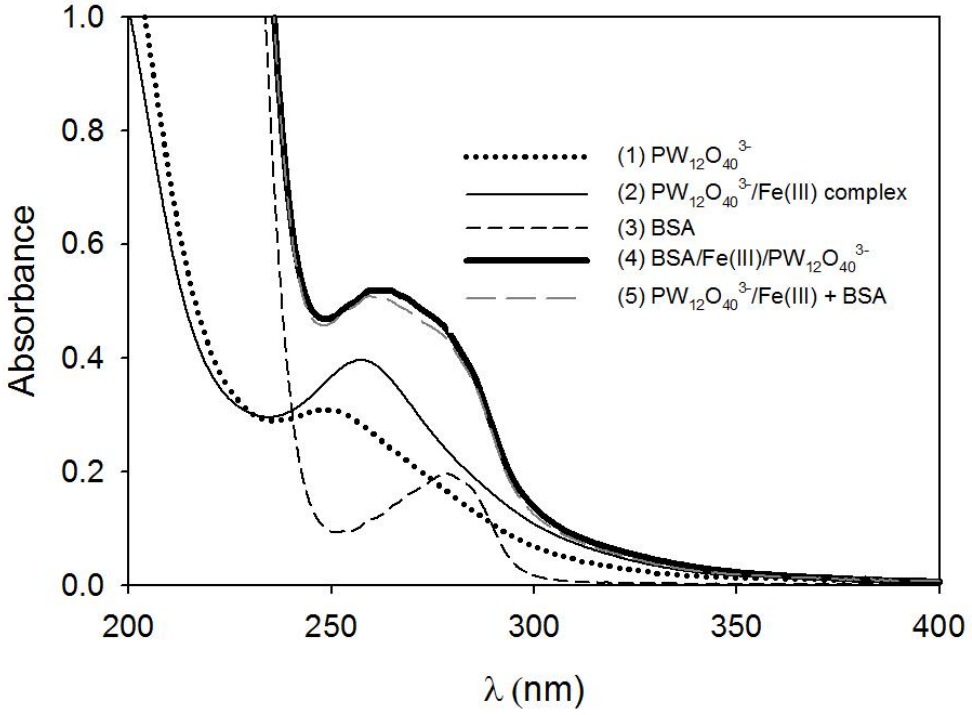


**Figure 5-4. UV-vis spectra of pH 7 solutions of:** (1) [$PW_{12}O_{40}^{3-}$] = 10μM; (2) [$PW_{12}O_{40}^{3-}$] = 10μM, [Fe(III)] = 10μM; (3) [BSA] = 3.3μM; (4) [$PW_{12}O_{40}^{3-}$] = 10μM, [Fe(III)] = 10μM; (5) is the UV-vis absorption summation of (2) and (3), which is equal to (4). This result indicates that BSA does not complex with Fe(III) under this experimental condition.

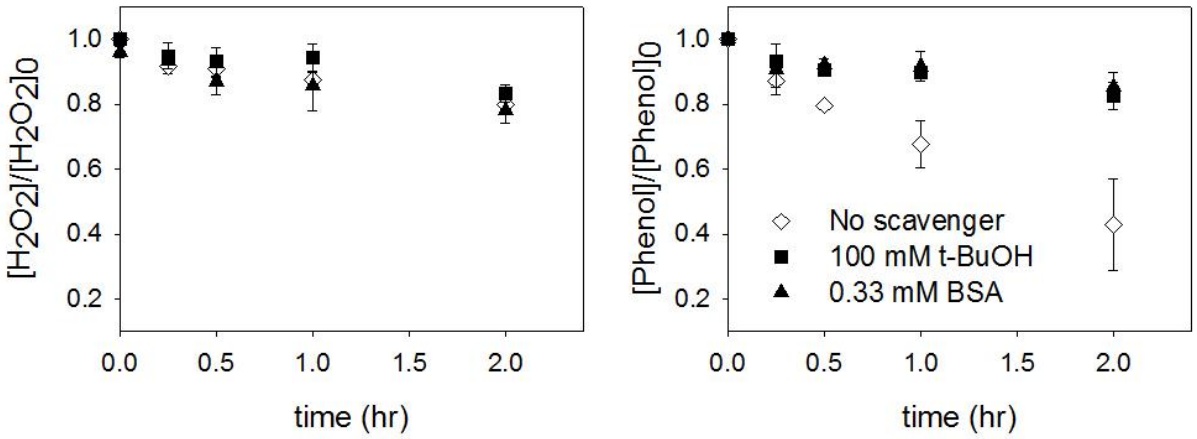


**Figure 5-5.** Hydrogen peroxide decomposition and phenol transformation in the presence of t-BuOH or BSA, which scavenge $^{\bullet}OH$, and in their absence, using homogeneous Fenton catalysis. $[Phenol]_{ini}$ = 0.5 mM; $[PW_{12}O_{40}^{3-}]$ = 1mM; [Fe(III)] = 2mM, $[H_2O_2]$ = 50 mM. Solutions were buffered with 1 mM PIPES. $pH_{average}$ = 6.7.

BSA was used in these experiments as a model high molecular weight compound. However, humic substances, rather than BSA, are likely to be more important $^{\bullet}OH$ scavengers in many situations. Our preliminary data suggest that some of the lower molecular weight humic acids enter the pores of the SBA15-$Fe_2O_3$ catalyst (Figure 5-6). In the presence of 25 mg/L humic acid the rate of disappearance of phenol increased by about 50% accompanied by significant leaching of iron (5-10 μM) and slightly faster losses of $H_2O_2$. Complexation of iron by humic substances is known to accelerate the rate of $H_2O_2$ decomposition in Fenton systems [125]. Nevertheless it still appears that partial size exclusion occurred: if all the humic acids could access the interior of the pores or if the $^{\bullet}OH$ was produced mainly in the bulk solution much slower transformation of phenol would have occurred under these conditions (Table 5-3). Future research should assess this effect and determine if smaller sized pores can be used to exclude a larger fraction of the humic substances.

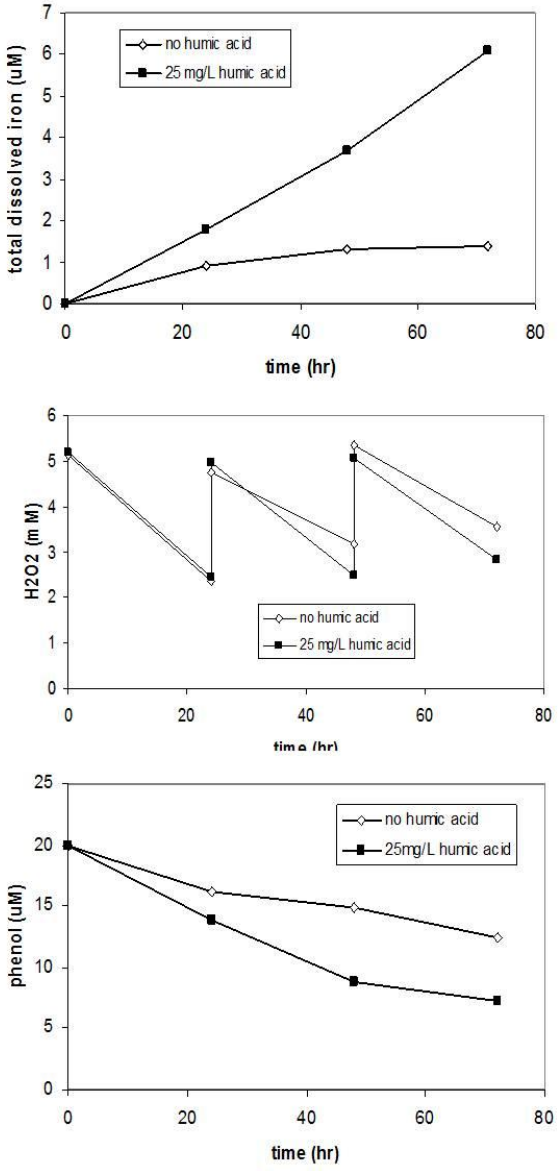


**Figure 5-6**. Total dissolved iron concentration, hydrogen peroxide decomposition and phenol transformation. [SBA15-$Fe_2O_3$] = 3 g/L; $[H_2O_2]_o$ = 5 mM; $[Phenol]_o$ = 20 μM; [PIPES] = 0.2 mM; [HA] = 25 mg/L; pH = 7 ± 0.4. The purpose of these experiments is to investigate the effect of humic acid (HA) to the rate of $H_2O_2$ decomposition and phenol transformation. HA (Aldrich) used in this study has the molecular weight ranging from 2 kDa. – 500 kDa and HA concentration in all experiments was 25 mg/L (challenges with phenol analysis in the presence of humic acid prevents the use of higher HA concentration solution). Initial $H_2O_2$, phenol and PIPES concentration were 5 mM, 20 μM and 0.2 mM, respectively. These values were chosen so that HA would be the main $^{\bullet}OH$ scavenger in these experiments (Table 5-3). After each period of 24 hours, an aliquot of hydrogen peroxide was added so that $[H_2O_2] = [H_2O_2]_o$ = 5 mM. This addition would maintain the constant quasi steady state $^{\bullet}OH$ concentration.

**Table 5-3.** Rate constant (k) and for the reaction between analytes present in the solution with $^{\bullet}OH$; initial first order rate constant $k' = k \times$ [ initial concentration] and the fraction of $^{\bullet}OH$ consumed by analytes.

| | Initial concentration (M) | k ($M^{-1}s^{-1}$) | $k'$ ($s^{-1}$) | fraction of $^{\bullet}OH$ consumed [d] |
|---|---|---|---|---|
| Phenol | $2\times10^{-5}$ | $6.6\times10^{9}$ | $1.32\times10^{5}$ | 18-24% |
| $H_2O_2$ | $5\times10^{-3}$ | $2.7\times10^{7}$ | $1.35\times10^{5}$ | 19-25% |
| PIPES | $2\times10^{-4}$ | $\sim10^{8}$-$10^{9}$ [a] | $\sim2\times10^{4}$-$2\times10^{5}$ [a] | 27-37% |
| Humic acid | 25 (mg/L) | $\sim2\times10^{4}$ [b] | $\sim2.5\times10^{5}$ [c] | 35-47% |

[a] Reaction rate constant between $^{\bullet}OH$ and PIPES is unknown. The value used here is typical for many organic compounds.
[b] Unit of $[(\text{mg C/L})^{-1}s^{-1}]$
[c] Calculation performed assuming that Humic acid contains 50 wt. % of Carbon.
[d] The fraction of $^{\bullet}OH$ react with the analyte (i) can be calculated based on the following equation: $f_{^{\bullet}OH,(i)} = k_{^{\bullet}OH,(i)}[i]/(k_{^{\bullet}OH,phenol}[phenol] + k_{^{\bullet}OH,H_2O_2}[H_2O_2] + k_{^{\bullet}OH,scavenger}[scavenger]^{*} + k_{^{\bullet}OH,PIPES}[PIPES])$
*scavenger: either t-BuOH or BSA

In conclusion, we have synthesized an iron oxide-containing mesoporous silica SBA15 catalyst that can convert $H_2O_2$ into $^{\bullet}OH$ at neutral pH. Most of the iron oxide precipitates are present in the narrow pores of SBA15 where they are accessible to $H_2O_2$ added to the bulk solution. The $^{\bullet}OH$ produced at these sites is accessible to small, model contaminants such as phenol, but is inaccessible to high molecular weight non-target compounds such as Bovine Serum Albumin. While humic acids are not fully excluded from the pores, it may be possible to develop more selective size exclusion supports with materials that have smaller pores (*e.g.*, MCM 41 mesoporous silica, zeolites). Nevertheless, the generation of $^{\bullet}OH$ in the microenvironment may improve the efficiency of AOPs used to treat complex wastes.

# Chapter 6. Dissolution of Mesoporous Silica Supports in Aqueous Solutions: Implications for Mesoporous Silica-based Water Treatment Processes

Reproduced with permission from Pham, A.L.T; Sedlak, D. L; Doyle, F.M. Dissolution of Mesoporous Silica Supports in Aqueous Solutions: Implications for Mesoporous Silica-based Water Treatment Processes. *Applied Catalysis B: Environmental* 126 (**2012**) 258-264.

## 6.1 Introduction

Owing to their high surface area and unique nano-porous structure, ordered mesoporous silica supports (*e.g.*, SBA-15 and MCM-41) have been proposed for water remediation [126]. For example, functionalized mesoporous silica has been used as an adsorbent for toxic metals [127, 128], anions [129, 130], radionuclides [131] and various organic contaminants [132-135]. Mesoporous silica catalysts impregnated with metal oxides, such as iron-, manganese- and copper-containing SBA-15, have also been used in hydrogen peroxide-based oxidative water treatment [65, 136, 137]. Many of these applications employ aqueous solutions at circumneutral pH values despite the fact that silica is relatively soluble under these conditions. Given the high surface area and poor crystalinity of these materials it is possible that they will dissolve rapidly in water. If so, the use of these materials in aqueous media needs to be carefully evaluated because the dissolution of functionalized mesoporous silica adsorbents could release adsorbed species and the organic functional compounds, many of which are toxic to aquatic life. Silica dissolution could also affect the long-term performance of the catalyst. Moreover, the presence of the dissolved silica species might lead to unexpected changes in the catalyst surface as silica interacts with catalytic active sites [101].

Previous investigators have reported dissolved silica concentration in excess of 100 mg/L when mesoporous silica materials were suspended in solutions at pH values between 5 and 6 [66, 67]. Measurement of the dissolution of $SiO_{2(s)}$ indicates that the mineral's solubility and dissolution rate are sensitive to pH, with higher solubility and faster dissolution observed in neutral and alkaline solutions [138]. To understand the stability of mesoporous silica supports, it is important to know the effect of pH on its dissolution rate. However, to the best of our knowledge, such information has not been reported. Here we have investigated the dissolution rate of three widely used types of mesoporous silica, namely SBA-15, HMS and MCM-41, in aqueous solutions at environmentally relevant pH values (pH 7 – 10). Recognizing the possibility that functionalized organic groups or precipitated oxides might significantly modify the aqueous solubility of silica [139], the dissolution of SBA-15 functionalized with different organic compounds (*i.e.*, propylthiol-, aminopropyl-, ethyldiaminopropyl- and diethylentriaminopropyl-) or SBA-15 that was coated with iron and aluminum oxide were also investigated. Because we observed the rapid release of dissolved silica in all cases, we also investigated how the presence of dissolved silica might change the catalytic activity of the iron oxide/SBA-15 system toward $H_2O_2$ decomposition.

## 6.2 Materials and methods

### 6.2.1 Synthesis of mesoporous silica supports

SBA-15, HMS and MCM-41 were synthesized following procedures reported elsewhere [121, 140, 141]. Iron oxide- and aluminum oxide- containing SBA15 (SBA15-Fe-oxide and SBA15-Al-oxide) was synthesized following the procedure described by Gervasini *et al.* [122].

Briefly, 1 gram of SBA-15 was suspended in a 120 mL solution of 1:1 water:propanol-1. The solution pH was kept at 10 with ammonium hydroxide and the temperature was maintained at 0ºC using an ice bath. Iron and aluminum precusor solutions, prepared by dissolving 0.015 mol of either iron-acetylacetonate or aluminum-acetylacetonate in a 500 mL solution of 1:1 water:propanol-1, were gently dropped into the SBA-15 solution. The mixtures were then removed from the ice bath and vigorously stirred at room temperature. The solids were recovered by filtration, air dried at 100ºC for 24 hours and calcined at 500ºC for 4 hours. All solutions were prepared using 18 MΩ Milli-Q water from a Millipore system.

SBA-15 functionalized with propylthiol-, aminopropyl-, ethyldiaminopropyl- and diethylenetriaminopropyl- were synthesized following the procedure reported by Aguado *et al.* [142, 143]. Briefly, 4 g of triblock copolymer P123 was dissolved in a solution of 125 ml of 1.9 M HCl and the mixture was heated to 40ºC. Subsequently, 8.2 g tetraethyl orthosilicate was added and the mixture was vigorously stirred for 45 min, followed by the addition of 2 mmol of (3-mercaptopropyl)trimethoxysilane (for propylthiol-SBA15), 4.1 mmol 3-aminopropyltrimethoxysilane (for SBA15-aminopropyl), N—[3-(trimoethoxysilyl)propyl]-ethylenediamine (for SBA15- ethyldiaminopropyl) or 3-[2-(2-aminoethylamino)ethylamino]propyl-trimethoxysilane (for diethylentriaminopropyl-SBA15). The mixture was stirred for 20 hours at 40ºC, then aged under static condition at 100 ºC for 24 hours. The functionalized-SBA15 was filtered and the P123 template was extracted by refluxing in ethanol for 24 hours.

### 6.2.2 Characterization

The surface area of mesoporous silica supports was determined using the 5 point BET (Brunauer–Emmett–Teller) nitrogen physiadsorption method. The measurements were made in the linear part of the isotherm where the BET equation is valid, namely in the pressure range of $0.06 < p/p_0 < 0.2$. The iron and aluminum content of SBA15-Fe-oxide and SBA15-Al-oxide were measured by dissolving the solids in concentrated HCl and measuring dissolved Fe and Al in the solution phase using an Inductively Coupled Plasma – Optical Emission Spectrometer (ICP-OES). The SBA15-Fe-oxide and SBA15-Al-oxide contained 9 wt. % of Fe and 4.7 wt. % of Al, respectively. The morphology of the solids was determined using a Philips CM200/FEG transmission electron microscope (TEM) at 200 kV and Zeiss Evo 10 scanning electron microscope (SEM) at 5 kV. X-ray diffraction analysis was performed with Cu Kα radiation using a Panalytical 2000 diffractometer.

### 6.2.3 Dissolution experiments

*Batch experiments.* All experiments were carried out at 25 ± 1ºC in a 50-mL polypropylene flask open to the atmosphere. 50 milligram of solid was added to 50 mL Milli-Q water and the suspension was vigorously stirred. The initial solution pH was adjusted using 1 M NaOH or 0.5 M $H_2SO_4$. Although sulfate can accelerate silica dissolution [144], this effect is only important in the presence of significant amount of sulfate (*e.g.*, 0.1 M $SO_4^{2-}$ in reference [144]). The maximum sulfate concentration in all of our experiments was approximately 50 μM and, therefore, its effect on silica dissolution is likely minimal. Solutions with pH 7 were

buffered with 1 mM of either piperazine-N,N'-bis(ethanesulfonic acid) (PIPES), bicarbonate or phosphate. Preliminary results indicated that the dissolution of SBA-15 was not affected by buffer types. Therefore, PIPES was used in all subsequent experiments. The use of PIPES, an organic buffer that does not adsorb on iron oxide surface or forms complexes with dissolved iron [145], allowed us to investigate the role of dissolved silica toward iron oxide reactivity (section 3.4). Solutions with pH 8 – 9 were buffered by 4 mM borate, while solutions with an initial pH of 10 were unbuffered. Samples were withdrawn at pre-determined time intervals, filtered immediately through a 0.2-μm nylon filter and analyzed for dissolved $SiO_2$.

*Column experiments with SBA-15.* Experiments were conducted in 10 mm ID glass columns. No dissolution of the column glass wall was detected in the control experiment. 0.25 gram SBA-15 was packed in the column and a pH 8.5 solution (buffered by 12 mM borate) was passed through the columns at a flow rate of 0.5 mL/min in a downward direction. The hydraulic retention time was ca. 0.4 min. A 0.45-μm nylon filter was attached to the outlet of the column to prevent elution of the solid out of the column (0.45-μm filter was used instead of 0.2-□m filter to avoid high back-pressure in the column). The concentration of dissolved $SiO_2$ in the column effluent was continuously measured throughout the course of the experiment.

### 6.2.4 Reactivity of iron oxide/SBA15 toward $H_2O_2$ decomposition

The effect of dissolution of SBA-15 on amorphous iron oxyhydroxide, (Fe-$ox_{(s)}$, Aldrich) reactivity toward catalytic $H_2O_2$ decomposition was investigated in both batch and column experiments. In batch experiments, the reactions were initiated by adding an aliquot of $H_2O_2$ stock solution to a pH-adjusted solution containing 1 g/L SBA-15 and 1 g/L Fe-$ox_{(s)}$. Samples were withdrawn at pre-determined time intervals and filtered immediately through a 0.2-μm nylon filter and analyzed for dissolved $SiO_2$ and $H_2O_2$. In column experiments, Fe-$ox_{(s)}$ and SBA-15 were packed in the column in different configurations (Figure 6-1), and pH 8.5 solution containing 5 mM $H_2O_2$ was passed through at a flow rate of 0.5 mL/min. The concentration of dissolved $SiO_2$ and $H_2O_2$ in the solution at the outlet was measured at predetermined time intervals.

### 6.2.5 Analytical methods

$H_2O_2$ was analyzed spectrophotometrically by the titanium sulfate method [85]. In the absence of $H_2O_2$, dissolved silica was measured either spectrophotometrically by the molybdosilicate method [146] or by ICP-OES. The molybdosilicate method only detects dissolved silica monomer and not other forms of silica (*e.g.*, $SiO_2$ in polymer forms or nano-sized $SiO_2$ particles), while the method using ICP-OES detects all forms of silica, including the particulate silica that passed through the filter. Two methods gave similar results (*i.e.*, $[SiO_2]_{molydosilicate} \sim 95\ \% [SiO_2]_{ICP\text{-}OES}$), indicating that minimal particulate silica was able to pass through the filter. ICP-OES was used to measure dissolved silica in the presence of $H_2O_2$, as interference from $H_2O_2$ precludes silica measurement by the molybdosilicate method. The deposition of $SiO_2$ on the Fe-$ox_{(s)}$ surface in column experiment was confirmed by using SEM with an EDAX Genesis energy dispersive X-ray unit (SEM-EDX).

To investigate the contribution of dissolved iron (leached from Fe-ox$_{(s)}$) toward $H_2O_2$ decomposition, total dissolved iron was quantified using the 1,10-phenanthroline method after adding hydroxylamine hydrochloride to the filtered samples [86]. The concentration of dissolved iron was always below the detection limit (*i.e.*, less than 5 μM), indicating that the amount of $H_2O_2$ decomposed by dissolved iron was negligible compared with that catalyzed by iron oxide surface.

All experiments were carried out at least in triplicate and average values along with one standard deviation are presented.

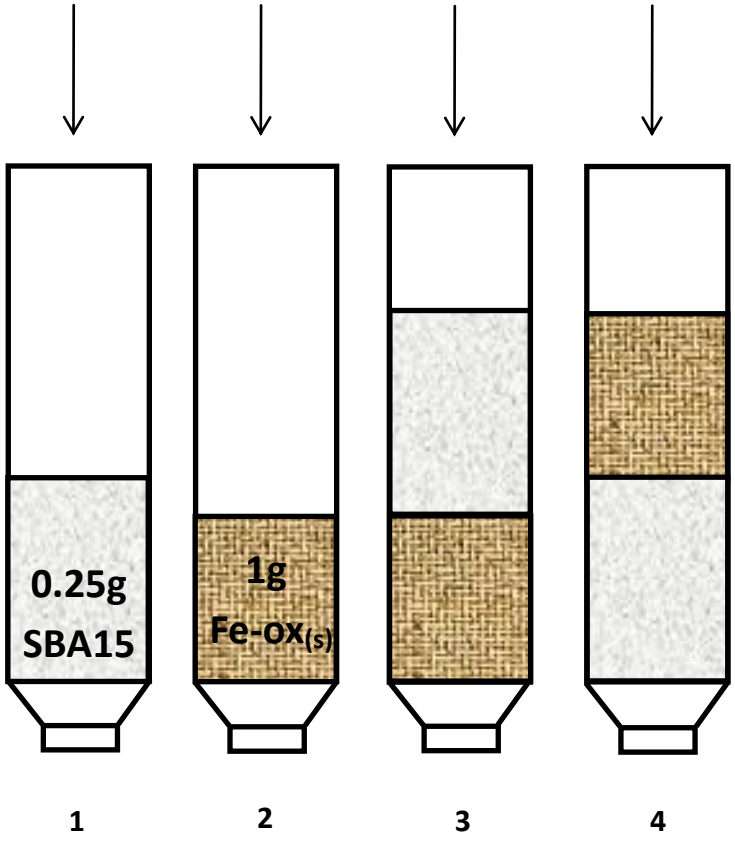


**Figure 6-1.** Investigation of $H_2O_2$ decomposition in column experiments (column ID = 10 mm). Column 1 and 2 contained only 0.25 gram SBA-15 or 1 gram Fe-ox$_{(s)}$ , respectively. Column 3 contained SBA-15 that was on the top of Fe-ox$_{(s)}$ while in column 4 Fe-ox$_{(s)}$ was on the top of SBA-15.

## 6.3 Results and discussion

### 6.3.1 Materials characterization

The BET surface area of the 9 mesoporous silica supports ranged from approximately 330 to 800 $m^2/g$ (Table 6-1), and the measured C values of the BET equation were between 50 and 250. The TEM micrographs (Figure 6-2) indicated that functionalization did not modify the mesoporous structure of the supports.

**Table 6-1**. Synthesis method and BET surface area.

| Material | Synthesis method | BET surface area ($m^2/g$) |
|---|---|---|
| SBA-15 | Structure directing agent: block copolymer P123 in aqueous solution of 130 ml $H_2O$ and 20 ml HCl 37%. Silica precursor: tetraethyl orthosilicate. Template removed by calcination. | 636 |
| HMS | Structure directing agent: dodecylamine in ethanol-water solution. Silica precursor: tetraethyl orthosilicate. Template removed by calcination. | 804 |
| MCM-41 | Structure directing agent: Cetyl trimethylammonium bromide in aqueous solution of ca. 6M $NH_4OH$. Silica precursor: tetraethyl orthosilicate. Template removed by calcination. | 501 |
| Propylthiol-SBA15 (SBA15-PT). Sulfur content: 0.54 mmol/gram. | Structure directing agent: block copolymer P123 in 125 ml aqueous solution of 1.9 M HCl. Silica precursor: tetraethyl orthosilicate.<br><br>Functional group precursor: 3-mercaptopropyl)trimethoxysilane. Template removed by extraction in ethanol. | 334 |

| | | |
|---|---|---|
| Aminopropyl-SBA15 (SBA15-AP). Nitrogen content: 0.9 mmol/gram. | As for SBA15-PT, except that the functional group precursor was 3-aminopropyltrimethoxysilane. | 570 |
| Ethylendiaminopropyl-SBA15 (SBA15-ED). Nitrogen content: 1.9 mmol/gram | As for SBA15-PT, except that the functional group precursor was: N—[3-(trimoethoxysilyl)propyl]-ethylenediamine | 530 |
| Diethylentriaminopropyl-SBA15 (SBA15-DT). Nitrogen content: 1.8 mmol/gram. | As for SBA15-PT, except that the functional group precursor was:3-[2-(2-aminoethylamino)ethyl-amino]propyl-trimethoxysilane | 380 |
| SBA15-Fe-oxide | Adsorption of iron-acetylacetonate $Fe(acac)_3$ onto bare SBA-15, followed by calcination at 500ºC for 4 hours. | 524 |
| SBA15-Al-oxide | Adsorption of aluminum-acetylacetonate $Al(acac)_3$ onto bare SBA-15, followed by calcination at 500ºC for 4 hours. | 373 |

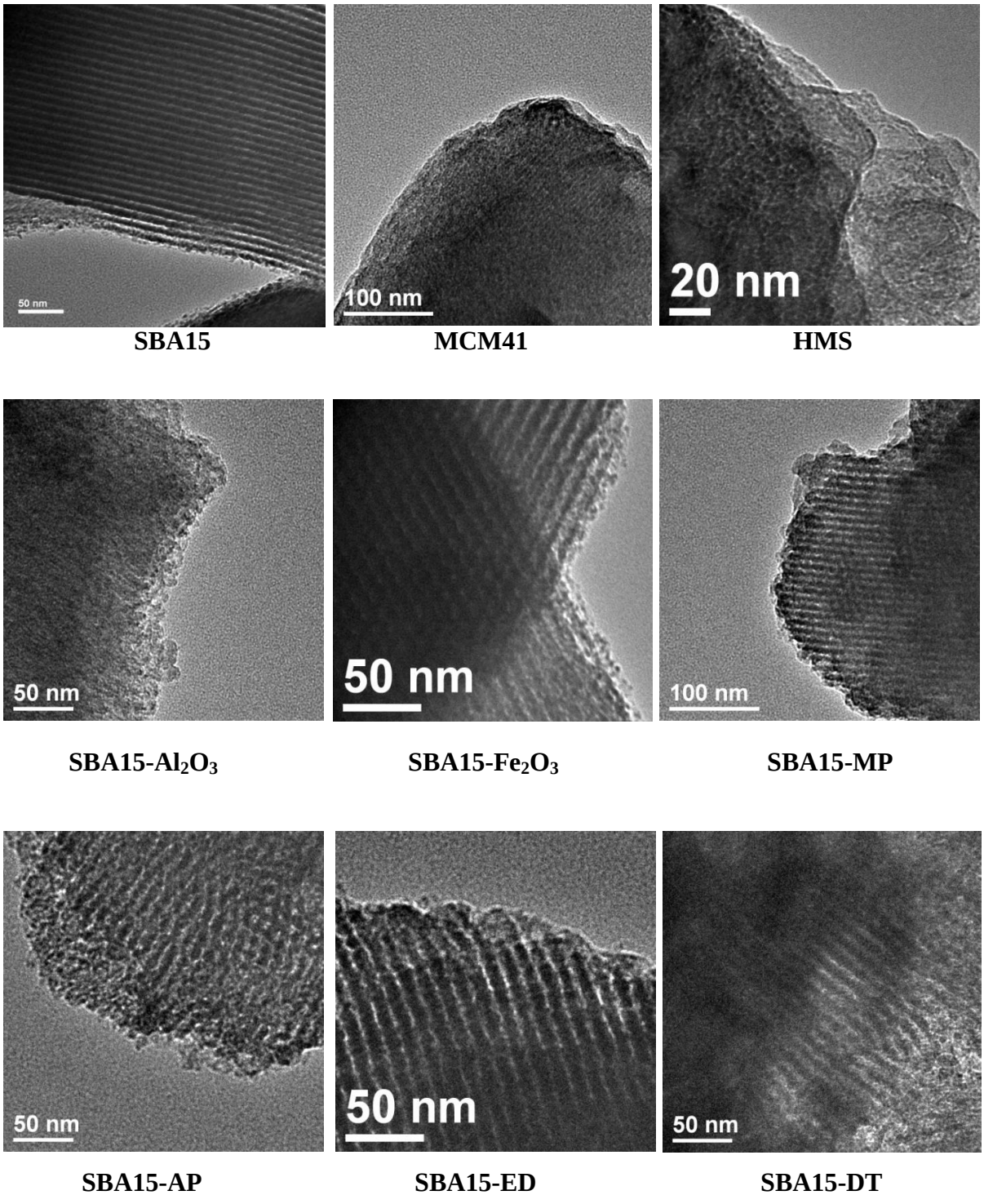


**Figure 6-2.** TEM images mesoporous silica materials.

### 6.3.2 Dissolution of SBA-15 in batch experiments

The dissolution of SBA-15 was investigated in well-mixed batch solutions containing 1 g/L SBA-15 (Figure 6-3). At pH values above 7, between 20 and 55 mg/L of dissolved silica (based on $SiO_2$) was released during the first 30 minutes. The dissolved silica concentration continued to increase throughout the 11-hour experiments, with no indication of saturation. The release of silica was attributable to the following reactions:

$$SiO_2 + 2H_2O \rightarrow H_4SiO_4 \ (pK_{s0} = 2.74) \ [138] \qquad (1)$$

$$H_4SiO_4 \Leftrightarrow H_3SiO_4^- + H^+ \ (pK_{a1} = 9.84) \ [138] \qquad (2)$$

The predicted concentration of dissolved silica in equilibrium with amorphous $SiO_{2(s)}$ at pH values between 7 and 9 is between 120 and 140 mg/L [138]. The dissolution of amorphous $SiO_{2(s)}$ in general, however, is a relatively slow process. Therefore, the rapid dissolution of SBA-15 is attributable to its high surface area and the unique wall and pore structure that provide convex surfaces with small radii of curvature, at which the activity of the amorphous silica exceeds that of the bulk material. The XRD pattern, SEM and TEM micrographs of the material that underwent the dissolution test were similar to those of the original SBA-15 (Figure 6-4, 6-5, and 6-6).

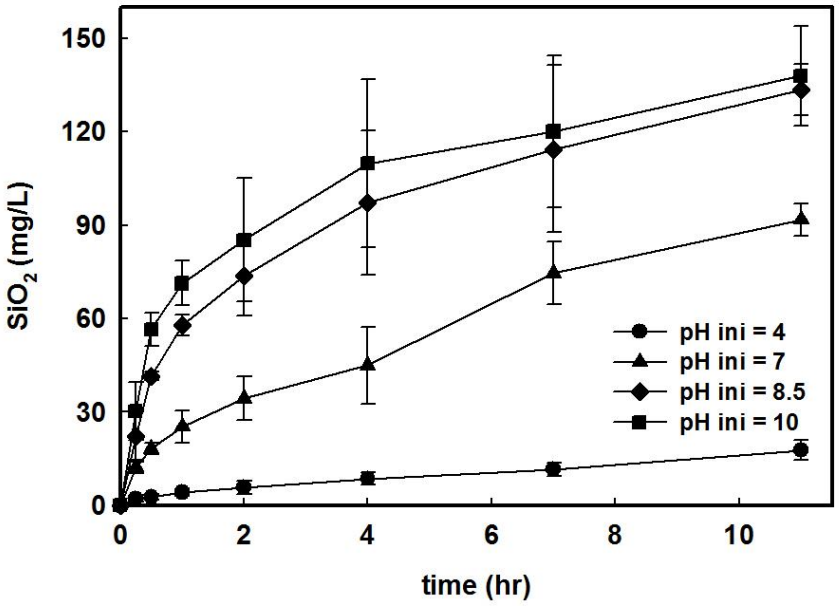


**Figure 6-3.** Dissolution of SBA-15 in well-mixed batch solution, 1 g/L SBA-15, $pH_{final}$ = 4.1 ± 0.1, 7 ± 0.1, 8.1 ± 0.1 and 8.6 ± 0.4 for $pH_{initial}$ of 4, 7, 8.5 and 10, respectively. Solutions with $pH_{initial}$ of 7 and 8.5 were buffered with 1 mM PIPES and 4 mM borate, respectively.

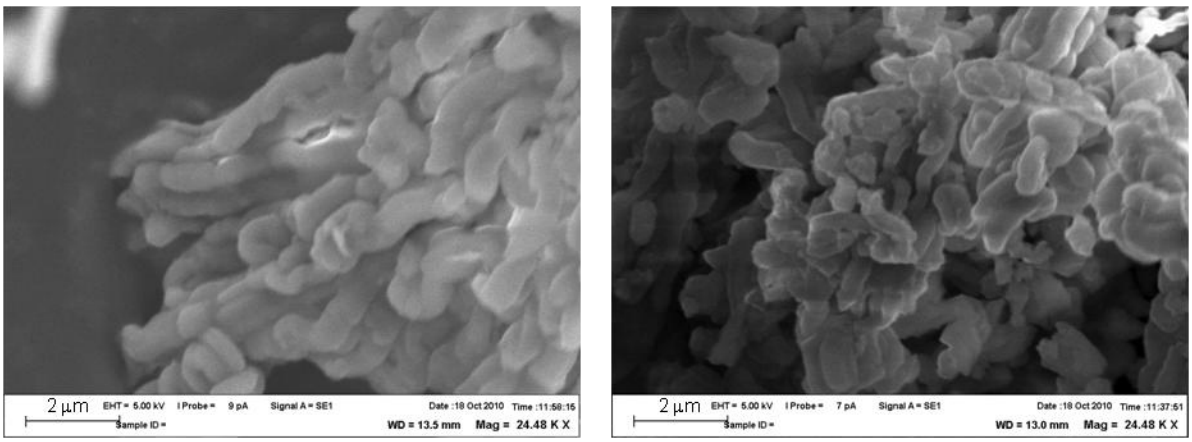


**Figure 6-4**. SEM images of the original SBA-15 (left) and the SBA-15 that was in the column for 45hr (right). No clear difference was observed.

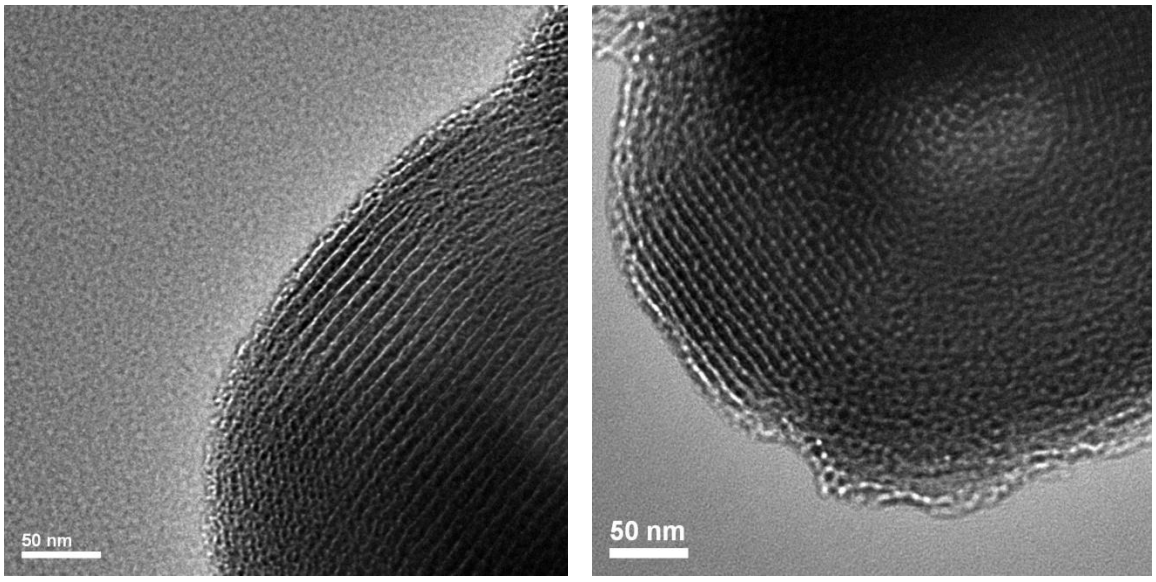


**Figure 6-5**. TEM images of SBA-15 recovered from the pH 8.5 solution after 20 hours. The original pore structure of the material was well observed.

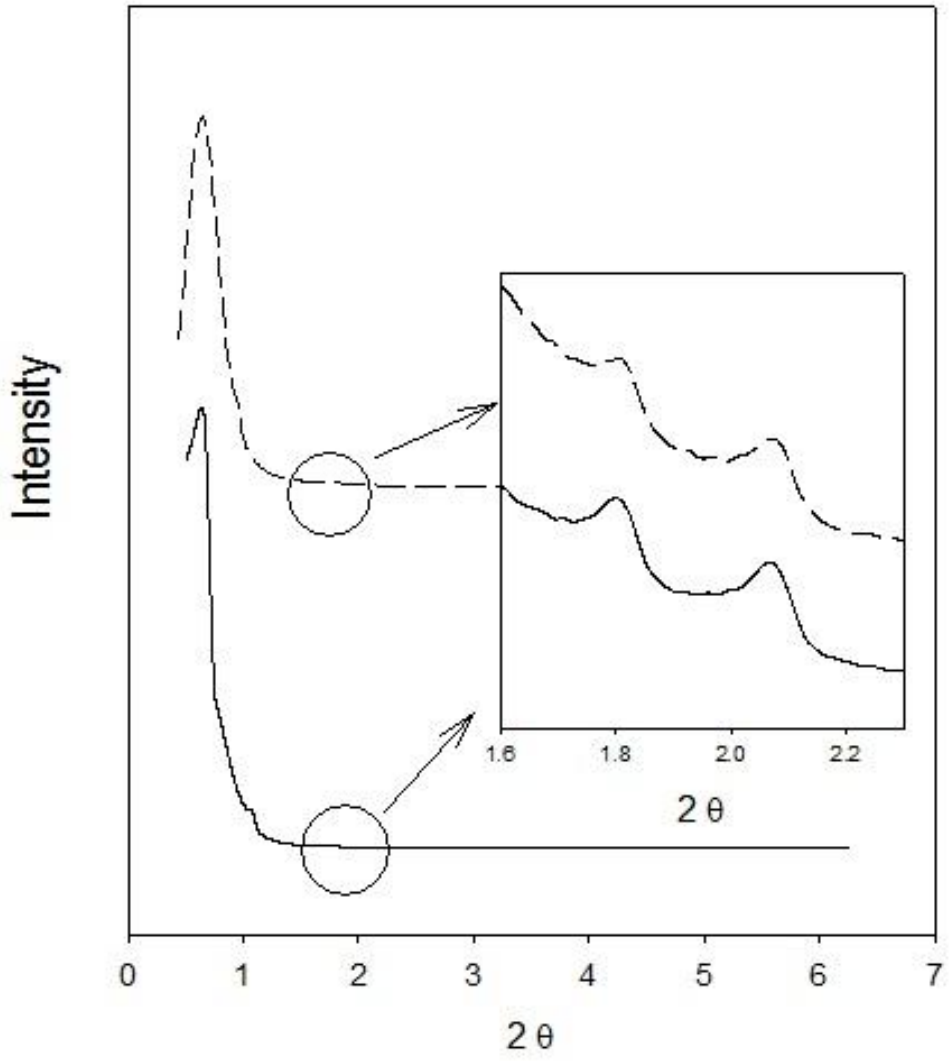


**Figure 6-6**. XRD spectrum of the original SBA-15 (dashed line) and the SBA-15 that was suspended in pH 7 solution for 24 hours (solid line).

### 6.3.3 Dissolution of HMS, MCM-41 and modified mesoporous supports

The dissolution of HMS and MCM-41, as well as modified materials such as propylthiol-, aminopropyl-, ethyldiaminopropyl-, diethylentriaminopropyl- functionalized SBA-15 (SBA15-PT, SBA15-AP, SBA15-ED and SBA15-DT, respectively), iron oxide-containing SBA-15 (SBA15-Fe-oxide) and alumina-containing SBA-15 (SBA15-Al.oxide) in pH 7 batch solution was also investigated. In these systems, the amount of dissolved silica released after a period of 4 hours ranged from approximately 7 mg/L (in the case of SBA15-Al-oxide) to 133 mg/L (in the case of SBA15-AP) (Figure 6-7, top). The concentration of dissolved silica in the SBA15-AP system exceeded the solubility of silica at pH 7 (*i.e.*, 120 mg/L [138]), suggesting that the solution was supersaturated with respect to amorphous $SiO_{2(s)}$. This phenomenon was also observed in a previous study with MCM-41 [66].

To gain insights into the relative stability among the mesoporous silica materials, their initial rate of dissolution in the batch experiment was calculated by normalizing the amount of dissolved silica released during the first 30 minutes against the materials' surface area. Despite the differences in the synthesis method (Table 6-1), SBA-15, HMS and MCM-41 dissolved at comparable rates (*i.e.*, ca. $3\times10^{-3} - 4\times10^{-3}$ mg×m$^{-2}$×hr$^{-1}$, Figure 6-4, bottom). Regarding the modified materials, three types of aminoalkyl-functionalized SBA-15 (namely SBA15-AP, SBA15-ED and SBA15-DT) dissolved at an initial rate that was approximately 1.5 to 3 times faster than that of SBA-15, HMS and MCM-41. In contrast, SBA15-PT, SBA15-Fe-oxide, and SBA15-Al-oxide dissolved 3 to 20 times slower than SBA-15, HMS and MCM-41 (Figure 6-4, bottom). The most stable material in this study was SBA15-Al-oxide (the initial dissolution rate of $2\times10^{-4}$ mg×m$^{-2}$×hr$^{-1}$). The effect of alumina on the stability of amorphous silica has been widely reported in the literature [139, 147, 148], although the mechanism through which alumina stabilizes silica remains unclear. The role of the iron oxide and propylthiol functional group on the enhanced stability of the SBA-15 support was also unclear. Regarding the aminoalkyl-functionalized SBA-15, faster dissolution of these materials was probably due to a high localized pH at the silica surface due to the basic nature of the amine groups (the $pK_a$ of aliphatic amines is above 10). Consequently, higher local pH values might cause faster dissolution and higher solubility of these materials.

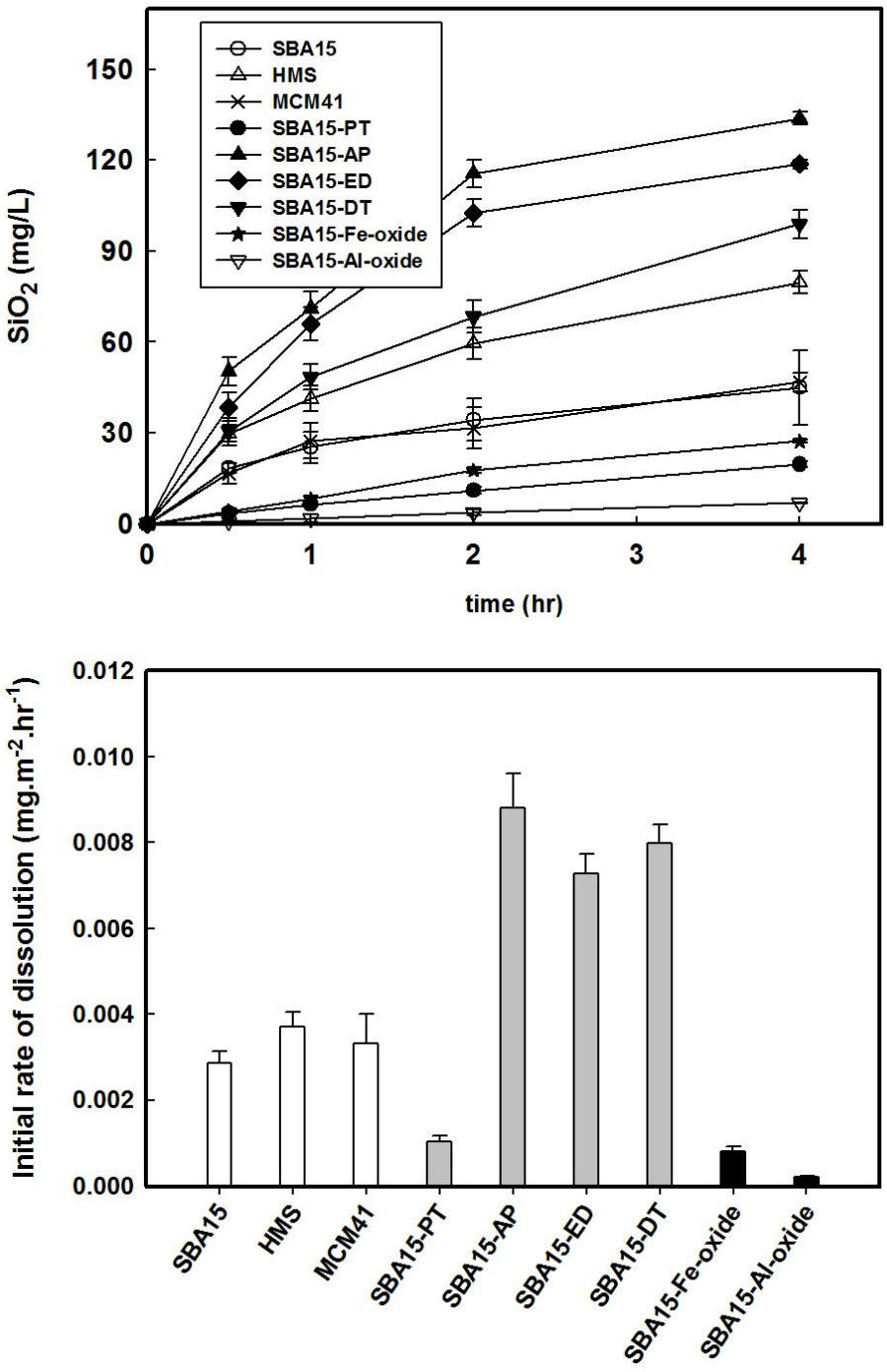


**Figure 6-7.** Dissolution of various mesoporous silica-based supports in well-mixed batch solution (top), and initial rates of dissolution during the first 30 minutes of the experiments (bottom). [solid] = 1 g/L, pH = 7 ± 0.1, buffered with 1 mM PIPES.

### 6.3.4 Long-term stability of SBA-15 in column experiment

The long term stability of SBA-15 was further investigated in a column experiment in which a pH 8.5 solution was passed continuously at 0.5 mL/min through SBA-15 packed in a 10 mm diameter column. The concentration of dissolved silica at the column outlet decreased gradually during the first 8.5 hours from more than 200 mg/L to approximately 90 mg/L then remained at this value for the next 18 hours (Figure 6-8). The higher-than-predicted concentration (*i.e.*, 120 – 140 mg/L [138]) observed initially was attributable to supersaturation with respect to amorphous $SiO_{2(s)}$. Approximately 120 mg of dissolved $SiO_2$ was recovered in the column effluent, which accounted for more than 45% of the initial mass of SBA-15 in the column (inset of Figure 6-8). The disappearance of SBA-15 in the column due to dissolution was visually observed after 45 hours (Figure 6-9).

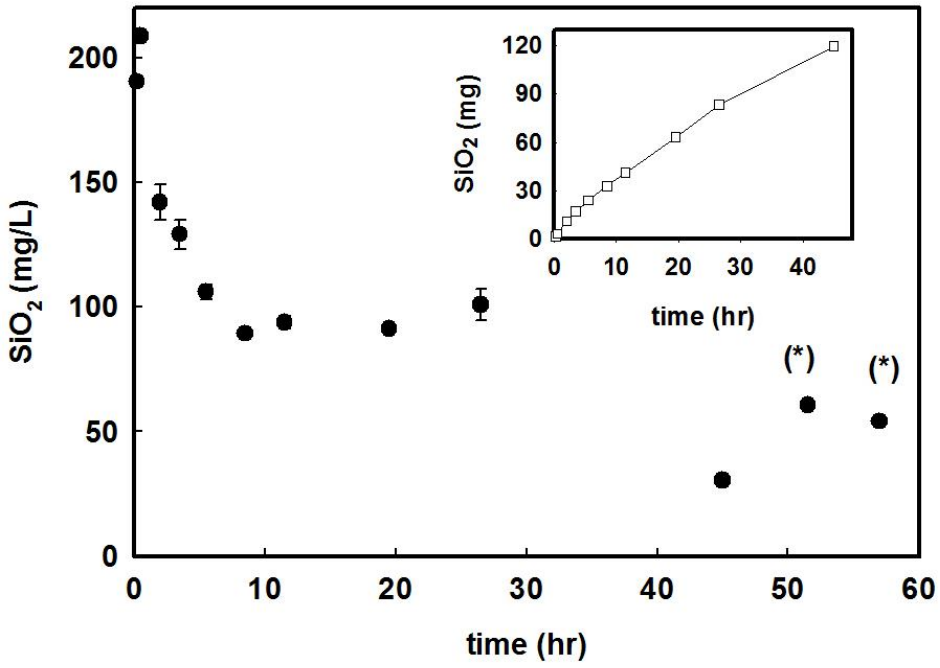


**Figure 6-8.** Column experiment containing 250 mg SBA-15. Flow rate = 0.5 mL/min, pH = 8.5, buffered with 12 mM borate. Inset: calculated cumulative amount of dissolved silica. (*): these data point were taken after the SBA-15 bed was compressed at t = 45 hr (see Figure 6-9 for detailed explanation).

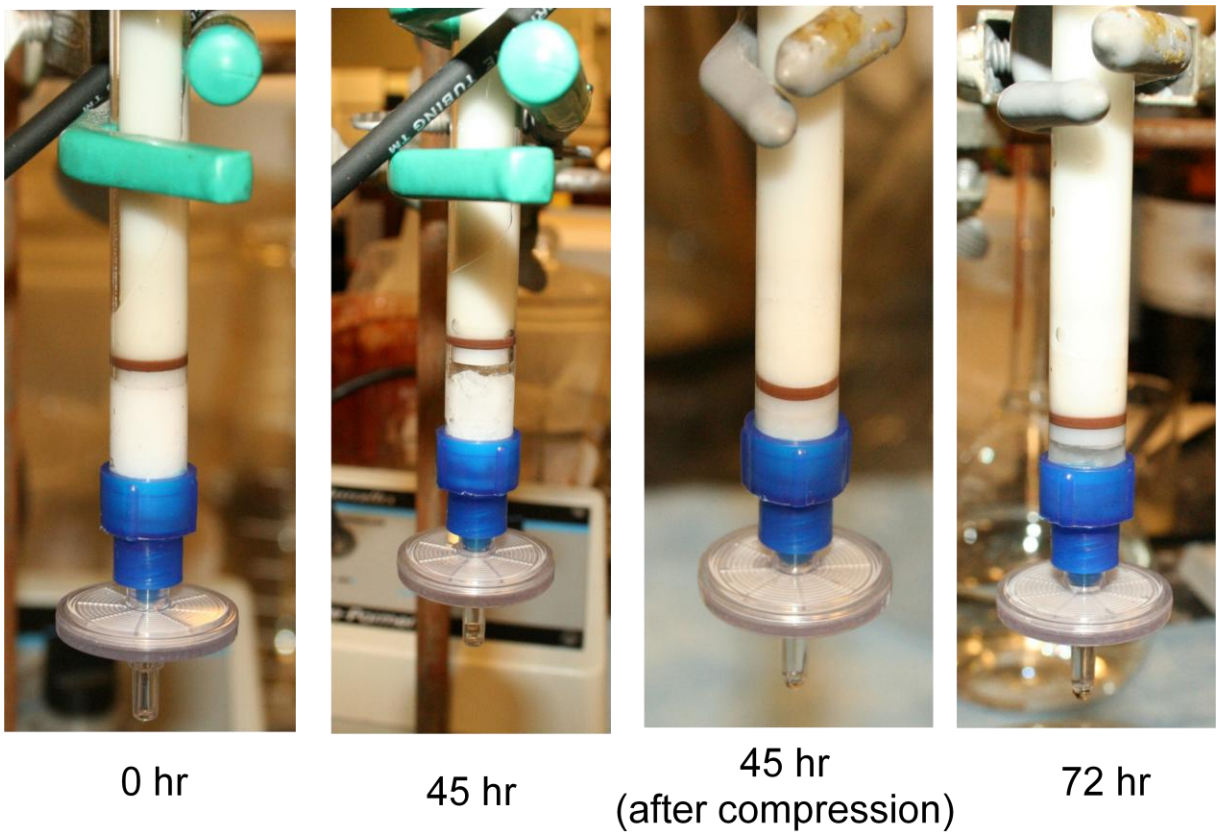


**Figure 6-9**. Dissolution of SBA-15 in the column experiment. After 45 hr, a significant amount of SBA-15 was dissolved. The remaining SBA-15 bed was then compressed in order to eliminate the void space in the column. Further dissolution created the void space again (image for t = 72 hr).

### 6.3.5 Impact of SBA-15 dissolution on reactivity of iron oxide in catalyzing $H_2O_2$ decomposition

Metal oxide-containing mesoporous silica catalysts have been used for $H_2O_2$-based oxidative water treatment [65, 136, 137]. However, the release of silica may alter the long term stability and reactivity of mesoporous silica-based catalysts, creating unexpected changes in the catalyst surface and hence the catalytic performance. To test this hypothesis, we studied the effect of SBA-15 dissolution on the kinetics of $H_2O_2$ decomposition catalyzed by Fe-$ox_{(s)}$ (reaction 3 and 4) [7, 24, 93].

$$\equiv Fe^{2+} + H_2O_2 \rightarrow \equiv Fe^{3+} + {}^{\bullet}OH + OH^- \quad (3)$$

$$\equiv Fe^{3+} + H_2O_2 \rightarrow \equiv Fe^{2+} + HO_2^{\bullet} + H^+ \quad (4)$$

$$HO_2^{\bullet} \Leftrightarrow H^+ + O_2^{\bullet -} \quad (5)$$

This process was selected as a case study because of the popularity of metal oxide-impregnated mesoporous silica/$H_2O_2$ systems in water treatment and organic synthesis. Organic solvents are often used in the latter application, but recent efforts to replace organic solvents with water have prompted interest in catalysts that are effective in water.

We studied the decomposition of $H_2O_2$ catalyzed by iron oxide in the presence of SBA-15. Although the catalytic activity of the iron oxide in this mixture does not represent that of iron-containing SBA-15 (where iron oxide is chemically deposited on the SBA-15 surface or is a part of the SBA-15 support), this approach allowed us to understand the role of dissolved silica released by SBA-15 unambiguously, which would not have been possible using iron-containing SBA-15.

In batch experiments, the rate of Fe-$ox_{(s)}$-catalyzed $H_2O_2$ decomposition was unaffected by the presence of SBA-15 at pH 4.2 ± 0.2, but significantly suppressed at pH 7.1 ± 0.1 (Figure 6-10). Because SBA-15 is not redox active and does not cause $H_2O_2$ decomposition, this difference was attributed to the dissolution of silica at higher pH, followed by adsorption onto the surface of Fe-$ox_{(s)}$, occupying iron sites responsible for $H_2O_2$ decomposition, thereby diminishing the reactivity of Fe-$ox_{(s)}$ [101]. SBA-15 dissolution was much slower at the lower pH value, and not enough silica was adsorbed on Fe-$ox_{(s)}$ to alter the rate of $H_2O_2$ decomposition.

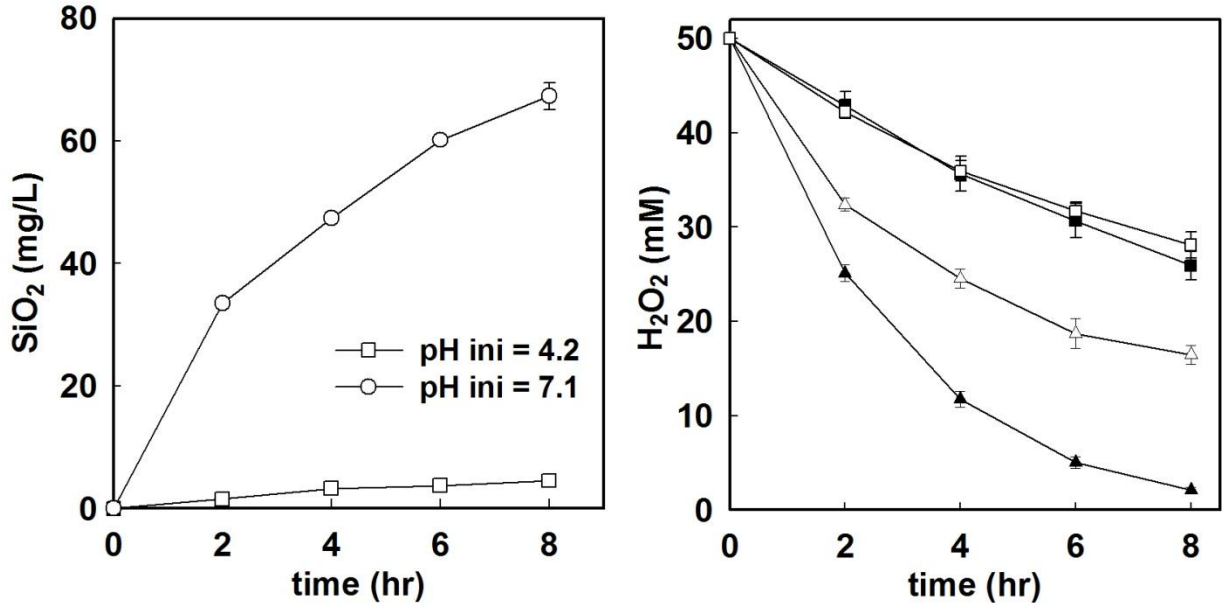


**Figure 6-10.** Dissolved silica and $H_2O_2$ concentration in batch experiment. [Fe-ox$_{(s)}$] = 1 g/L, [SBA-15] = 1 g/L, $[H_2O_2]_{inital}$ = 50 mM. Solution with pH = 7 ± 0.1 was buffered with 1mM PIPES. Squares: pH 4.2, triangles: pH 7 ± 0.1. Fe-ox$_{(s)}$ (filled symbol), Fe-ox$_{(s)}$ and SBA-15 (open symbol).

To confirm that the $H_2O_2$ decomposition was suppressed by deposition of dissolved silica onto the iron oxide rather than by some unanticipated interaction between SBA-15 and iron oxide, the catalytic decomposition of $H_2O_2$ was studied further using column experiments (Figure 6-11). The $H_2O_2$ concentration at the outlet of column 1, containing only SBA-15, was unaffected by passage through the column because SBA-15 does not catalyze $H_2O_2$ decomposition. More than 97% of the initial $H_2O_2$ was decomposed as the solution passed through column 2 (containing only Fe-ox$_{(s)}$) and column 4 (in which the solution passed through the Fe-ox$_{(s)}$ before encountering SBA-15) due to reaction (3) and (4). For column 3 (in which the solution passed through SBA-15 before Fe-ox$_{(s)}$), the concentration of $H_2O_2$ increased gradually during the experiment as would be expected if the activity of the catalyst was decreasing over time.

Comparison of the dissolved silica concentrations leaving columns 1 and 3 indicates that the dissolved silica was adsorbed by Fe-ox$_{(s)}$, resulting in lower dissolved silica concentrations at the outlet of column 3. This adsorption was confirmed by SEM/EDS analysis of the Fe-ox$_{(s)}$ from column 3 after the test, which showed a Si peak (Figure 6-12). With time, adsorption of dissolved silica lowered the catalytic activity of the Fe-ox$_{(s)}$ and therefore the $H_2O_2$ concentration at the outlet gradually increased.

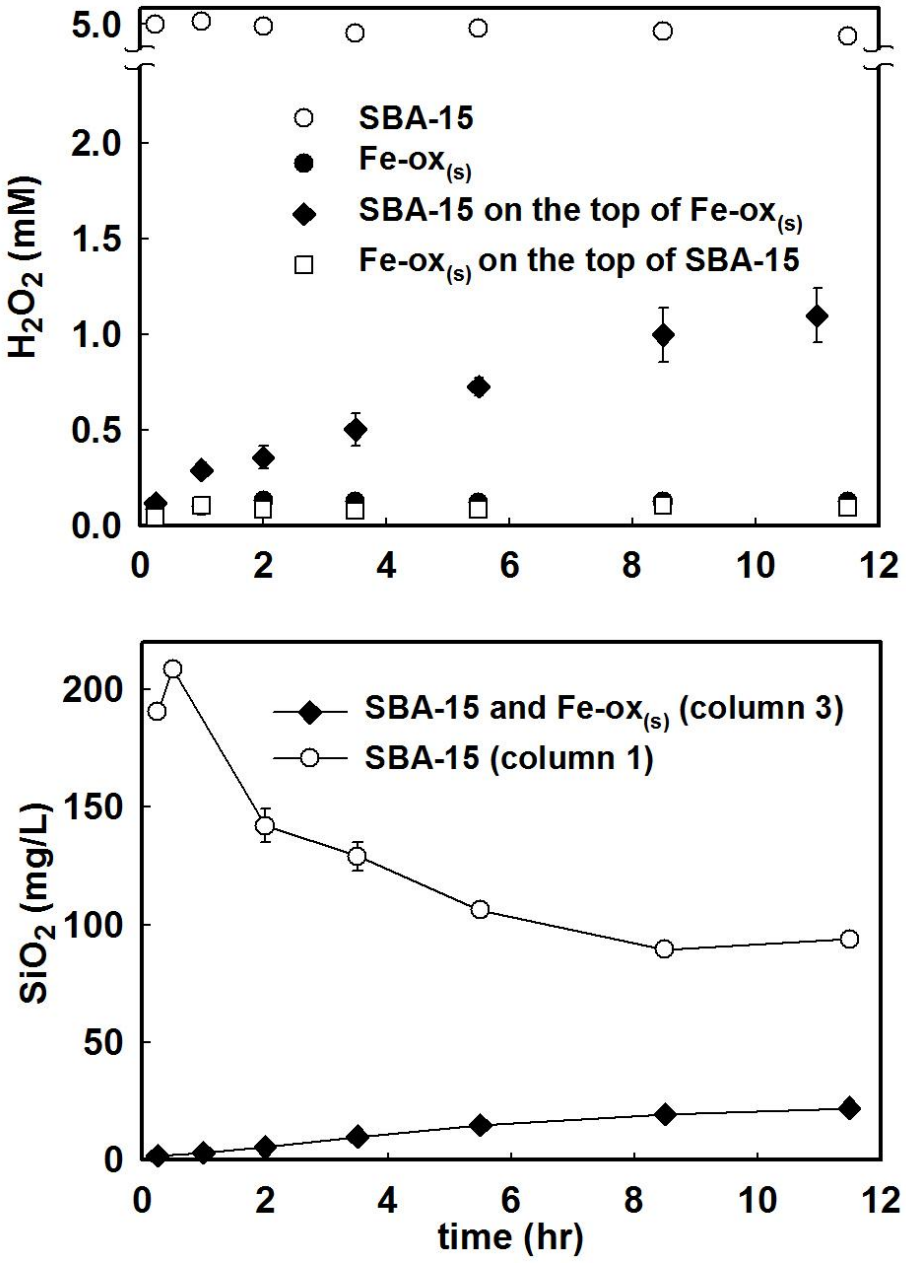


**Figure 6-11.** Hydrogen peroxide and dissolved silica concentration at outlet of 10 mm ID columns through which pH = 8.5 ± 0.1 solutions containing 5 mM $H_2O_2$ were flowed at a 0.5 mL/min. Column was packed with 0.25 g SBA-15 and/or 1g $Fe\text{-}ox_{(s)}$.

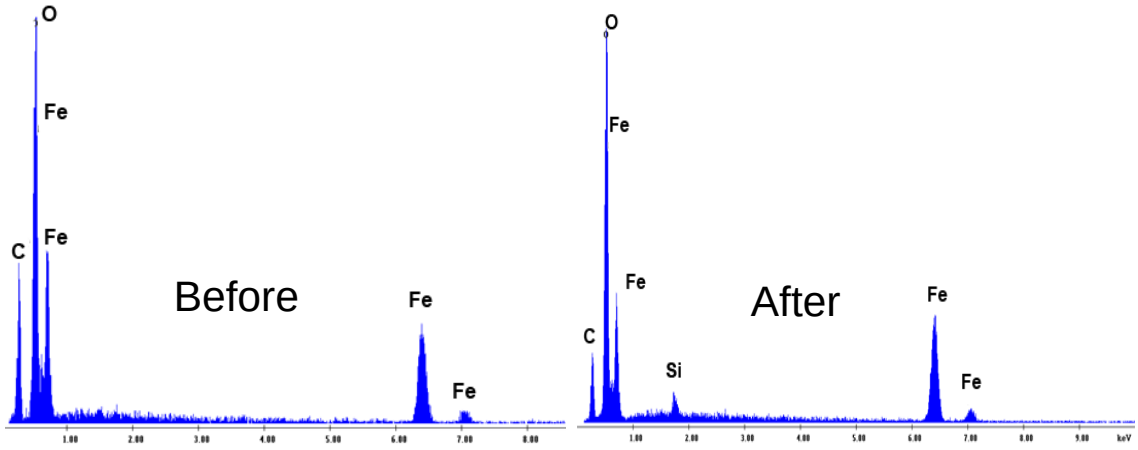


**Figure 6-12.** EDS spectrum of the Fe-ox$_{(s)}$ surface before and after the column experiment. The Fe-ox$_{(s)}$ sample was collected from column 3 at the end of the experiment. The carbon peak is due to the carbon coating needed to prevent charging in the SEM.

### 6.3.6 Dissolution of mesoporous silica supports – a broader implication

In addition to being used in advanced oxidation processes for water treatment, mesoporous silica-based supports also have been proposed for applications such as adsorption, separation, and sensing [132, 149]. The results of our study, however, raise significant questions about the merits of their application in aqueous media. For example, when mesoporous silica is used to encapsulate enzymes and proteins [150], a process that is routinely conducted at pH values ranging from 5 to 11, significant dissolution of the substrate would be expected over a time scale of hours to days. Functionalized mesoporous silica also has been proposed as an adsorbent for removing toxic metals, anions, radionuclides and organic contaminants from polluted water. The dissolution of these adsorbents could release not only adsorbed contaminants but also the organic functional compounds, many of which are toxic to aquatic life. In addition, it was observed that adsorption of Cr(VI) [130] and organic contaminants [134] on various functionalized SBA-15 and HMS substrates was a pH dependent process, with lower adsorption affinity at neutral and alkaline pH. The dissolution of adsorbent might explain why adsorption capacity decreased at higher pH. Additional research is needed to evaluate the performance of mesoporous silica materials in these applications.

## 6.4 Conclusion

In summary, we have demonstrated that mesoporous silica materials such as SBA-15, HMS and MCM-41, four types of functionalized SBA-15, and iron and aluminum oxide-containing SBA-15 are unstable in aqueous solution, especially at circumneutral and more basic pH values. The results raise questions about the use of these materials in aqueous-based applications such as adsorption and catalysis, suggesting that these materials may only be suitable under acidic conditions, where silica dissolves slowly. We also showed that silica dissolved from mesoporous silica supports such as SBA-15 may change the reactivity of catalysts. Our experiments have shown that silica-containing iron oxide, produced from adsorption of dissolved silica on Fe-$ox_{(s)}$, was less active in catalyzing the decomposition of $H_2O_2$ than pure iron oxide.

Among the studied materials, the SBA-15 support that was functionalized with propylthiol or contained iron or aluminum oxide was more stable than the bare SBA-15. Although the mechanism through which the propylthiol group and metal oxides enhance the stability of silica is still unclear, our findings suggest that it might be possible to design more stable mesoporous silica based materials. Given the complex nature of functional group/metal center and support interaction, additional research is required to further investigate this issue.

# Chapter 7. Conclusions

The research described in this dissertation investigated the ability of various silica- and alumina-containing iron catalysts, minerals, and aquifer materials to convert $H_2O_2$ into $^{\bullet}OH$ for use in water treatment. New insights have been gained into the role of silica and alumina, as well as solution conditions, such as pH and dissolved silica, in iron-mediated $H_2O_2$ activation. These findings have important implications for the development of effective catalysts for $H_2O_2$ activation in *ex situ* water treatment systems, as well as for the design and operation of $H_2O_2$-based *in situ* chemical oxidation technologies for groundwater and soil remediation.

## 7.1 Iron-containing catalysts for $H_2O_2$ activation

One of the major contributions of the research described in this dissertation was related to the activation of $H_2O_2$ by iron-containing minerals and catalysts under *circumneutral* pH conditions. Although the synthesis of catalysts capable of effectively activating $H_2O_2$ has been an active research field, most previous studies have focused on $H_2O_2$ activation under *acidic* pH conditions. Therefore, the results and conclusions reported in this dissertation are likely more relevant to the water treatment scenarios where bicarbonate buffering is strong and pH adjustment is problematic.

The research described in Chapter 2 explored the ability of silica- and alumina-containing iron catalysts to activate $H_2O_2$ under circumneutral pH conditions. The results of this study indicated that the catalysts that were synthesized by a sol-gel process exhibited a stoichiometric efficiency which was 10 to 80 times higher than that of common iron oxides. The significant enhancement in $^{\bullet}OH$ production is attributable to the interaction of Fe with Al and Si in the mixed oxides, which alters the surface redox processes, favoring the production of $^{\bullet}OH$ during $H_2O_2$ decomposition. The silica- and alumina-containing iron oxide catalyst has the potential to be more effective in the *ex situ* oxidative treatment of industrial waste and contaminated water at circumneutral pH than iron oxides that have been proposed for this application.

Iron-containing mesoporous silica SBA-15 catalyst, synthesized by immobilizing iron on the SBA-15 support, also exhibited a stoichiometric efficiency that was approximately 10 times higher than that of common iron oxides (Chapter 5). This indicates that the efficiency improvement is not unique to the sol-gel synthesis process; therefore, various synthesis techniques can be employed to obtain a better iron catalyst. Furthermore, the use of the iron-containing mesoporous silica SBA-15 catalyst offer the potential for selectively oxidizing phenol in the presence of bovine serum albumin, a macromolecule that was employed as a model for proteins and natural organic matter. This selective oxidation increases the stoichiometric efficiency when the presence of natural organic matter in water competes with contaminants for $^{\bullet}OH$.

Iron-containing aluminosilicates (*i.e.*, montmorillonite and nontronite) also were shown to be as effective as synthetic catalysts in $H_2O_2$ activation (Chapter 3). These materials are naturally available, relatively cheap, and have the potential to be employed in *ex situ* advanced oxidation processes for water remediation.

The stability of the silica supports and the effect of silica dissolution on the long-term performance of the catalysts were investigated in Chapter 6. In previous research, the dissolution of silica supports was often ignored by researchers who studied the heterogeneous Fenton reaction, because it was assumed that silica does not dissolve at an appreciable rate, and that dissolved silica does not affect the reactivity of iron-containing solids with $H_2O_2$. The research in Chapter 6 showed that mesoporous silica supports dissolved rapidly under circumneutral conditions due to their high surface area and poor crystalinity. More importantly, the released dissolved silica adsorbed onto the iron surface and lowered its reactivity with $H_2O_2$. Thus, the rapid dissolution of most mesoporous silica materials raises questions about their use not only for $H_2O_2$ activation, but also for other applications in water treatment, such as separation and adsorption, because silica dissolution might alter the behavior of the material.

## 7.2 The activation of $H_2O_2$ in *in situ* remediation

The ability of iron-containing sediments and aquifer materials to activate $H_2O_2$ has been investigated previously, but the correlation between the surface properties of these materials and their reactivity remains poorly understood. Thus, it is currently difficult to predict the performance of $H_2O_2$-based *in situ* chemical oxidation (ISCO) treatment systems.

To gain new insights into factors that control the activation of $H_2O_2$ in ISCO, the reactivity of ten aquifer materials was investigated and correlated with their surface properties (Chapter 3). The results of this study showed that the stoichiometric efficiency of aquifer materials was comparable with that of iron-containing minerals. The surface property-reactivity analysis indicated that aquifer materials containing high concentrations of manganese oxides decomposed $H_2O_2$ at a faster rate but generated less $^{\bullet}OH$ (*i.e.*, they had a lower stoichiometric efficiency). The strong correlation between Mn content and $H_2O_2$ loss rate and $^{\bullet}OH$ yield suggests that the amount of Mn in aquifer materials could serve as a proxy for predicting the material's efficiency in $H_2O_2$ activation.

To explore possible approaches to enhance $^{\bullet}OH$ yield in the aquifer materials systems, aquifer materials were treated with citrate-bicarbonate-dithionite (CBD) solution to remove iron and manganese oxide coatings, components that are ineffective in activating $H_2O_2$ (Chapter 3). Compared with the original aquifer materials, the CBD treated counterparts exhibited a lower reactivity with $H_2O_2$ yet a higher stoichiometric efficiency, so they are more effective for the activation of $H_2O_2$ in ISCO.

Chapter 3 and 4 of this dissertation addressed a major issue associated with $H_2O_2$-based ISCO, namely the short lifetime of $H_2O_2$ in the subsurface. The fast decomposition of $H_2O_2$ in the subsurface is often considered detrimental, because $H_2O_2$ may be consumed before it reaches contaminated zones. The research described in Chapter 3 and 4 indicated that dissolved silica in groundwater decreased the reactivity of iron-containing minerals and aquifer materials with $H_2O_2$, thereby increased $H_2O_2$ persistence. Therefore, in systems where the subsurface is deficient in dissolved silica, dissolved silica could be injected together with $H_2O_2$ to increase the

persistence of $H_2O_2$ and move the zone of remediation further from the injection well. Dissolved silica is inexpensive and benign, and can replace other $H_2O_2$-stabilizing agents that are currently being used, such as phosphate or citrate.

## 7.3 Future research

The research described in this dissertation has addressed various fundamental and practical questions related to the use of the heterogeneous Fenton reaction for *ex situ* and *in situ* water remediation. One major finding of this research was that the reactivity of iron can be tailored for more effective production of $^{\bullet}OH$ during the decomposition of $H_2O_2$. Although significant improvement in stoichiometric efficiency was achieved, the highest stoichiometric efficiency reported in this research, however, was only a few percent, which is approximately an order of magnitude lower than the theoretical stoichiometric efficiency (see the footnote of Table 1-2). Therefore, additional research is needed to improve the $H_2O_2$ utilization efficiency and reduce the treatment cost. Several areas for future research are suggested below.

First, increased understanding of the $H_2O_2$ activation mechanism is needed to develop better catalysts. Although the research in Chapter 2 indentified the importance of silica and alumina in $H_2O_2$ activation, the exact mechanism through which silica and alumina affect iron reactivity is not well understood. Future research addressing this fundamental issue could involve the use of surface characterization techniques to understand the interaction among iron, silicon and aluminum, and/or the distribution of these elements on the catalyst surface. In addition, detailed correlation between the structure of well-characterized materials (*e.g.*, montmorillonite and nontronite in Chapter 3) and their ability to produce $^{\bullet}OH$ from $H_2O_2$ may provide further insights into the role of silica and alumina.

It has been proposed that in addition to $^{\bullet}OH$, the decomposition of $H_2O_2$ in the heterogeneous Fenton system also produces surface-bound ferryl species (Chapter 2, Scheme 2). In agreement with this hypothesis, Gonzalez-Olmos *et al.* recently demonstrated that methanol oxidation in a zeolite/$H_2O_2$ system was due to the reaction with an oxidant that was different from $^{\bullet}OH$, possibly surface bound ferryl [151]. Notably, the stoichiometric efficiency was calculated to be approximately 30%, which was 10 to 1000 times higher than that in the systems where contaminants are oxidized by $^{\bullet}OH$. The high stoichiometric efficiency associated with the surface-bound ferryl species suggests that the heterogeneous Fenton reaction might be effective for the treatment of contaminants that can react with surface-bound ferryl, such as As[III]. Additional research is needed to assess the production and reactivity of surface-bound ferryl in the heterogeneous Fenton system.

The research described in Chapter 5 investigated the use of an iron-containing mesoporous silica SBA-15 catalyst for selective oxidation of phenol in the presence of non-target compounds (*i.e.*, bovine serum albumin and humic acid). One limitation of this catalyst is that only a partial selective oxidation was observed in the presence of humic acid, as some of humic acid was able to enter the mesopores of SBA-15 and scavenge $^{\bullet}OH$. More selective oxidation

may be achieved through the use of supports with smaller pores (*e.g.*, MCM-41 mesoporous silica, zeolites) that could allow better exclusion of natural organic matter. In addition to size exclusion, other approaches to achieve selective oxidation could involve the synthesis of a catalyst that enhances the preferential adsorption (*e.g.*, by molecular recognition or molecular imprinting) followed by oxidation of the target contaminant.

Silica-supported iron catalysts are susceptible to dissolution under circumneutral pH conditions. The research in Chapter 6 indicated that functionalizing with propylthiol, or immobilizing aluminum or iron oxides onto SBA-15 mesoporous silica support enhanced its stability in aqueous solution. Given the complex nature of functional group/metal center and support interaction, additional research is needed to further investigate the approaches to design more stable catalysts.

For *in situ* treatment systems, the stoichiometric efficiency could be enhanced by modifying the surface of aquifer materials to remove components that are ineffective at $^{\bullet}OH$ production. One approach used in this research was to treat aquifer materials with citrate-bicarbonate-dithionite solution to remove surface manganese and iron oxides (Chapter 3). Although the addition of this solution into soil and groundwater is unlikely to be practical, other approaches that remove these oxides could include the injection of a metal-complexing agent, such as ethylenediaminetetracetic acid (*i.e.*, EDTA), and the adjustment of redox conditions in the subsurface to favor the reductive dissolution of manganese and iron oxides.

The research described in Chapter 3 and 4 led to a proposal that dissolved silica could be injected together with $H_2O_2$ to enhance $H_2O_2$ stability in *in situ* remediation systems. One concern associated with this approach is the precipitation of silica in the subsurface, which could decrease the permeability of the aquifer. Studies that monitor $H_2O_2$ lifetime and permeability in a column reactor would be needed to assess the practicality of injecting dissolved silica into the subsurface.

Understandings of the correlation between the physico-chemical properties of aquifer materials and their reactivity will help predict the performance of $H_2O_2$-based ISCO systems. The research in Chapter 3 suggested that the rate of $H_2O_2$ decomposition and $^{\bullet}OH$ yield are strongly correlated with the Mn content of the aquifer materials samples. Additional research with more aquifer materials is needed to assess the predictive strength of this correlation, and to gain insights into the role of other aquifer materials properties, such as surface area, particle size, organic matter and inorganic carbon content.

# References


1. Jones, C. W., In *Applications of hydrogen peroxide and derivatives*, Royal Society of Chemistry: 1999.

2. Beltran, F. J., Ozone – UV radiation – hydrogen peroxide oxidation technologies. In *Chemical Degradation Methods for Wastes and Pollutants*, CRC Press: 2003.

3. Tarr, M. A., Fenton and modified Fenton methods for pollutant degradation. In *Chemical Degradation Methods for Wastes and Pollutants*, CRC Press: 2003.

4. Ravikumar, J. X.; Gurol, M. D., Chemical oxidation of chlorinated organics by hydrogen peroxide in the presence of sand. *Environmental Science & Technology* **1994,** *28*, 394-400.

5. Miller, C. M.; Valentine, R. L., Hydrogen peroxide decomposition and quinoline degradation in the presence of aquifer material. *Water Research* **1995,** *29*, 2353-2359.

6. Valentine, R. L.; Wang, H. C. A., Iron oxide surface catalyzed oxidation of quinoline by hydrogen peroxide. *Journal of Environmental Engineering* **1998,** *124*, 31.

7. Pignatello, J. J.; Oliveros, E.; MacKay, A., Advanced oxidation processes for organic contaminant destruction based on the Fenton reaction and related chemistry. *Critical Reviews in Environmental Science and Technology* **2006,** *36*, 1.

8. Suthersan, S. S.; Payne, F. C., *In situ remediation engineering*. CRC Press: 2005.

9. Siegrist, R. L.; Crimi, M. L.; Simpkin, T. J., *In Situ Chemical Oxidation for groundwater remediation*. Springer: 2011.

10. Huling, S. G.; Pivetz, B. E., In-Situ Chemical Oxidation. In *U.S. Environmental Protection Agency Engineering Issue*, 2006.

11. Chou, S.; Huang, C., Application of a supported iron oxyhydroxide catalyst in oxidation of benzoic acid by hydrogen peroxide. *Chemosphere* **1999,** *38*, 2719-2731.

12. Lim, H.; Lee, J.; Jin, S.; Kim, J.; Yoon, J.; Hyeon, T., Highly active heterogeneous Fenton catalyst using iron oxide nanoparticles immobilized in alumina coated mesoporous silica. *Chemical Communications* **2006**, 463-465.

13. Luo, M.; Bowden, D.; Brimblecombe, P., Catalytic property of Fe-Al pillared clay for Fenton oxidation of phenol by $H_2O_2$. *Applied Catalysis B: Environmental* **2009,** *85*, 201-206.

14. Garrido-Ramírez, E. G.; Theng, B. K. G.; Mora, M. L., Clays and oxide minerals as catalysts and nanocatalysts in Fenton-like reactions — A review. *Applied Clay Science* **2010,** *47*, 182-192.

15. Lipczynska-Kochany, E.; Sprah, G.; Harms, S., Influence of some groundwater and surface waters constituents on the degradation of 4-chlorophenol by the Fenton reaction. *Chemosphere* **1995,** *30*, 9-20.

16. Watts, R. J.; Foget, M. K.; Kong, S.-H.; Teel, A. L., Hydrogen peroxide decomposition in model subsurface systems. *Journal of Hazardous Materials* **1999,** *69*, 229-243.

17. Pokrovski, G. S.; Schott, J.; Farges, F.; Hazemann, J.-L., Iron (III)-silica interactions in aqueous solution: insights from X-ray absorption fine structure spectroscopy. *Geochimica et Cosmochimica Acta* **2003,** *67*, 3559-3573.

18. Anderson, P. R.; Benjamin, M. M., Effect of silicon on the crystallization and adsorption properties of ferric oxides. *Environmental Science & Technology* **1985,** *19*, 1048-1053.

19. Cameron, A. J.; Liss, P. S., The stabilization of "dissolved" iron in freshwaters. *Water Research* **1984,** *18*, 179-185.

20. Buxton, G. V.; Greenstock, C. L.; Helman, W. P.; Ross, A. B., Critical review of rate constants for reactions of hydrated electrons, hydrogen atoms, and hydroxyl radicals ($OH/O^-$) in aqueous solution. *Journal of Physical Chemistry Reference Data* **1988,** *17*, 513-886.

21. Fenton, H. J. H., LXXIII.-Oxidation of tartaric acid in presence of iron. *Journal of the Chemical Society, Transactions* **1894,** *65*, 899-910.

22. Haber, F.; Weiss, J., The catalytic decomposition of hydrogen peroxide by iron salts. *Proceedings of the Royal Society of London. Series A - Mathematical and Physical Sciences* **1934,** *147*, 332-351.

23. Sedlak, D. L.; Andren, A. W., Oxidation of chlorobenzene with Fenton's reagent. *Environmental Science & Technology* **1991,** *25*, 777-782.

24. Lin, S.-S.; Gurol, M. D., Catalytic decomposition of hydrogen peroxide on iron oxide: kinetics, mechanism, and implications. *Environmental Science & Technology* **1998,** *32*, 1417-1423.

25. Kanel, S. R.; Neppolian, B.; Jung, H.; Choi, H., Comparative removal of polycyclic aromatic hydrocarbons using iron oxide and hydrogen peroxide in soil slurries *Environmental Engineering Science* **2004,** *21*, 741-751.

26. Huang, H. H.; Lu, M. C.; Chen, J. N., Catalytic decomposition of hydrogen peroxide and 2-chlorophenol with iron oxides. *Water Research* **2001,** *35*, 2291.

27. Matta, R.; Hanna, K.; Chiron, S., Fenton-like oxidation of 2,4,6-trinitrotoluene using different iron minerals. *Science of The Total Environment* **2007,** *385*, 242-251.

28. Huling, S. G.; Arnold, R. G.; Sierka, R. A.; Miller, M. R., Influence of peat on Fenton oxidation. *Water Research* **2001,** *35*, 1687-1694.

29. Xue, X.; Hanna, K.; Deng, N., Fenton-like oxidation of Rhodamine B in the presence of two types of iron (II, III) oxide. *Journal of Hazardous Materials* **2009,** *166*, 407-414.

30. Kwan, W. P.; Voelker, B. M., Decomposition of hydrogen peroxide and organic compounds in the presence of dissolved iron and ferrihydrite. *Environmental Science & Technology* **2002,** *36*, 1467-1476.

31. Petigara, B. R.; Blough, N. V.; Mignerey, A. C., Mechanisms of hydrogen peroxide decomposition in soils. *Environmental Science & Technology* **2002,** *36*, 639-645.

32. Spain, J. C.; Milligan, J. D.; Downey, D. C.; Slaughter, J. K., Excessive bacterial decomposition of $H_2O_2$ during enhanced biodegradation. *Ground Water* **1989,** *27*, 163-167.

33. Morgan, P.; Watkinson, R. J., Factors limiting the supply and efficiency of nutrient and oxygen supplements for the in situ biotreatment of contaminated soil and groundwater. *Water Research* **1992,** *26*, 73-78.

34. Hinchee, R. E.; Downey, D. C.; Aggarwal, P. K., Use of hydrogen peroxide as an oxygen source for in situ biodegradation: Part I. Field studies. *Journal of Hazardous Materials* **1991,** *27*, 287-299.

35. Pardieck, D. L.; Bouwer, E. J.; Stone, A. T., Hydrogen peroxide use to increase oxidant capacity for in situ bioremediation of contaminated soils and aquifers: A review. *Journal of Contaminant Hydrology* **1992,** *9*, 221-242.

36. Anid, P. J.; Alvarez, P. J. J.; Vogel, T. M., Biodegradation of monoaromatic hydrocarbons in aquifer columns amended with hydrogen peroxide and nitrate. *Water Research* **1993,** *27*, 685-691.

37. Miller, C. M.; Valentine, R. L., Mechanistic studies of surface catalyzed $H_2O_2$ decomposition and contaminant degradation in the presence of sand. *Water Research* **1999,** *33*, 2805-2816.

38. Krembs, F. J.; Siegrist, R. L.; Crimi, M. L.; Furrer, R. F.; Petri, B. G., ISCO for groundwater remediation: analysis of field applications and performance. *Ground Water Monitoring & Remediation* **2010,** *30*, 42-53.

39. Nyer, E. K.; Vance, D., Hydrogen peroxide treatment: the good, the bad, the ugly. *Ground Water Monitoring & Remediation* **1999,** *19*, 54-57.

40. U.S. Department of Defense *Technology status review: in situ oxidation*; 1999.

41. Watts, R. J.; Teel, A. L., Chemistry of modified Fenton's reagent (catalyzed $H_2O_2$ propagations-CHP) for in situ soil and groundwater remediation. *Journal of Environmental Engineering* **2005,** *131*, 612-622.

42. Watts, R. J.; Finn, D. D.; Cutler, L. M.; Schmidt, J. T.; Teel, A. L., Enhanced stability of hydrogen peroxide in the presence of subsurface solids. *Journal of Contaminant Hydrology* **2007,** *91*, 312-326.

43. Elprince, A. M.; Mohamed, W. H., Catalytic decomposition kinetics of aqueous hydrogen peroxide and solid magnesium peroxide by birnessite. *Soil Sci. Soc. Am. J. 56*, 1784-1788.

44. Furman, O.; Laine, D. F.; Blumenfeld, A.; Teel, A. L.; Shimizu, K.; Cheng, I. F.; Watts, R. J., Enhanced reactivity of superoxide in water−solid matrices. *Environmental Science & Technology* **2009,** *43*, 1528-1533.

45. Pera-Titus, M.; García-Molina, V.; Baños, M. A.; Giménez, J.; Esplugas, S., Degradation of chlorophenols by means of advanced oxidation processes: a general review. *Applied Catalysis B: Environmental* **2004,** *47*, 219-256.

46. Stefansson, A., Iron(III) hydrolysis and solubility at 25°C. *Environ. Sci. Technol.* **2007,** *41*, 6117.

47. Kwan, W. P.; Voelker, B. M., Rates of hydroxyl radical generation and organic compound oxidation in mineral-catalyzed Fenton-like systems. *Environmental Science & Technology* **2003,** *37*, 1150-1158.

48. Chou, S.; Huang, C., Decomposition of hydrogen peroxide in a catalytic fluidized-bed reactor. *Applied Catalysis A: General* **1999,** *185*, 237-245.

49. Hermanek, M.; Zboril, R.; Medrik, I.; Pechousek, J.; Gregor, C., Catalytic efficiency of iron(III) oxides in decomposition of hydrogen peroxide: competition between the surface area and crystallinity of nanoparticles. *Journal of the American Chemical Society* **2007,** *129*, 10929-10936.

50. De Laat, J.; Gallard, H., Catalytic decomposition of hydrogen peroxide by Fe(III) in homogeneous aqueous solution: mechanism and kinetic modeling. *Environmental Science & Technology* **1999,** *33*, 2726-2732.

51. Huling, S. G.; Arnold, R. G.; Sierka, R. A.; Miller, M. R., Measurement of hydroxyl radical activity in a soil slurry using the spin trap α-(4-pyridyl-1-oxide)- N-tert-butylnitrone. *Environmental Science & Technology* **1998,** *32*, 3436-3441.

52. Christensen, H.; Sehested, K.; Corfitzen, H., Reactions of hydroxyl radicals with hydrogen peroxide at ambient and elevated temperatures. *The Journal of Physical Chemistry* **1982,** *86*, 1588-1590.

53. Jayson, G. G.; Parsons, B. J.; Swallow, A. J., Some simple, highly reactive, inorganic chlorine derivatives in aqueous solution. Their formation using pulses of radiation and their role in the mechanism of the Fricke dosimeter. *Journal of the Chemical Society, Faraday Transactions 1: Physical Chemistry in Condensed Phases* **1973,** *69*, 1597-1607.

54. Haag, W. R.; Hoigné, J., Photo-sensitized oxidation in natural water via ˙OH radicals. *Chemosphere* **1985,** *14*, 1659-1671.

55. Chou, S.; Huang, C.; Huang, Y.-H., Heterogeneous and homogeneous catalytic oxidation by supported γ-FeOOH in a fluidized-bed reactor: kinetic approach. *Environmental Science & Technology* **2001,** *35*, 1247-1251.

56. Keenan, C. R.; Sedlak, D. L., Factors affecting the yield of oxidants from the reaction of nanoparticulate zero-valent iron and oxygen. *Environmental Science & Technology* **2008,** *42*, 1262-1267.

57. Bossmann, S. H.; Oliveros, E.; Göb, S.; Siegwart, S.; Dahlen, E. P.; Payawan, L.; Straub, M.; Wörner, M.; Braun, A. M., New Evidence against hydroxyl radicals as reactive intermediates in the thermal and photochemically enhanced Fenton reactions. *The Journal of Physical Chemistry A* **1998,** *102*, 5542-5550.

58. Keenan, C. R.; Sedlak, D. L., Ligand-enhanced reactive oxidant generation by nanoparticulate zero-valent iron and oxygen. *Environmental Science & Technology* **2008,** *42*, 6936-6941.

59. Xiang, L.; Royer, S.; Zhang, H.; Tatibouët, J. M.; Barrault, J.; Valange, S., Properties of iron-based mesoporous silica for the CWPO of phenol: a comparison between impregnation and co-condensation routes. *Journal of Hazardous Materials* **2009,** *172*, 1175-1184.

60. Cornu, C.; Bonardet, J. L.; Casale, S.; Davidson, A.; Abramson, S.; André, G.; Porcher, F.; Grčić, I.; Tomasic, V.; Vujevic, D.; Koprivanac, N., Identification and location of iron species in Fe/SBA-15 catalysts: interest for catalytic Fenton reactions. *The Journal of Physical Chemistry C* **2011,** *116*, 3437-3448.

61. Martínez, F.; Calleja, G.; Melero, J. A.; Molina, R., Heterogeneous photo-Fenton degradation of phenolic aqueous solutions over iron-containing SBA-15 catalyst. *Applied Catalysis B: Environmental* **2005,** *60*, 181-190.

62. Khieu, D. Q.; Quang, D. T.; Lam, T. D.; Phu, N. H.; Lee, J. H.; Kim, J. S., Fe-MCM-41 with highly ordered mesoporous structure and high Fe content: synthesis and application in heterogeneous catalytic wet oxidation of phenol. *Journal of inclusion phenomena and macrocyclic chemistry* **2009,** *65*, 73-81.

63. Gokulakrishnan, N.; Pandurangan, A.; Sinha, P. K., Catalytic wet peroxide oxidation technique for the removal of decontaminating agents ethylenediaminetetraacetic acid and oxalic

acid from aqueous solution using efficient Fenton type Fe-MCM-41 mesoporous materials. *Industrial & Engineering Chemistry Research* **2008,** *48,* 1556-1561.

64. Navalon, S.; Alvaro, M.; Garcia, H., Heterogeneous Fenton catalysts based on clays, silicas and zeolites. *Applied Catalysis B: Environmental* **2010,** *99,* 1-26.

65. Calleja, G.; Melero, J. A.; Martínez, F.; Molina, R., Activity and resistance of iron-containing amorphous, zeolitic and mesostructured materials for wet peroxide oxidation of phenol. *Water Res.* **2005,** *39,* 1741.

66. Guthrie, C. P.; Reardon, E. J., Metastability of MCM-41 and Al-MCM-41. *The Journal of Physical Chemistry A* **2008,** *112,* 3386-3390.

67. Galarneau, A.; Nader, M.; Guenneau, F.; Di Renzo, F.; Gedeon, A., Understanding the stability in water of mesoporous SBA-15 and MCM-41. *The Journal of Physical Chemistry C* **2007,** *111,* 8268-8277.

68. Ramirez, J. H.; Costa, C. A.; Madeira, L. M.; Mata, G.; Vicente, M. A.; Rojas-Cervantes, M. L.; López-Peinado, A. J.; Martín-Aranda, R. M., Fenton-like oxidation of Orange II solutions using heterogeneous catalysts based on saponite clay. *Applied Catalysis B: Environmental* **2007,** *71,* 44-56.

69. Chirchi, L.; Ghorbel, A., Use of various Fe-modified montmorillonite samples for 4-nitrophenol degradation by $H_2O_2$. *Applied Clay Science* **2002,** *21,* 271-276.

70. Neamţu, M.; Zaharia, C.; Catrinescu, C.; Yediler, A.; Macoveanu, M.; Kettrup, A., Fe-exchanged Y zeolite as catalyst for wet peroxide oxidation of reactive azo dye Procion Marine H-EXL. *Applied Catalysis B: Environmental* **2004,** *48,* 287-294.

71. Neamţu, M.; Catrinescu, C.; Kettrup, A., Effect of dealumination of iron(III)-exchanged Y zeolites on oxidation of Reactive Yellow 84 azo dye in the presence of hydrogen peroxide. *Applied Catalysis B: Environmental* **2004,** *51,* 149-157.

72. Gonzalez-Olmos, R.; Roland, U.; Toufar, H.; Kopinke, F. D.; Georgi, A., Fe-zeolites as catalysts for chemical oxidation of MTBE in water with $H_2O_2$. *Applied Catalysis B: Environmental* **2009,** *89,* 356-364.

73. Doocey, D. J.; Sharratt, P. N.; Cundy, C. S.; Plaisted, R. J., Zeolite-mediated advanced oxidation of model chlorinated phenolic aqueous waste: part 2: solid phase catalysis. *Process Safety and Environmental Protection* **2004,** *82,* 359-364.

74. Parkhomchuk, E. V.; Vanina, M. P.; Preis, S., The activation of heterogeneous Fenton-type catalyst Fe-MFI. *Catalysis Communications* **2008,** *9,* 381-385.

75. Kuznetsova, E. V.; Savinov, E. N.; Vostrikova, L. A.; Parmon, V. N., Heterogeneous catalysis in the Fenton-type system FeZSM-5/$H_2O_2$. *Applied Catalysis B: Environmental* **2004,** *51*, 165-170.

76. Xu, X.; Thomson, N. R., Hydrogen peroxide persistence in the presence of aquifer materials. *Soil and Sediment Contamination: An International Journal* **2010,** *19*, 602-616.

77. Sigg, L.; Stumm, W., The interaction of anions and weak acids with the hydrous goethite (a-FeOOH) surface. *Colloids and Surfaces* **1981,** *2*, 101-117.

78. Hiemstra, T.; Barnett, M. O.; van Riemsdijk, W. H., Interaction of silicic acid with goethite. *Journal of Colloid and Interface Science* **2007,** *310*, 8-17.

79. Jordan, N.; Marmier, N.; Lomenech, C.; Giffaut, E.; Ehrhardt, J.-J., Sorption of silicates on goethite, hematite, and magnetite: experiments and modelling. *Journal of Colloid and Interface Science* **2007,** *312*, 224-229.

80. Yeh, C. K. J.; Chen, W. S.; Chen, W. Y., Production of hydroxyl radicals from the decomposition of hydrogen peroxide catalyzed by various iron oxides at pH 7. *Pract. Period. Hazard.,, Toxic, Radioact. Waste Manage.* **2004,** *8*, 161-165.

81. Crowther, N.; Larachi, F. ç., Iron-containing silicalites for phenol catalytic wet peroxidation. *Applied Catalysis B: Environmental* **2003,** *46*, 293-305.

82. Barrault, J.; Abdellaoui, M.; Bouchoule, C.; Majesté, A.; Tatibouët, J. M.; Louloudi, A.; Papayannakos, N.; Gangas, N. H., Catalytic wet peroxide oxidation over mixed (Al–Fe) pillared clays. *Applied Catalysis B: Environmental* **2000,** *27*, L225-L230.

83. Cheng, M.; Song, W.; Ma, W.; Chen, C.; Zhao, J.; Lin, J.; Zhu, H., Catalytic activity of iron species in layered clays for photodegradation of organic dyes under visible irradiation. *Applied Catalysis B: Environmental* **2008,** *77*, 355-363.

84. Schwertmann, U.; Cornell, R. M., *Iron Oxides in the Laboratory: Preparation and Characterization*. Wiley-VCH Publishers: Weinheim, Germany: 2000.

85. Eisenberg, G., Colorimetric determination of hydrogen peroxide. *Industrial & Engineering Chemistry Analytical Edition* **1943,** *15*, 327.

86. Tamura, H.; Goto, K.; Yotsuyanagi, T.; Nagayama, M., Spectrophotometric determination of iron(II) with 1,10-phenanthroline in the presence of large amounts of iron(III). *Talanta* **1974,** *21*, 314.

87. Corma, A., From microporous to mesoporous molecular sieve materials and their use in catalysis. *Chemical Reviews* **1997,** *97*, 2373-2420.

88. Voegelin, A.; Hug, S. J., Catalyzed oxidation of arsenic(III) by hydrogen peroxide on the surface of ferrihydrite: an in situ ATR-FTIR study. *Environmental Science & Technology* **2003,** *37*, 972-978.

89. Lee, Y. N.; Lago, R. M.; Fierro, J. L. G.; González, J., Hydrogen peroxide decomposition over $Ln_{1-x}A_xMnO_3$ (Ln = La or Nd and A = K or Sr) perovskites. *Applied Catalysis A: General* **2001,** *215*, 245-256.

90. Amonette, J. E.; Workman, D. J.; Kennedy, D. W.; Fruchter, J. S.; Gorby, Y. A., Dechlorination of Carbon Tetrachloride by Fe(II) Associated with Goethite. *Environmental Science & Technology* **2000,** *34*, 4606-4613.

91. Esshington, M. E., *Soil and water chemistry: an integrative approach*. CRC Press: Boca Raton, FL: 2004.

92. Zeglínski, J.; Piotrowski, G. P.; Piękós, R., A study of interaction between hydrogen peroxide and silica gel by FTIR spectroscopy and quantum chemistry. *Journal of Molecular Structure* **2006,** *794*, 83-91.

93. Pham, A. L.-T.; Lee, C.; Doyle, F. M.; Sedlak, D. L., A silica-supported iron oxide catalyst capable of activating hydrogen peroxide at neutral pH values. *Environmental Science & Technology* **2009,** *43*, 8930-8935.

94. Taujale, S.; Zhang, H., Impact of interactions between metal oxides to oxidative reactivity of manganese dioxide. *Environmental Science & Technology* **2012,** *46*, 2764-2771.

95. Nico, P. S.; Stewart, B. D.; Fendorf, S., Incorporation of oxidized uranium into Fe (hydr)oxides during Fe(II) catalyzed remineralization. *Environmental Science & Technology* **2009,** *43*, 7391-7396.

96. Kunze, G. W.; Dixon, J. B., *Pretreatment for mineralogical analysis. In: Methods of soil analysis*. American Society of Agronomy, Inc. Soil Science Society of America, Inc.: 1986.

97. Keeling, J. L.; Raven, M. D.; Gates, W. P., Geology and characterization of two hydrothermal nontronites from weathered metamorphic rocks at the Uley graphite mine, South Australia. *Clays and Clay Minerals* **2000,** *48*, 537-548.

98. Teel, A. L.; Finn, D. D.; Schmidt, J. T.; Cutler, L. M.; Watts, R. J., Rates of trace mineral-catalyzed decomposition of hydrogen peroxide. *Environmental Engineering Science* **2007,** *133*, 853-858.

99. Crimi, M. L.; Siegrist, R. L., Factors affecting effectiveness and efficiency of DNAPL destruction using potassium permanganate and catalyzed hydrogen peroxide. *Journal of Environmental Engineering* **2005,** *131*, 1724-1732.

100. Bissey, L. L.; Smith, J. L.; Watts, R. J., Soil organic matter–hydrogen peroxide dynamics in the treatment of contaminated soils and groundwater using catalyzed $H_2O_2$ propagations (modified Fenton's reagent). *Water Research* **2006,** *40,* 2477-2484.

101. Pham, A. L.-T.; Doyle, F. M.; Sedlak, D. L., Inhibitory effect of dissolved silica on $H_2O_2$ decomposition by iron(III) and manganese(IV) oxides: implications for $H_2O_2$-based in situ chemical oxidation. *Environmental Science & Technology* **2012,** *46,* 1055-1062.

102. Kakarla, P. K. C.; Watts, R. J., Depth of Fenton-like oxidation in remediation of surface soil. *Journal of Environmental Engineering-ASCE* **1997,** *123,* 11-17.

103. Langmuir, D., *Aqueous environmental geochemistry*. Prentice Hall, Inc.: 1997.

104. Davis, C. C.; Chen, H.-W.; Edwards, M., Modeling silica sorption to iron hydroxide. *Environmental Science & Technology* **2002,** *36,* 582-587.

105. Kohn, T.; Kane, S. R.; Fairbrother, D. H.; Roberts, A. L., Investigation of the inhibitory effect of silica on the degradation of 1,1,1-trichloroethane by granular iron. *Environmental Science & Technology* **2003,** *37,* 5806-5812.

106. Browman, M. G.; Robinson, R. B.; Reed, G. D., Silica polymerization and other factors in iron control by sodium silicate and sodium hypochlorite additions. *Environmental Science & Technology* **1989,** *23,* 566-572.

107. Robinson, R. B.; Frasier, B.; Reed, G. D., Iron and manganese sequestration facilities using sodium-silicate. *Journal American Water Works Association* **1992,** *84,* 77.

108. Davis, C. C.; Knocke, W. R.; Edwards, M., Implications of aqueous silica sorption to iron hydroxide: mobilization of iron colloids and interference with sorption of arsenate and humic substances. *Environmental Science & Technology* **2001,** *35,* 3158-3162.

109. Zachara, J. M.; Girvin, D. C.; Schmidt, R. L.; Resch, C. T., Chromate adsorption on amorphous iron oxyhydroxide in the presence of major groundwater ions. *Environmental Science & Technology* **1987,** *21,* 589-594.

110. Jordan, N.; Lomenech, C.; Marmier, N.; Giffaut, E.; Ehrhardt, J.-J., Sorption of selenium(IV) onto magnetite in the presence of silicic acid. *Journal of Colloid and Interface Science* **2009,** *329,* 17-23.

111. Sastra, V. S., *Corrosion inhibitors. Principles and applications*. 1998.

112. Rushing, J. C.; McNeill, L. S.; Edwards, M., Some effects of aqueous silica on the corrosion of iron. *Water Research* **2003,** *37,* 1080-1090.

113. Swedlund, P. J.; Hamid, R. D.; Miskelly, G. M., Insights into $H_4SiO_4$ surface chemistry on ferrihydrite suspensions from ATR-IR, Diffuse Layer Modeling and the adsorption enhancing effects of carbonate. *Journal of Colloid and Interface Science* **2010,** *352*, 149-157.

114. Swedlund, P. J.; Webster, J. G., Adsorption and polymerisation of silicic acid on ferrihydrite, and its effect on arsenic adsorption. *Water Research* **1999,** *33*, 3413-3422.

115. Icopini, G. A.; Brantley, S. L.; Heaney, P. J., Kinetics of silica oligomerization and nanocolloid formation as a function of pH and ionic strength at 25°C. *Geochimica et Cosmochimica Acta* **2005,** *69*, 293-303.

116. Dzombak, D. A.; Morel, F. M., *Surface complexation modeling: hydrous ferric oxide*. 1990.

117. Legrini, O.; Oliveros, E.; Braun, A. M., Photochemical processes for water treatment. *Chemical Reviews* **1993,** *93*, 671-698.

118. Ghosh-Mukerji, S.; Haick, H.; Schvartzman, M.; Paz, Y., Selective photocatalysis by means of molecular recognition. *Journal of the American Chemical Society* **2001,** *123*, 10776-10777.

119. Yoneyama, H.; Haga, S.; Yamanaka, S., Photocatalytic activities of microcrystalline titania incorporated in sheet silicates of clay. *The Journal of Physical Chemistry* **1989,** *93*, 4833-4837.

120. Shiraishi, Y.; Sugano, Y.; Inoue, D.; Hirai, T., Effect of substrate polarity on photocatalytic activity of titanium dioxide particles embedded in mesoporous silica. *Journal of Catalysis* **2009,** *264*, 175-182.

121. Zhao, D.; Feng, J.; Huo, Q.; Melosh, N.; Fredrickson, G. H.; Chmelka, B. F.; Stucky, G. D., Triblock copolymer syntheses of mesoporous silica with periodic 50 to 300 angstrom pores. *Science* **1998,** *279*, 548-552.

122. Gervasini, A.; Messi, C.; Carniti, P.; Ponti, A.; Ravasio, N.; Zaccheria, F., Insight into the properties of Fe oxide present in high concentrations on mesoporous silica. *Journal of Catalysis* **2009,** *262*, 224-234.

123. Katiyar, A.; Ji, L.; Smirniotis, P.; Pinto, N. G., Protein adsorption on the mesoporous molecular sieve silicate SBA-15: effects of pH and pore size. *Journal of Chromatography A* **2005,** *1069*, 119-126.

124. Lee, C.; Sedlak, D. L., A novel homogeneous Fenton-like system with Fe(III)–phosphotungstate for oxidation of organic compounds at neutral pH values. *Journal of Molecular Catalysis A: Chemical* **2009,** *311*, 1-6.

125. Voelker, B. M.; Sulzberger, B., Effects of fulvic acid on Fe(II) oxidation by hydrogen peroxide. *Environmental Science & Technology* **1996,** *30*, 1106-1114.

126. Cooper, C.; Burch, R., Mesoporous materials for water treatment processes. *Water Research* **1999,** *33*, 3689-3694.

127. Burke, A. M.; Hanrahan, J. P.; Healy, D. A.; Sodeau, J. R.; Holmes, J. D.; Morris, M. A., Large pore bi-functionalised mesoporous silica for metal ion pollution treatment. *Journal of Hazardous Materials* **2009,** *164*, 229-234.

128. Yang, H.; Xu, R.; Xue, X.; Li, F.; Li, G., Hybrid surfactant-templated mesoporous silica formed in ethanol and its application for heavy metal removal. *Journal of Hazardous Materials* **2008,** *152*, 690-698.

129. McKimmy, E.; Dulebohn, J.; Shah, J.; Pinnavaia, T. J., Trapping of arsenite by mercaptopropyl-functionalized mesostructured silica with a wormhole framework. *Chemical Communications* **2005**, 3697-3699.

130. Li, J.; Wang, L.; Qi, T.; Zhou, Y.; Liu, C.; Chu, J.; Zhang, Y., Different N-containing functional groups modified mesoporous adsorbents for Cr(VI) sequestration: Synthesis, characterization and comparison. *Microporous and Mesoporous Materials* **2008,** *110*, 442-450.

131. Yantasee, W.; Fryxell, G. E.; Addleman, R. S.; Wiacek, R. J.; Koonsiripaiboon, V.; Pattamakomsan, K.; Sukwarotwat, V.; Xu, J.; Raymond, K. N., Selective removal of lanthanides from natural waters, acidic streams and dialysate. *Journal of Hazardous Materials* **2009,** *168*, 1233-1238.

132. Walcarius, A.; Mercier, L., Mesoporous organosilica adsorbents: nanoengineered materials for removal of organic and inorganic pollutants. *Journal of Materials Chemistry* **2010,** *20*, 4478-4511.

133. Anbia, M.; Lashgari, M., Synthesis of amino-modified ordered mesoporous silica as a new nano sorbent for the removal of chlorophenols from aqueous media. *Chemical Engineering Journal* **2009,** *150*, 555-560.

134. Zhu, D.; Zhang, H.; Tao, Q.; Xu, Z.; Zheng, S., Surface functionalized mesoporous silicas as adsorbents for aromatic contaminants in aqueous solution. *Environmental Toxicology and Chemistry* **2009,** *28*, 1400-1408.

135. Sawicki, R.; Mercier, L., Evaluation of mesoporous cyclodextrin-silica nanocomposites for the removal of pesticides from aqueous media. *Environmental Science & Technology* **2006,** *40*, 1978-1983.

136. Han, Y.-F.; Chen, F.; Ramesh, K.; Zhong, Z.; Widjaja, E.; Chen, L., Preparation of nanosized $Mn_3O_4$/SBA-15 catalyst for complete oxidation of low concentration EtOH in aqueous solution with $H_2O_2$. *Applied Catalysis B: Environmental* **2007,** *76*, 227-234.

137. Navalon, S.; Alvaro, M.; Garcia, H., Heterogeneous Fenton catalysts based on clays, silicas and zeolites. *Applied Catalysis B: Environmental* **2010,** *99*, 1-26.

138. Iler, R. K., *The chemistry of silica: solubility, polymerization, colloid and surface properties, and biochemistry*. 1979.

139. Dunphy, D. R.; Singer, S.; Cook, A. W.; Smarsly, B.; Doshi, D. A.; Brinker, C. J., Aqueous stability of mesoporous silica films doped or grafted with aluminum oxide. *Langmuir* **2003,** *19*, 10403-10408.

140. Tanev, P. T.; Pinnavaia, T. J., A neutral templating route to mesoporous molecular sieves. *Science* **1995,** *267*, 865-867.

141. Beck, J. S.; Vartuli, J. C.; Roth, W. J.; Leonowicz, M. E.; Kresge, C. T.; Schmitt, K. D.; Chu, C. T. W.; Olson, D. H.; Sheppard, E. W., A new family of mesoporous molecular sieves prepared with liquid crystal templates. *Journal of the American Chemical Society* **1992,** *114*, 10834-10843.

142. Aguado, J.; Arsuaga, J. M.; Arencibia, A., Adsorption of aqueous mercury(II) on propylthiol-functionalized mesoporous silica obtained by cocondensation. *Industrial & Engineering Chemistry Research* **2005,** *44*, 3665-3671.

143. Aguado, J.; Arsuaga, J. M.; Arencibia, A.; Lindo, M.; Gascón, V., Aqueous heavy metals removal by adsorption on amine-functionalized mesoporous silica. *Journal of Hazardous Materials* **2009,** *163*, 213-221.

144. Bai, S.; Urabe, S.; Okaue, Y.; Yokoyama, T., Acceleration effect of sulfate ion on the dissolution of amorphous silica. *Journal of Colloid and Interface Science* **2009,** *331*, 551-554.

145. Yu, Q.; Kandegedara, A.; Xu, Y.; Rorabacher, D. B., Avoiding interferences from Good's buffers: a contiguous series of noncomplexing tertiary amine buffers covering the entire range of pH 3–11. *Analytical Biochemistry* **1997,** *253*, 50-56.

146. Green Berg, A. E.; Clesceri, L. S.; Eaton, A. D., *Standard methods for the examination of water and wastewater*. 1992.

147. Bickmore, B. R.; Nagy, K. L.; Gray, A. K.; Brinkerhoff, A. R., The effect of Al(OH)4- on the dissolution rate of quartz. *Geochimica et Cosmochimica Acta* **2006,** *70*, 290-305.

148. Glasspoole, B. W.; Webb, J. D.; Crudden, C. M., Catalysis with chemically modified mesoporous silicas: Stability of the mesostructure under Suzuki-Miyaura reaction conditions. *Journal of Catalysis* **2009,** *265*, 148-154.

149. Melde, B.; Johnson, B.; Charles, P., Mesoporous silicate materials in sensing. *Sensors* **2008,** *8*, 5202-5228.

150. Hartmann, M., Ordered mesoporous materials for bioadsorption and biocatalysis. *Chemistry of Materials* **2005,** *17*, 4577-4593.

151. Gonzalez-Olmos, R.; Holzer, F.; Kopinke, F.-D.; Georgi, A., Indications of the reactive species in a heterogeneous Fenton-like reaction using Fe-containing zeolites *Applied Catalysis A: General* **2011**, *398*, 44-53.